Application for EURATOM Priority Support of Additional Heating for ASDEX Upgrade, Phase I and Phase II

prepared by the

ASDEX Upgrade Project Group
Neutral Injection Group
Ion Cyclotron Resonance Heating Group

IPP 1/237 April 1985

MAX-PLANCK-INSTITUT FÜR PLASMAPHYSIK

8046 GARCHING BEI MÜNCHEN

MAX-PLANCK-INSTITUT FÜR PLASMAPHYSIK

GARCHING BEI MÜNCHEN

Application for EURATOM Priority Support of Additional Heating for ASDEX Upgrade, Phase I and Phase II

prepared by the

ASDEX Upgrade Project Group
Neutral Injection Group
Ion Cyclotron Resonance Heating Group

IPP 1/237 April 1985

Die nachstehende Arbeit wurde im Rahmen des Vertrages zwischen dem Max-Planck-Institut für Plasmaphysik und der Europäischen Atomgemeinschaft über die Zusammenarbeit auf dem Gebiete der Plasmaphysik durchgeführt.

A S D E X U p g r a d e - Additional Heating

Prepared by the

ASDEX Upgrade Project Group:

W.Köppendörfer, M.Blaumoser, K.Ennen, J.Gruber, O.Gruber, O.Jandl, M.Kaufmann, H.Kollotzek, H.Kotzlowski, E.Lackner, K.Lackner, T.v.Larcher, J.Neuhauser, M.Pillsticker, R.Pöhlchen, H.Preis, H.Schneider[1], U.Seidel, B.Sombach, B.Streibl, F.Werner, A.Wieczorek

Neutral Injection Group:

E.Speth, F.P.Pennigsfeld, J.H.Feist, K.Freudenberger, J.Kolos, R.C.Kunze, H.Lohnert, W.Melkus[2], W.Ott, H.Riedler, A.Stäbler, O.Vollmer, K.Wittenbecher, G.Wulff

Ion Cyclotron Resonance Heating Group:

J.M.Noterdaeme, F.Wesner, J.Bäumler, F.Braun, R.Fritsch, F.Hofmeister, E.v.Mark, S.Puri, M.Söll, K.Steinmetz, H.Wedler

Max-Planck-Institut für Plasmaphysik, EURATOM Association, D-8046 Garching, West-Germany

Contributions by:
J.B.Lister
Centre de Recherches en Physique des Plasmas, Association EURATOM Confédération Suisse, Ecole Polytechnique Fédérale de Lausanne/Switzerland.
R.Wilhelm, E.Räuchle
Institut für Plasmaforschung, Universität Stuttgart, D-7000 Suttgart, West-Germany.

---

1 INTERATOM, West-Germany

2 ZTE

March 1985

Content

1. Summary

1.1 Introduction

The physical aims and the technical features of ASDEX Upgrade have been described in several papers and reports /1,2,3,4/. They shall be summarized in the following with regard to additional heating.

ASDEX Upgrade has been designed in order to extent the favourable features found in ASDEX divertor discharges to poloidal divertor plasmas which are physically and technically compatible with reactor requirements. These requirements concern:

1. the plasma configuration and the poloidal field (PF) system;
2. the plasma parameters affecting plasma wall interaction, namely the plasma line density $\overline{n_e \cdot a}$ and temperature gradient in the boundary;
3. the energy flux density in the plasma boundary and to the material evironment;
4. the additional heating, as required by the above points, and by plasma refuelling.

In a reactor the plasma configuration and the location of the poloidal field coils have to provide space for blanket structure and for a single null (SN) divertor plasma. In the ASDEX Upgrade design those reactor relevant distances have been scaled to smaller size. The unavoidably vertically elongated plasma is in any case desireable with elongations of at least b/a = κ = 1.6 for achieving large β_t values. Those elongated plasmas are vertically unstable but are easier to stabilize at high β_p values because the associated outward shift in the plasma current distribution leads to an improved coupling to the passive stabilizing coils. High ß values can only be reached with additional heating.

The function of a divertor requires a zone of high particle recycling in front of the material structure which intersects the

diverted scrape-off layer. A narrow flux tube and a closed divertor chamber facilitated the formation of a recycling layer in ASDEX. The fanning out of the flux tubes and the impossibility to form a closed divertor chamber in the "open" ASDEX Upgrade configuration call for larger plasma density in the bulk and boundary and a sufficient energy flux in order to reach the high recycling regime at the target plates. Large line density in the average plasma boundary combined with a proper temperature gradient can also considerably reduce sputtering at the wall by reducing fast charge exchange neutrals. This is another reason for demanding high average density. There is also a good chance to model the temperature decay of a reactor plasma in the boundary perpendicular to magnetic flux surfaces provided the plasma bulk is sufficiently heated /5/.

All these objectives require additional heating which should be available as early as possible in the experimental programme.

1.2 Plasma Parameters and Heating Powers

The attainable plasma parameters of ASDEX Upgrade are subject to several limits.

The ß-limit, or plasma pressure limit /6/ is

$$\beta_t = c_\beta \frac{I_p\ (MA)}{a(m)\ B_t(T)} \qquad (1)$$

Experimentally a value of $c_\beta = 0.031$ was found in ASDEX discharges. The maximum average plasma pressure is thus

$$p\ \left(\frac{MN}{m^2}\right) = \beta_t \frac{B_t^2 \cdot 10^{-6}}{2\ \mu_o} = 0.012 \frac{I_p(MA)\ B_t(T)}{a(m)} \qquad (2)$$

It is finally limited by the permissible shear stresses in the toroidal field coils:

$$B_t I_p \leq c_m = \begin{cases} 4.5 \text{ for SN} & \text{single null} \\ 3.9 \text{ for DN} & \text{double null} \\ 6.5 \text{ for L} & \text{limiter} \end{cases} \qquad (3)$$

The heating power required to reach this pressure $\bar{p}$ is given by:

$$P_h \text{ (MW)} = \frac{3}{2} \frac{\bar{p} \cdot V_{pe}}{\tau_E} \quad .$$

The energy confinement time τ_E can be taken from H-mode discharges of ASDEX as

$$\tau_E = 0.107 \cdot I_p \text{ (MA)} \cdot A_i^{1/2} \qquad (4)$$

with A_i denoting the atomic mass number. Setting for $V_{pl} = 2\pi^2 \kappa R_o a^2$, with major plasma radius R_o and $\kappa = \frac{b}{a}$, the heating power needed to reach the ASDEX Upgrade ß-limits becomes:

$$P_h \text{ (MW)} = 3.41 \cdot \frac{B_t R a \kappa}{A_i^{1/2}} \qquad (5)$$

The density limit (Murakhami/Hugill) determines the largest attainable average density:

$$\bar{n}_c \text{ (m}^{-3}\text{)} = 0.825 \cdot 10^{20} \frac{I_p \text{ (MA)}}{a^2 (1 + \kappa^2)} \qquad (6)$$

Together with (2) the maximum average plasma temperature is also determined.

Figure 1 shows for the SN plasma configuration the attainable plasma temperature in dependence on I_p and $\bar{n}_c$ and on the different limits described above. Lines of constant $q_I = 2.5 \frac{a^2 (1 + \kappa^2) B_t \text{ (T)}}{R_o \cdot I_p \text{ (MA)}}$ are also shown. The $q_I = 2$ line can be regarded as a lower limit although one has to bear in

mind that $q_I = 2$ corresponds to a flux surface averaged q_ψ-value at the plasma boundary of $q_\psi \simeq 3$. Relation (5) yields heating powers for hydrogen of $P_{hH} = 4.5 \cdot B_t$ and for deuterium of $P_{hD} = 3.2 \cdot B_t$. At the critical density $\bar{n}_c$ the temperature depends solely on the heating power:

$$\frac{\overline{T_e + T_i}}{2} = c_h \cdot P_h$$

with $c_h = 0.19$ for hydrogen and $c_h = 0.25$ for deuterium. Larger temperatures can still be achieved if the average plasma density is kept below the critical density:

$$\frac{\overline{T_e + T_i}}{2}/\text{kev} = c_h \frac{\bar{n}_c}{\bar{n}_e} \cdot P_h \quad .$$

Reactor similar parameters and proper conditions for the SN divertor operation are found in Fig. 1 in the area of the triangle given by the line $I_p \gtrsim 1$ MA ($\bar{n}_c \gtrsim 10^{20}$ m^{-3}) the β_t-limit line and the $q_I = 2$ line. The heating powers required to reach this area is about $P_h \simeq 6$ MW and to fully cover it $P_h \simeq 12$ MW for deuterium. ASDEX with circular plasma reaches barely the lower point of the triangle. Optimum conditions in ASDEX Upgrade are met at the right point, $I_p = 1.6$ MA, $\bar{n}_c \simeq 1.5 \cdot 10^{20}$ m^{-3} with $P_h = 12$ MW for hydrogen and $P_h = 8.5$ MW for deuterium.

The accessible parameter range for fixed machine parameters are shown in Fig. 2 and 3.

SN configurations with parameter of Fig. 1 can be sustained for 5 to 10 seconds depending on the choice of I_p and B_t. The 5 seconds correspond to the SN reference discharge with $B_t \simeq 2.7$ T and $I_p = 1.6$ MA.

1.3 The Choice of Auxiliary Heating Methods

The basic auxiliary heating of ASDEX Upgrade shall be accomplished by half neutral injection (NI) and half ICRH. Both shall be installed in steps during 1988 and 1989. This choice reduces the risc of relying solely on ICRH and provides increased flexibility for heating and refuelling the plasma. Later they may be supplemented by lower hybrid (LH) for current build up and current drive and by ECRH as soon as proper generators are available and Alfvèn Wave Heating. The total heating power finally available shall be 15 MW. The definition of heating power P_h was given in Section 1.2.

The following conditions and requirements determined the choice of the basic heating system:

- optimal heating of hydrogen and deuterium plasmas;
- heating of the plasma core in order to simulate α-particle heating;
- small power deposition at the plasma boundary to avoid losses by fast CX neutrals;
- heating for toroidal field values $2.5 \leq B_t \leq 4$ T;
- wave heating from the low toroidal field side;
- heating of plasmas with $\frac{\omega_{pe}}{\omega_{ce}} > 1$.

THIS APPLICATION FOR ADDITIONAL HEATING OF ASDEX UPGRADE CONCERNS THE BASIC SYSTEM CONSISTING OF NEUTRAL INJECTION AND ION CYCLOTRON RESONANCE HEATING. BOTH ARE DESCRIBED IN DETAIL. THE OTHER OPTIONS FOR THE LONG RANGE PROGRAMME ARE DESCRIBED FOR INFORMATION ONLY.

1.3.1 Neutral Injection

Originally NI heating was discarded because of the large opacity of the plasma $\bar{n}_e \cdot a \simeq 10^{20}$ m^{-2} and the decreased neutralization efficiency of ion beams with 100 keV particle energies. Recent experiments on ASDEX with very different injection energies (25, 13, 9 keV species averaged energy pro nucleon) showed little differences in the radial temperature profiles although the energy deposition profiles differed considerably /6/. This is essentially in agreement with theory.

It implies that ASDEX Upgrade can be heated with beam particle energies (H°) around 60 keV, with an average injection angle of 25° to the radial direction at R_o = 1.7 m. This injection angle is essentially determined by the port geometry. The good penetration at this angle and the reduced CX losses are bought at the expense of enhanced ripple losses and the danger of triggering fishbone instabilities.

The toroidal field ripple reaches

$$\frac{B_{max} - B_{min}}{B_{max} + B_{min}} = 0.8\ \%$$

at the outer edge at R = 2.15 m. Extensive calculations for fast ion ripple losses were carried through during the ZEPHYR design study /7/. Because of the 16 fold symmetry of both TF-magnets and similar radial distances, results from these calculations can be applied to ASDEX Upgrade. Ripple losses of $\leq$ 15 % have to be expected for 60 to 80 keV protons in ASDEX Upgrade. These ripple losses and CX losses of fast neutrals lead to an estimated loss of 20 to 25 % of the NI power entering the vacuum vessel.

In PDX neutral injection heated (14° to perpendicular at R_o = 1.43 m) experiments so called fishbone instabilities were observed at high heating power /8/. A theoretical model explains these as internal kink modes being destabilized by trapped high energy particle pressure /9/. The slowing down distribution of ASDEX Upgrade beam particles may be similar to PDX because the higher density is compensated by higher temperature leading to equal relaxation times. However, the injection angle of 24° of ASDEX Upgrade is closer to that of Doublett III with 27° were fishbone instabilities were usually not observed or at least not found to affect significantly the energy balance.

IPP Garching proposes to use modified JET sources optimized to 60 kV and 80 A per source. One NI box with four sources provides 6 MW for 10 sec steady state hydrogen injection.

NI concept summarized:

- One injection box equipped with 4 sources;
- Hydrogen operation; 1 source delivers 60 kV, 80 A, 10 s, 1 box yields 6.0 MW;
- Deuterium operation: 1 source delivers 70 kV, 70 A, 10 s, 1 box yields 9.0 MW;

The powers are those entering through the vacuum vessel port.

1.3.2 Ion Cyclotron Heating

Figure 2 shows the dependence of the ion cyclotron resonances of hydrogen, deuterium and Helium 3 on magnetic field and frequency.

A frequency range $30 \leq f_{IC} \leq 120$ MHz and magnetic field range $2.5 \leq B_t \leq 4$ T cover He_3 and H minority heating of deuterium and H and D 2nd harmonic heating. Low field side excitation, central plasma heating and high single path absorption favour this choice. A similar tuneable frequency range was realized for ASDEX /10/.

In order to provide 6 MW ICRH power for ASDEX Upgrade 4 of the 16 vacuum vessel sectors will be equipped with antenna arrays of 1.5 MW each. In principle every other sector (2,4,6 ...), in total 8, could take up an antenna array. The antenna was developed and optimized for second harmonic heating based on the experience gained in other ICR heated tokamaks and on calculations with ray tracing /11/ and antenna coupling codes /12/.

Two types of antenna frames were developed. One, of medium width, can be equipped with a dipole, or eventually at reduced power with a quadrupole whose spectrum peaks at $k \simeq 12\ m^{-1}$. A second,

wider frame was specifically designed to accomodate a quadrupole at full power with a spectrum peaking at $k \simeq 8\ m^{-1}$. Both types can be adapted, with minimal changes to single null, double null, or limiter configurations.

Four 1.5 MW generators provide the required power for up to 10 seconds every 5 minutes. Study contracts with several industrial companies on the development of such generators and power tetrodes were carried out yielding sufficient confidence that the required parameters can be achieved.

The ASDEX system presently in operation is rather similar to what is planned for ASDEX Upgrade.

ICRH concept summarized:

- Four antenna arrays for 4 x 1.5 MW installed at the low field side;
- frequency range $30 \leq f \leq 120$ MHz with full power up to 100 MHz;
- He_3 and H minority in D, $2\omega_{ci}$ for D and H;
- 4 tuneable generators of 1.5 MW, each with tetrodes for long pulse (10 s) operation.

1.3.3 Advantages of the combination of NI and ICRH

Neutral injection can reliably heat plasmas independently of the initial temperature and the toroidal field value. Neutral injection is connected with refuelling of the bulk plasma by the injected particle flux. This can be advantageous or detrimental depending on the amount of recycling at the walls. Even at the highest density 25 % of hydrogen would be refuelled by 12 MW H° injection with 60 keV in the SN reference plasma of ASDEX Upgrade, if the particle confinement time is twice the energy confinement time. The injection will change the plasma composition if the injected species mix differs from the plasma particle composition. The injected power loss is estimated to be 20 %. Half due to ripple losses and half to CX losses. Both lead to fast particles which can cause sputtering and impurity production at the vacuum vessel structure.

Neutral injection applied prior to ICRH can support ICRH, since, in general, wave absorption is larger at elevated temperature. ICRH delivers energy to the plasma without adding particles. More freedom with regard to the refuelling flux and method is therefore gained by combining NI and ICRH.

Since switching and control of the ICRH power is easy in contrast to the NI power a feedback control of the heating power up to 50 % can be achieved by combining NI and ICRH.

In Fig. 5 a horizontal cross-section of tokamak midplane and environment is shown. 1 NI box for 6 MW leaves still 7 large ports (0.4 x 0.8 m^2) to diagnostics. The neutral beam particles themselves can be utilized for diagnostic purposes like fast particle energy spectra and CX excited impurity lines of fully stripped ions.

1.4 Supplementary Heating in the Long Range Programme

This section deals with the possible extension of auxiliary heating which may become necessary to be installed in a later stage of the experimental programme.

1.4.1 Lower Hybrid Current Drive

Lower hybrid (LH) waves shall be used in a later stage. Rather than for heating they shall be optimized for current drive. Current drive is basically understood from several tokamak experiments /13/ and a theory by Fisch /14/.

The efficiency of LH heating is limited to a narrow density window and restricted to distinct frequency and N profile shaping. Therefore LH heating is not primarily considered.

Ramp up of part of the plasma current by LH waves can save OH flux which can than be utilized to prolong the hot plasma discharge. The flux connected with the plasma is:

$$\phi(\mathrm{Vs}) = 0.4\,\pi\, R_o \Delta I_p \left(\ln \frac{8A}{\sqrt{R}} - 2 + \frac{h_i}{2}\right) = 3.6\, I_p\ (\mathrm{MA})$$

Providing I_p = 0.5 MA by LH current drive would thus save 1.8 Vs.

For ASDEX Upgrade a current rise rate of $\dot{I}_p$ = 0.24 MA/s for $Z_{eff} \simeq$ 1 and 0.31 MA/s for Z_{eff} = 2 are estimated as feasible from the theory by Fisch and from ASDEX experimental results extrapolated to large power. For 3 MW LH power and a density of $\bar{n}_e \simeq 10^{19}$ m^{-3} a plasma current of I_p = 0.5 MA should be reached in 2.5 seconds starting from small or zero plasma current. The choice of the proper frequency depends on the acessibility to the plasma and on the density. A frequency of 1.5 to 3 GHz and a spectrum with $N_{\parallel} \simeq$ 1.3 seems adequate. Accessibility supports the lower frequency, however, ion coupling limits the attainable density. At higher frequencies the accessibility depends only weakly on frequency but according to theory the current drive efficiency is already decreasing.

The choice of frequency shall be supported by ASDEX experiments through investigation of the density limit at low frequency (1.5 GHz) and the current drive efficiency in dependence on the $N_{\parallel}$ spectrum. In addition current drive experiments over a large range of plasma current are desireable. The data envisaged for current drive on ASDEX Upgrade are:

LH current drive:

$\dot{I}_{pLH} \simeq$ 0.25 MA/sec

$\Delta I_{pLH} \simeq$ 0.5 MA (t = 2.5 sec)

$\Delta \phi_{plLH} \simeq$ 1.8 Vsec

$f_{LH} \simeq$ 1.5 ÷ 3 GHz

$P_{LH} \simeq$ 3 MW

required port: A-port 0.4 x 0.6 m².

1.4.2 Electron Cyclotron Resonance Heating (ECRH)

ECRH has several attractive features like: high-power flux density, small wave guides, localized power deposition within the plasma which can be used for profile shaping, and heating independent of the ion species.

Tokamak experiments and W VII A / 15 / have successfully applied ECRH. Especially when polarized waves were used instead of the gyrotron mode pattern wave mixture, narrow power deposition profiles and efficient heating could be observed.
The high plasma density of ASDEX Upgrade with $\frac{\omega_{pe}}{\omega_{ce}} < 1$ makes access to the plasma difficult.
Figure 6 shows the cut-offs and principal resonances for ordinary (O) and extraordinary (X) waves perpendicular to the magnetic field. Index 1 denotes the fundamental frequency ω_{ce} and Index 2 the second harmonic $2\omega_{ce}$. Since absorption of the O_2 waves is still small at 2 - 3 keV plasma temperature the X_1 wave launched from the inside should be preferred. Gyratrons with 70 GHz (B_o = 2.5 T, $n_{crit} = 1.2 \cdot 10^{20}$ m^{-3}) and 200 kW power are already available. Gyrotrons with 90 GHz (B_o = 3.2 T, $n_{crit} = 2 \cdot 10^{20}$ m^{-3}) exist in the USSR. The trace of an X_1 wave into the ASDEX Upgrade plasma is shown in Fig. 7. It requires a mirror which can enhance absorption if it is tilted to incline the wave 45° into the toroidal direction. Full absorption close to the resonance layer can be achieved this way. This seems to be the only method to achieve heating up to $n_{eo} = 1 \div 2 \cdot 10^{20}$ m^{-3} at frequencies of already or in near future available gyrotrons.

IPP intends to prepare for installation of 2 MW ECRH power in a later stage of the ASDEX Upgrade programme. As a first step ASDEX shall investigate absorption of a 70 GHz X-wave transmitted by a mirror from the high field side to the plasma.

2 MW ECRH power requires gyrotrons of output powers larger than 200 kW, long pulse. Although those are not available at present, the intense worldwide development programme can be expected to produce 70 to 90 GHz gyrotrons in due course.

1.4.3 Alfvèn Wave Heating

The TCA Group of the Ecole Polytechnique Fédérale de Lausanne has successfully applied Alfvèn Wave Heating (AWH) to a tokamak. Although the damping process is physically less clear the mode structure and resonance layer position are theoretically well understood. The radial profiles of the resonance frequency for different n and m values in dependence on q- and density profiles were calculated in cylindrical approximation. The coupling process between antenna current and shear Alfvèn wave resonance layers were studied with an appropriately modified 2-D ERATO ideal MHD stability code. In TCA global eigenmodes with $n/m > o$ were experimentally observed. Modes not present in cylindrical geometry, which were excited by the antennae structure via toroidal coupling, could also be observed and confirmed by the ERATO model calculations. These experimental findings and theoretical interpretation produced sufficient confidence in the theoretical models for predicting Alfvèn Wave Heating also for other tokamaks /16/.

The TCA group explored the possibility to use the ASDEX Upgrade ICRH antennae for plasma heating. The group concluded that low-n (4 and 8) Alfvèn Wave Heating would be an interesting alternative. The use of N = 4 and N = 8 antennae would allow mode control over the whole density range (10^{19} to $2 \cdot 10^{20}$ m^{-3}) at fixed frequency 4.47 MHz in the case where 8 toroidal antenna locations were available. If only 4 antennae are available, N = 1, 2, 4 would be optimal, even with asymmetric toroidal locations, and a lower frequency would be used. The ICRH antennae planned for ASDEX Upgrade could be used for AWH studies, also at high power, provided current capability of the transmission lines is increased.

The conclusion is that AWH in a later stage of the experiment is highly attractive. Therefore all measures shall be taken to prepare for some MW AWH power and to adjust antennae and feeds to the increased losses at this lower frequency as good as possible. A cooperative programme shall be discussed together with TCA Lausanne in time in order to prepare the physics preparation and the technical installation required.

1.5 The Discharge Programme of ASDEX Upgrade

Basic ASDEX Upgrade operation shall be in hydrogen. However the shielding house with 2 m thick concrete walls and 1.8 m thick concrete roof allows emission of 10^{19} neutrons/y or about 500 D-D discharge seconds per year at full SN plasma parameters. Since the main aim is stable SN divertor plasma operation and since limiter controlled circular and elongated plasmas are covered by many other tokamaks (TORE SUPRA, FTU, TFTR, JET) limiter bound plasmas in ASDEX Upgrade shall only be used for machine component and control system tests during the comissioning phase.

The experimental programme of ASDEX Upgrade can be devided into 3 phases:

1. ohmically heated plasmas
2. plasma heated by NI and ICRH up to 12 MW
3. additional use of LH and ECRH

1.5.1 Ohmic Heating Phase

Ohmically heated plasmas shall predominantly serve the following aims:

- to optimize breakdown and early plasma and current build-up;
- to learn how to produce SN and DN plasma configurations and to keep them during current ramp-up;
- to practice plasma position control and stabilization for SN and DN configurations;
- to practice density and current feedback control and density refuelling through plasma boundary and divertor;
- to investigate divertor operation in the recycling regime accessible by ohmic heating power:

The plasma temperature attainable ($Z_{eff} = 1$) for the SN reference plasma, $I_p = 1.6$ MA, is $\bar{T}_e \simeq \bar{T}_i \simeq 0.5$ keV at $\bar{n}_e \simeq 1.5 \cdot 10^{20}$ m^{-3}.

1.5.2 Additional Heating

The required heating power of 12 ÷ 15 MW in order to reach full plasma parameter performance has to be successively installed according to the overall time schedule and to the assembly of the machine.

6 MW heating power shall be provided in the middle of 1988. Four antenna arrays shall provide 6 MW. It is expected that the decision between the dipole or quadrupole antenna will have been taken by then, e.g. on the basis of the JET results. The pulse duration can be up to 10 seconds every 5 minutes limited by the power supply. This heating power of 6 MW is insufficient to exploit the plasma parameters as provided by the tokamak machine performance (Fig. 1). The parameters which can be reached are shown in Fig. 2 and 3 for 2 different modes of tokamak operation.

The heating pulse duration may start with short pulses in order to investigate the power and heat load distribution over the vacuum vessel structure in order to adjust it properly before damage occurs. The programme of this about one year period with 6 MW heating power shall encompass:

- optimization of the ICR coupling e.g. by variation of plasma to antenna distance;
- adjustment of secondary heat shield and protection structure; search for and examination of the H-mode confinement regime;
- study of the scrape-off layer and divertor plasma;
- study and optimization of the plasma position control and stabilization;
- supplement of diagnostics especially with regard to the analysis of plasma heating;
- investigation of long pulse heated (several seconds) discharges with feedback control of current, density and heating power (profile shaping?);

- search for methods to minimize energetic particles and fast CX neutrals in the plasma boundary;
- exploiting of ß-limits at reduced plasma, and machine parameters.

Additional 6 MW heating power shall be provided early in 1989. such that 12 MW heating power is available. This power consists of a neutral injection box equipped with four JET sources. This power should then allow to reach full plasma performance and cover the area of parameter space indicated in Fig. 1. This additional heating power can be effectively applied from the beginning because of the experience gained during stage I. However it shall start with short heating pulses in order to learn to control power and energy deposition on heat shield and target structure. Plasma parameter adjustment can help to reduce damage. Research of stage II with full heating power will then be devoted to the investigation and the optimization of open divertor operations:

- high density operation ($\bar{n}_e = 1.5 \cdot 10^{20}$ m^{-3}) with sufficient plasma heating $\frac{T_e + T_i}{2} = 2.2$ keV for producing a dense recycling zone in the divertor;
- study of particle and energy flux in scrape-off layer and divertor, comparison with theory;
- study of impurity flow and sources;
- study of the opacity of the plasma boundary, of CX neutrals leading to sputtering, evaluation of sputtering fluxes for reactor;
- optimization of plasma control at high $ß_p$;
- plasma control and stabilization of plasmas with increased elongation $1.6 \leq \kappa \leq 2$, $ß_t$-limits at high elongation;
- density control and refuelling of open divertor configurations;
- study of α-particle pumping and divertor pumping;
- feedback control of steady state SN divertor plasmas up to 5 seconds;
- optimization of plasma position and shape control and stabilization with the aim to minimize effort and to maximize reliability for future tokamaks.

1.5.3 Supplement of Additional Heating after 1989

1.5.3.1 LH Heating

3 MW power of LH waves at a frequency in the range $1.5 \leq f_{LH} \leq 3$ GHz shall be used for current drive. The programme shall serve two aims:

- current ramp up of 0.5 MA in 2.5 sec for stretching the OH flux by 1.8 Vs
- investigations of quasi steady tokamak operation with intermediate current drive for recharging the OH transformer.

1.5.3.2 ECR Heating

2 MW ECR power at a frequency in the interval $75 \leq f_{EC} \leq 85$ GHz ($2.7 \leq B_t \leq 2.85$ T). The aims are:

- investigation of plasma heating by the extraordinary fundamental wave, launched under oblique angle from the high field side using mirrors
- experiments utilizing EC power deposition profiles for profile shaping and transport studies.

1.5.3.3 Alfvèn Wave Heating

Up to 4 MW AWH power at 4.47 MHz can be launched through 8 ICRH antennas, if they can be designed to accomodate higher currents. Of interest are:

- investigation of mode structures and resonance layers
- investigation of heating, power deposition profile and impurities.

1.6 Time Schedule

The time schedule of installation of the different heating sources and the basic programme is shown by Fig. 8.

1.7 Cost Estimates for Additional Heating for ASDEX Upgrade

1.7.1 Neutral Injection System

The estimate is based on information by JET concerning the sources and power supplies. The cost for the other components are extrapolated from the ASDEX/WVII AS neutral injection systems.

	MDM
1 complete box	7.4
5 sources	4.3
power supplies and cooling	8.0
test stand	5.7
prototype source and development	1.0
control and data acquisition	2.0
	28.4

Fly wheel generator for the additional power required for NI (25 MVA, 120 MJ for 5 sec) (fraction of larger generator ordered) 5.0

1.7.2 ICRH System

The estimate is based on ASDEX component cost experience.

	MDM
HF generators (8 MW)	9.6
HF transmission lines, antenna, control	9.6
high voltage power supply	4.8
	24.0

Total investment costs for NI and ICRH 57.4 MDM

Acknowledgement

IPP Garching gratefully acknowledges the support and contributions by the Centre de Recherches en Physique des Plasmas, Association EURATOM Confédération Suisse, Ecole Polytechnique Fédérale de Lausanne/Switzerland and the Institut für Plasmaforschung, Universität Stuttgart, D-7000 Stuttgart, Germany.

References

/1/ O.Gruber, M.Kaufmann, W.Köppendörfer, K.Lackner, J.Neuhauser.
Journ. Nucl. Materials 121 (1984) 407 - 414.

/2/ ASDEX Upgrade Design Team and Tokamak Theory Group.
ASDEX Upgrade, Definition of a Tokamak Experiment with a Reactor Compatible Poloidal Divertor
IPP Garching Report IPP 1/197, March 1982.

/3/ Supplement to /2/
IPP Garching Report IPP 1/211, November 1982.

/4/ ASDEX Upgrade Project Team.
ASDEX Upgrade Project Proposal Phase II
IPP Garching Report IPP 1/217, Mai 1983.

/5/ IPP Garching Report IPP 1/197 (reference /2/) page 23, March 1982.

/6/ E.Speth, A.Staebler, O.Vollmer, and ASDEX Team.
To be published. Proc. 12th Europ. Conf. on Controlled Fusion and Plasma Physics, Budapest, September 1985.

/7/ O.Gruber, K.Lackner, G.Lister.
Computations on Neutral Beam Injection Heating, Ripple Recommendations and Varying Compression Ratio in ZEPHYR,
IPP Garching Report IPP 1/199.

/8/ D.Johnson et. al.
IAEA 9th Conf. Proceedings, Plasma Phys. and Contr. Nucl. Fusion Research, Baltimor 1982, Vol. 1, p.9.

/9/ R.B.White, L.Chen, R.Hay.
Proc. of the 4th Int. Symp. on Heating in Toroidal Plasmas, Vol. 1, p. 57, Rom, March 1984.

/10/ IPP Annual Report 1984.

/11/ M.Brambilla.
IPP Garching Report IPP 4/216, February 1984.

/12/ M.Söll, E.Springmann.
IPP Garching Report IPP 4/215, February 1984.

/13/ F.Leuterer et al.
Tenth Conf. Proceedings of Plasma Physics and Controlled Nucl. Fusion Research, IAEA, Vol. 1, p. 597, London, September 1984.

/14/ N.Fisch.
Princeton Plasma Physics Laboratory Report PPPL-2108 (1984).

/15/ K.Erckmann G.Hanzen, G.Müller, P.G.Schüller, K.Schwörer, M. Thumm, R.Wilhelm.
Proc. 4th Intern. Symp. on Heating in Toroidal Plasmas, Vol. II, p. 846, Rome, 1984.

/16/ A. de Chambrier et al.
10th Conf. Proceedings of Plasma Phys. and Controlled Nucl. Fusion Research IAEA, Vol. 1, p. 531, London, September 1984.

Figure Captions

Fig. 1: The attainable average plasma temperature of ASDEX Upgrade in SN operation in dependence on plasma density and heating power. The critical density links the plasma current and density.

Fig. 2: Average plasma temperature in dependence on density and heating power for reduced machine parameters I_p = 1.2 MA, B_t = 2 T ($q_c \simeq 2.3$).

Fig. 3: Average plasma temperature in dependence on density and heating power for the SN reference data: I_p = 1.6 MA, B_t = 2.7 T ($q_c \simeq 2.3$).

Fig. 4: ICRH frequency range and resonances for H, D, He_3, for typical ASDEX Upgrade toroidal field values.

Fig. 5: Horizontal cross-section of ASDEX Upgrade indicating neutral injection and ICRH access.

Fig. 6: Resonance frequencies and cutt offs for ordinary and extraordinary ECRH waves.

Fig. 7: The use of a mirror allows to launch the extraordinary fundamental EC wave from the high field side.

Fig. 8: Time schedule for installation and application of additional heating in ASDEX Upgrade.

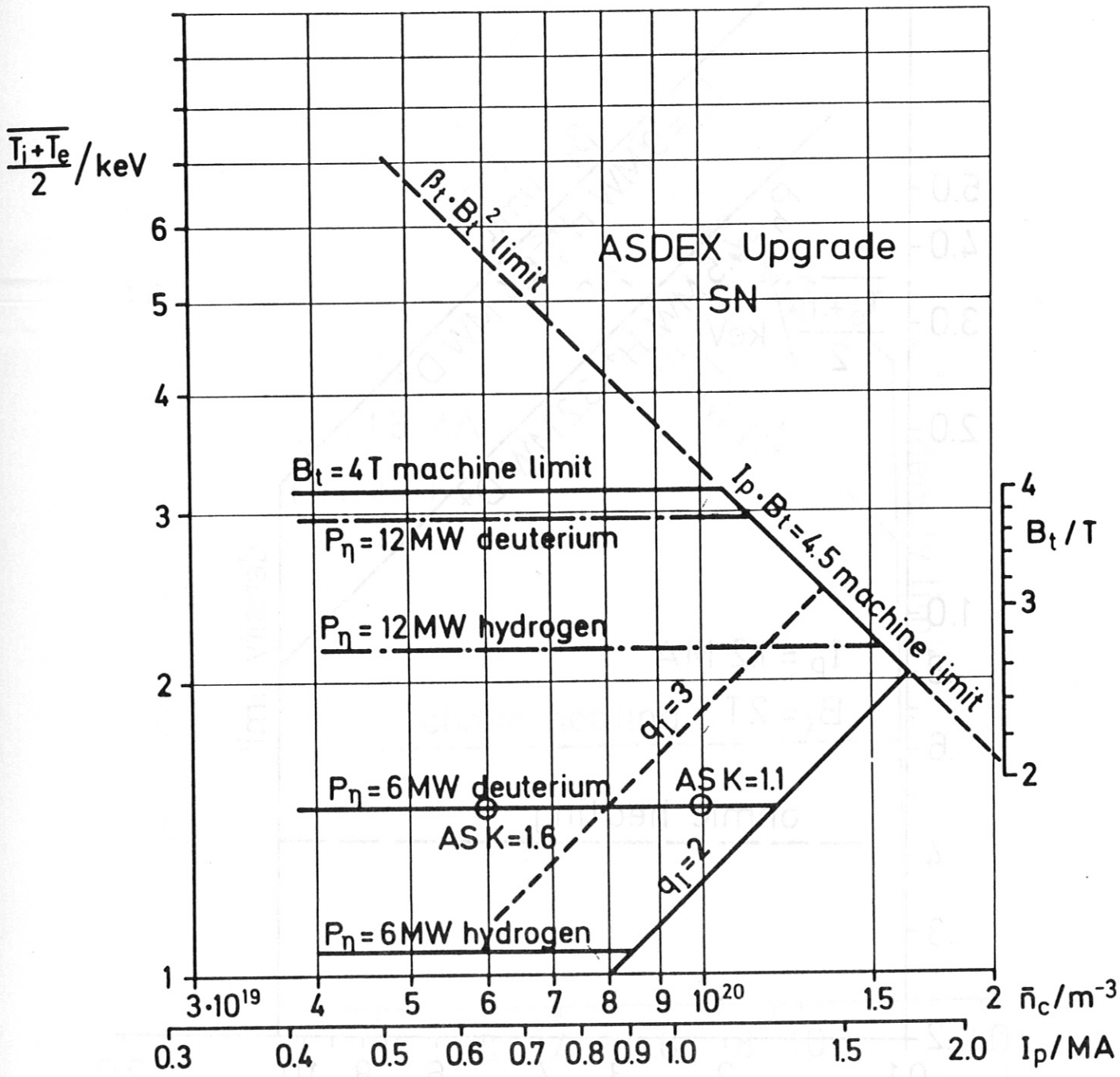
$\frac{\overline{T_i+T_e}}{2}$/keV
$\beta_t \cdot B_t^2$ limit
ASDEX Upgrade
SN
B_t = 4 T machine limit
$I_p \cdot B_t$ = 4.5 machine limit
P_η = 12 MW deuterium
P_η = 12 MW hydrogen
q_I = 3
P_η = 6 MW deuterium
AS K=1.1
AS K=1.6
q_I = 2
P_η = 6 MW hydrogen
B_t / T
$\bar{n}_c$/m^{-3}
I_p/MA

Fig. 1

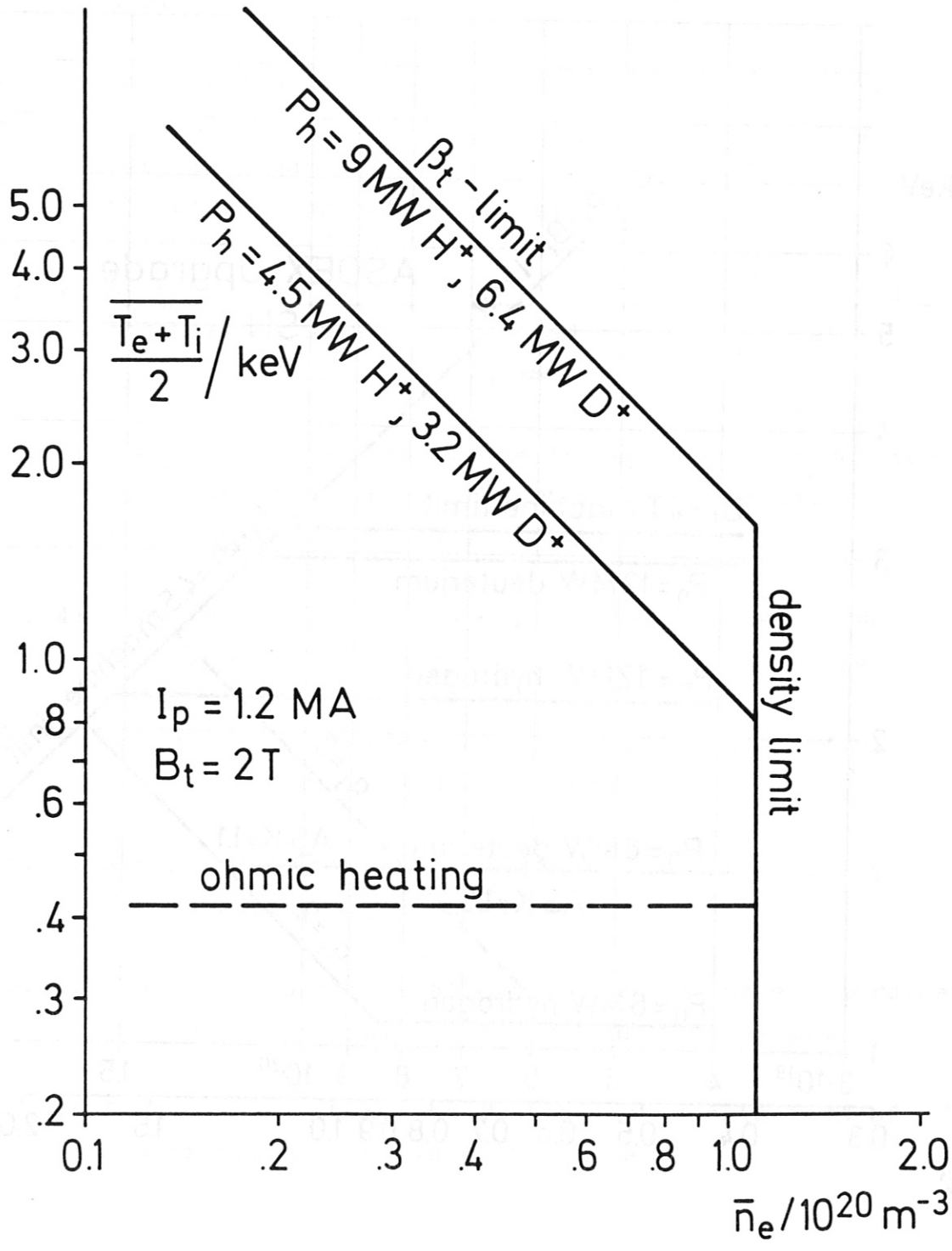
P_h = 9 MW H⁺, 6.4 MW D⁺
β_t - limit
P_h = 4.5 MW H⁺, 3.2 MW D⁺
density limit
$\frac{\overline{T_e + T_i}}{2}$ / keV
5.0
4.0
3.0
2.0
1.0
.8
.6
.4
.3
.2
I_p = 1.2 MA
B_t = 2 T
ohmic heating
0.1
.2
.3
.4
.6
.8
1.0
2.0
$\bar{n}_e / 10^{20}\ m^{-3}$

Fig. 2

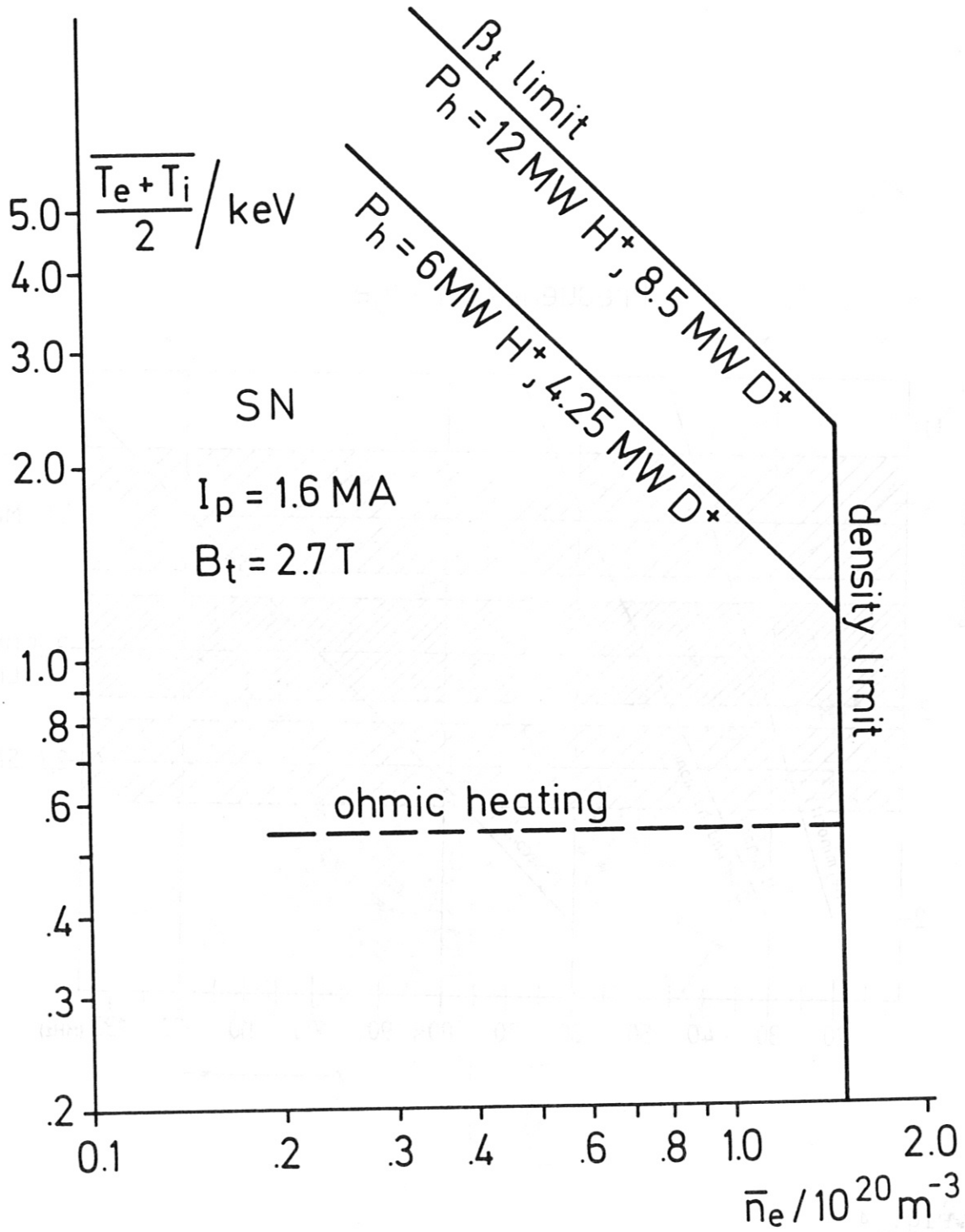
β_t limit
P_h = 12 MW H^+, 8.5 MW D^+
P_h = 6 MW H^+, 4.25 MW D^+
density limit
ohmic heating
$\frac{T_e + T_i}{2}$ / keV
5.0
4.0
3.0
2.0
1.0
.8
.6
.4
.3
.2
SN
I_p = 1.6 MA
B_t = 2.7 T
0.1
.2
.3
.4
.6
.8
1.0
2.0
$\bar{n}_e / 10^{20} m^{-3}$

Fig. 3

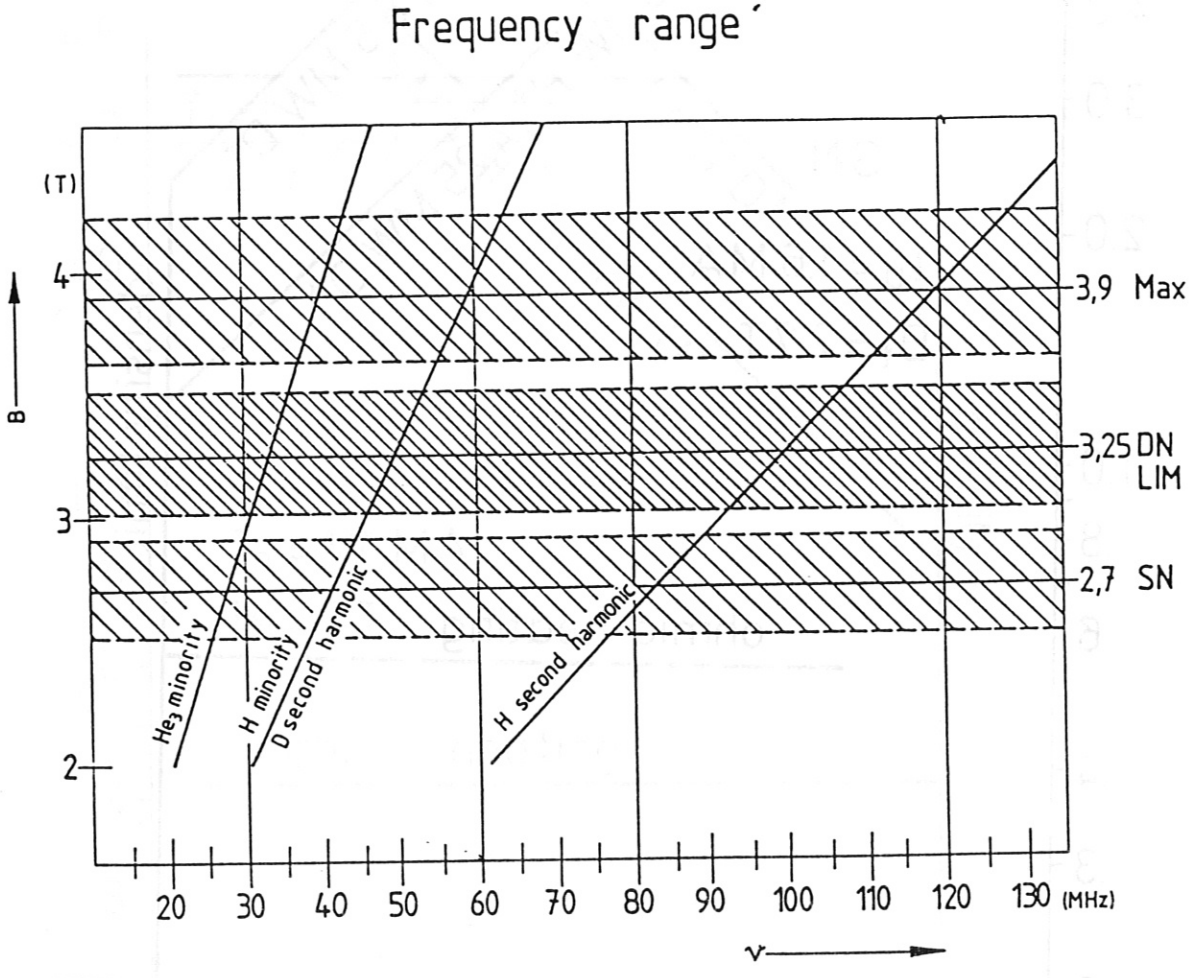
Frequency range
(T)
B
4
3
2
3,9 Max
3,25 DN LIM
2,7 SN
He3 minority
H minority
D second harmonic
H second harmonic
20
30
40
50
60
70
80
90
100
110
120
130
(MHz)
ν

Fig. 4

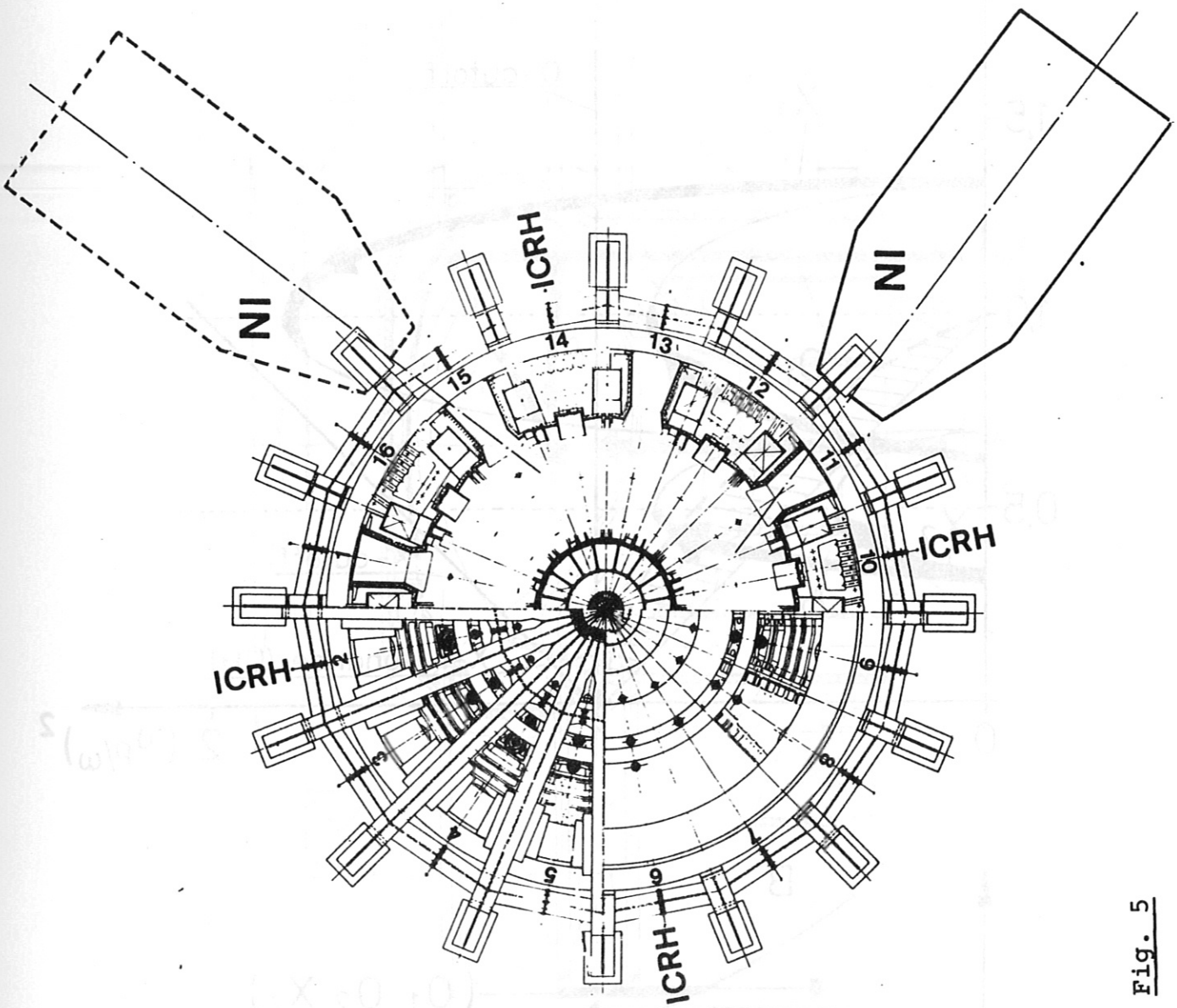

Fig. 5

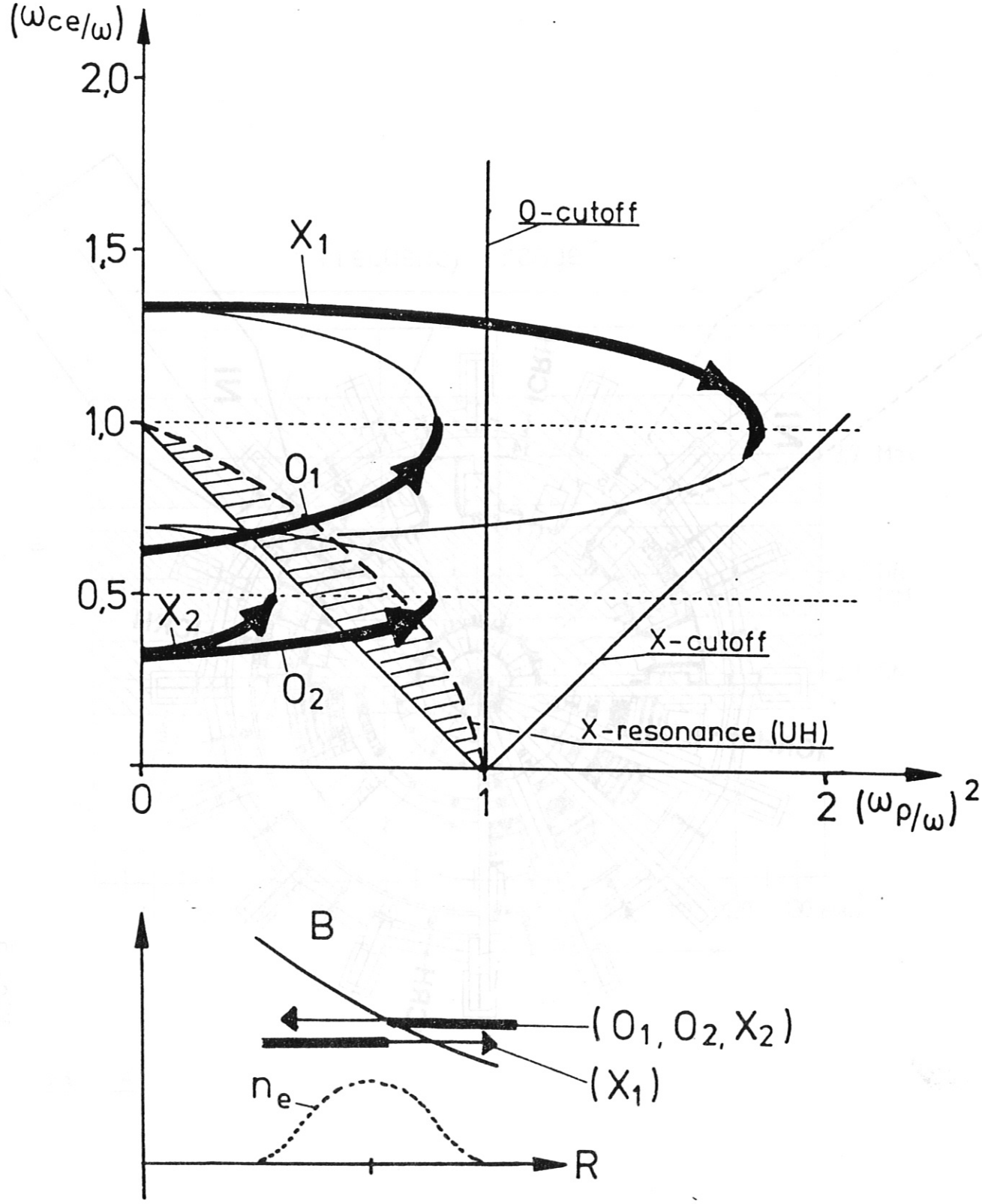
(ωce/ω)
2,0
1,5
1,0
0,5
0
1
2 (ωp/ω)²
X1
O1
X2
O2
O-cutoff
X-cutoff
X-resonance (UH)
B
(O1, O2, X2)
(X1)
ne
R

Fig. 6

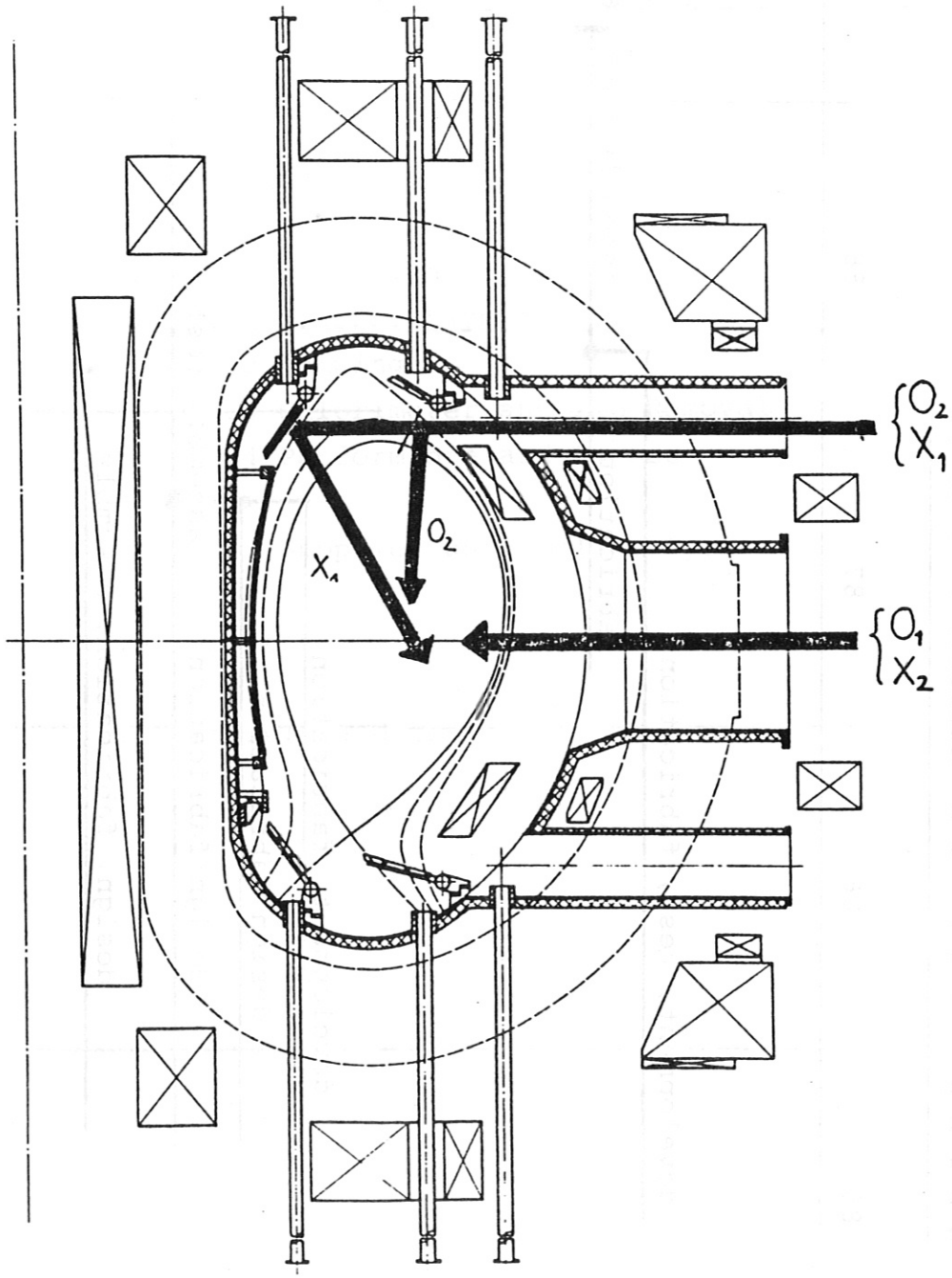

Fig. 7

A S D E X U P G R A D E Additional Heating

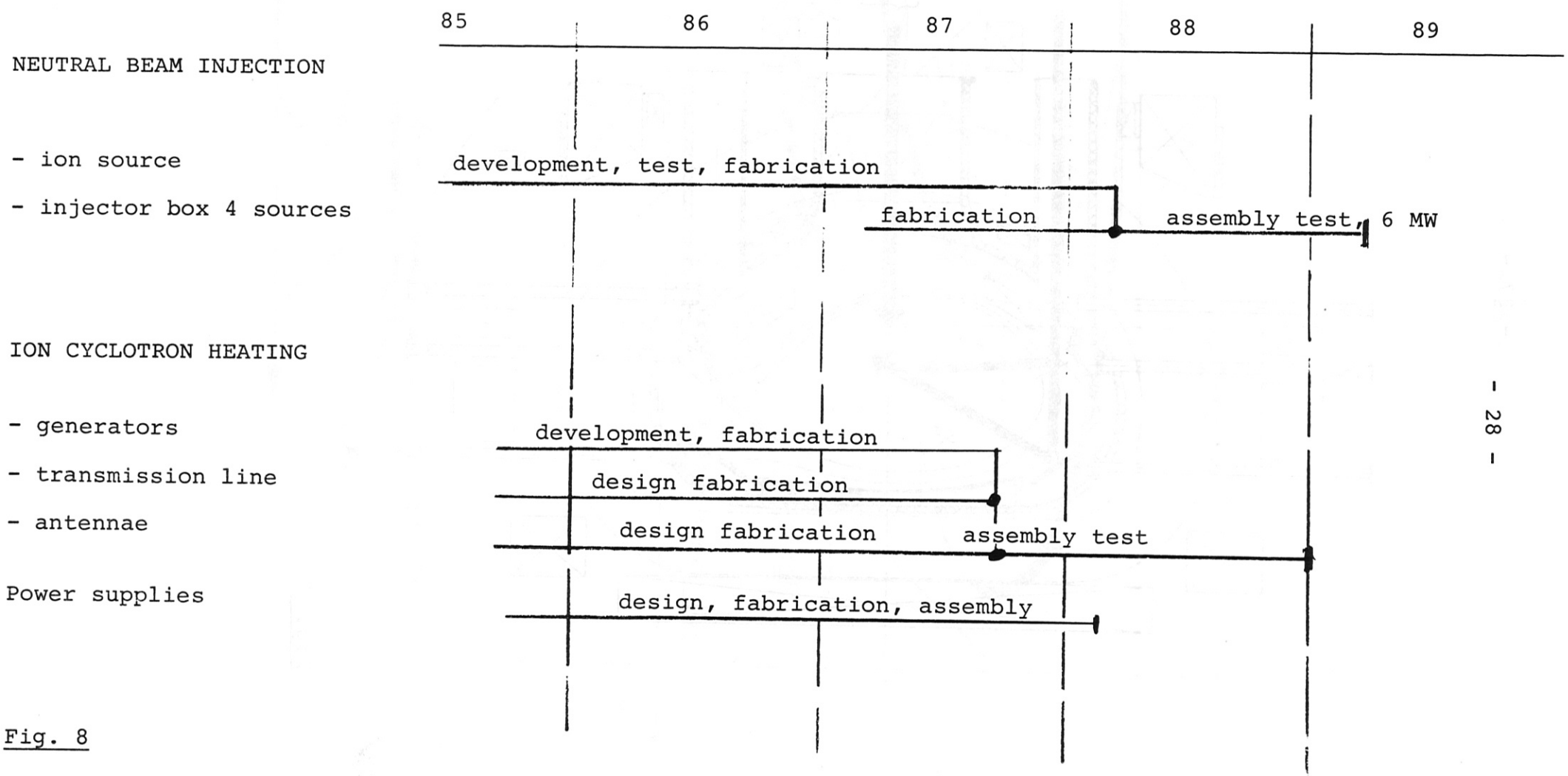

Fig. 8

2. Description of the Neutral Injection System

2.1 General Overview

2.2 Modified PINI

2.3 Beamline Design
- 2.3.1 General Layout
- 2.3.2 Pumping
- 2.3.3 Calorimeter and Ion Removal
- 2.3.4 Performance and Losses

2.4 Power Supplies and Cooling System

2.5 Teststand

2.6 Schedule and Cost

2.1 General Overview

As described under section 1.3 a total neutral power (integrated over all species) of 6 MW H° at an energy around 60 keV hydrogen is required. The space restrictions on ASDEX Upgrade call for a minimum number of injector boxes: at most two boxes, however preferably only a single box may be installed.

The proposed concept for the injector box is an upgraded ASDEX LPNI (longpulse neutral injection) box, equipped with four modified JET PINIS (60 kV, 80 A each). This concept has been chosen for a number of obvious reasons.

(i) The JET PINI is a well established and thoroughly tested piece of equipment; the required modifications require minor extrapolations and coincide with the plans of KFA Jülich for TEXTOR.

(ii) Only one box is required to provide the full power of 6 MW.

(iii) The beamline concept with four sources utilizing a four-quadrant flux-linking reflexion magnet is familiar from ASDEX LPNI and many of the design solutions can be transferred directly to ASDEX Upgrade injection.

For ASDEX Upgrade, deuterium operation is limited due to the neutron problem, and hence the standard scenario will be hydrogen injection. However, if the system is run in deuterium, the power supplies would allow 70 kV, 70 A for each source for unchanged extraction geometry, thereby yielding altogether 9 MW of neutral deuterium.

The choice of the beam energy has already been described in section 1.3; energies even below 60 keV would be acceptable from the penetration point of view. The choice of the injection angle of 25° w.r.t. perpendicular measured at R = 1.7 m (or 15° w.r.t. perpendicular at R = 2.84 m) represents a compromise between transmission losses through the given porthole geometry and losses due to ripple trapping.

In the following sections first the modified PINI and then the beamline design are described. Subsequently the power supplies and the cooling system are outlined and the test-stand will be discussed. Finally schedule and cost round off the technical description.

2.2 Modified PINI

In order to produce 1.5 MW of neutral hydrogen per source at 60 kV a drain current of around 80 A is required. The precise figure depends on the species distribution and on the overall beamline efficiency. In Fig. 1 the efficiency vs. extraction voltage is shown for three different species compositions. The underlying assumptions on the various power losses are discussed in section 2.3. For the case of 85 % H^+ an overall efficiency of 0.33 at 60 kV results in about 80 A of drain current, which fits very nicely with the capabilities of the H.V. power supplies (see Fig. 2). For details of the power supplies see section 2.4. The variation of the required current with extraction voltage as shown in Fig. 2 has been studied on purpose, because the beam energy of 60 keV derived from the penetration requirements is not a sharp limit and the precise figure should be determined by applying technical and other criteria (e.g. optimisation of the extraction parameters, efficient use of power supplies etc.). For example Fig. 2 shows, how much current would be required for 55 kV to produce a neutral power of 1.5 MW per source and how much current could be taken out of the power supply at 55 kV). Together with Fig. 3 this allows to evaluate the maximum neutral power per source compatible with the power supply characteristics (e.g. at 55 kV a current of 85 A could be drawn from the power supply and this would result in a neutral power of $\sim$ 1.75 MW per source).

The standard hydrogen version of the JET PINI is designed to produce 60 $\div$ 65 A at 80 kV, and utilises a four-electrode-extraction system. The extraction area is roughly a rectangle of 18 x 46 cm^2, and the current density in the 262 apertures is around 220 $\frac{mA}{cm^2}$. The single-beamlet $1/e$-divergence reaches values below 0.7°. The proton content is around 85 % if the bucket-

configuration SC15S3 is utilised as a plasma generator /1/.

In order to generate 80 A instead of 65 A either the current density must be increased or the net extraction area (or a combination of both). Both possibilities are related to the question of whether to apply a triode or a tetrode extraction system. Ion-optical experiments with a triode accelerating system at Fontenay-aux-Roses have shown that a divergence of $\leq 0.7°$ can also be achieved /2/. It is therefore proposed to apply the less complex three-electrode-system to ASDEX Upgrade injection.

The following details on the extraction system are to be understood as a first approximation to the problem. KFA Jülich is at present (April 1985) investigating a 55 kV, 80 A-version of the PINI. The ion optics will be computed both at Jülich and Fontenay-aux-Roses and the results will also be applicable to ASDEX Upgrade. For the time being a more direct approach is chosen: a scaling-down of the french results in /2/ to ASDEX Upgrade injection.

Taking $j = 120\ mA/cm^2$ at $U = 120$ kV as a perveance match for the optics shown in /2/, the metal-to-metal gap d has to be reduced to a value between 10 and 11 mm in order to achieve a current density of $220 \div 250\ mA/cm^2$ at 60 kV. Reducing the aperture diameter Ø from 10 mm Ø to 8 mm Ø (in order to keept the aspect ratio Ø/d < 1) and by scaling all other geometrical dimensions (except d) down to 8/10, yields the following two alternatives:

a) 626 holes over 180 x 468 mm^2
$j = 254\ \frac{mA}{cm^2}$

b) 740 holes over 204 x 490 mm^2
$j = 221\ \frac{mA}{cm^2}$

The latter alternative is feasible by transforming the PINI extraction system from a tetrode into a triode and making use of the space available due to the reduced number of grid holder boxes. The proposed ion optics is shown in Fig. 4. The resulting currents vs. voltage for the two alternatives and for different gap settings are shown in Figs. 5 and 6.

The final decision will depend on plasma source tests at elevated current densities (under investigation by Culham for KFA Jülich), the result of the ion optics optimisation mentioned above and general beamline design trade-off considerations.

If one runs the 60 kV, 80 A hydrogen PINI in deuterium without changing the gap under the constraint of constant drain power from the power supplies one derives 70 A at 70 kV of deuterium. Due to the higher neutralisation the neutral deuterium power per source is then 2.25 MW.

2.3 Beam Line Concept

2.3.1 General Layout

The overall views of the proposed beamline are shown in Fig. 7. The arrangement of four PINIS on a beamline is dictated by their outer diameter, by transmission considerations through the porthole/duct at the torus and by internal beamline constraints. In the case of ASDEX Upgrade the injection porthole is a conical rectangular duct, 800 mm high and 410 mm wide in its waist (see Fig. 8).

Transmission losses through this duct have been computed in order to assess the maximum allowable injection angle. In the horizontal direction the PINIS have been put as close together as possible (0.9 m) in order to maximise overall transmission. With a total length l_h of 6.5 m from the earth grid to the cross-over point in the duct center the beam axis form an angle of about $\pm$ 4° in the horizontal midplane w.r.t. the beamline

axis. Transmission losses of this arrangement as a whole vs. injection angle φ (angle of the beamline axis w.r.t. perpendicular, measured at R = 2.84 m) are shown in Fig. 9 for different $1/e$ -divergences. An injection angle of $\varphi = 15°$ has been chosen as the maximum permissible since above 15° transmission decreases rapidly. At 15° the losses are 1.5 % for 0.7° divergence and 4.5 % for 0.9° divergence.

In the vertical direction transmission is less critical and the PINIS can be located somewhat more apart (1.2 m) in order to ensure a beam path through the magnet at a reasonable distance above and below the midplane. The choice of cross-over point in the vertical direction is determined by the same motivation. Furthermore the beam should pass through the plasma not too far above and below the midplane for penetration reason. Therefore the distance l_v from the earth grid to the vertical cross-over can reasonably be chosen around 7 to 7.5 m. The corresponding angle between the beam axes and the beamline axis in the vertical direction is about $\pm$ 5°. Displacing the sources further apart vertically or chosing $l_v > 7.5$ m encounters transmission problems though the box exit, which is determined by a 800 mm ø valve and bellows. Due to mechanical constraints on the ASDEX Upgrade field coil structure a bigger valve/bellows is not possible.

The same constraint limits the choice of the focal length. Figure 10 shows the peak power density at the apex of the long pulse calorimeter vs. focal length (vertical and horizontal focal length have been assumed identical). Clearly a focal length of e.g. 8.5 m reduces the power density by about a factor two compared to 6 m focal length. However above f = 7 m transmission losses through the box exit start to increase and a reasonable compromise may therefore be around f = 8.5 m (see Fig. 11).

2.3.2 Pumping

The main gas load in the ASDEX Upgrade injection system, as in many others, stems from the neutraliser. The thermalised ions on

the ion dump typically represent only 20 % of the total gas load.

In order to achieve 90 % F_0^{∞} for 60 kV hydrogen a neutralisation target of about $9 \times 10^{15} \frac{\text{molecules } H_2}{\text{cm}^2}$ or 0.22 Torr cm are required. Depending on the precise shape and the length of the neutraliser this requires a gas flow which varies considerably. Choosing a length of 2 m and assuming molecular flow conditions /3/ one derives a gas flow between 11 Tl/sec and 17 Tl/sec for an average cross-section of 18 x 43 cm² (tapered) and 20 x 50 cm² (straight) respectively. For the three-electrode-systems of standard dimensions a gas flow of 20 Tl/sec D_2 generates a source pressure of 10 m Torr D_2 /4/; hence it may be viable to get away without additional gas into the neutraliser.

The ions represent a gas load of typically 4 Tl/sec per ion dump. As a working figure for the pumping requirements we assume a gas load of 25 Tl/sec per beam or a total gas flow of 100 Tl/sec for the whole box.

The proposed pumping system utilises Ti-getter of the type recently developed at Fontenay-aux-Roses /5/. These evaporators combine the advantages of compact structure (35 cm ⌀, 4 m high), simple manufacture and the capability of being regenerated by baking at 300° C. Each pump has a pumping speed of around 350 000 l/sec for H_2. In the beamline concept of Fig. 7 at least eight pumps can be installed to yield a total pumping speed of $2.8 \cdot 10^6$ l/sec, 50 % in the first pumping chamber (PR I), 50 % in the second one (PR II).

The conductance from the neutraliser exit (distance to magnet 0.6 m) into PR I is about twice the conductance through the magnet (length 0.8 m, gap width 0.25 m) and hence the gas flow of 100 Tl/sec will be subdivided in the ratio 2 : 1. The corresponding pressures are then around $6 \cdot 10^{-5}$ Torr and $3 \cdot 10^{-5}$ Torr in PR I and PR II respectively, taking into account some conductance limitations.

If we assume PR I to be magnetically shielded, the total reionisation target from the magnet entrance to the duct is about $4.8 \cdot 10^{14} \frac{\text{molecules } H_2}{cm^2}$. The reionisation losses are then distributed as follows:

magnet	1.9 %
drift space	2.5 %
torus valve/bellows	1.0 %
duct	1.6 %

These figures are valid for 60 kV hydrogen. The conditions for 70 kV deuterium will not be very much different, since on the one hand the required neutralisation target will be thinner, the conductance of the neutraliser will be smaller, and the unneutralised ion current will be smaller, all three resulting in a reduced gas flow. On the other hand the pumping speed will be smaller, the reionisation cross section will be higher and the neutral power will be higher.

2.3.3 Calorimeter and Ion Removal

The long pulse calorimeter shall be suitable to stand the full neutral power for full pulse length, i.e. 2.25 MW (deuterium case) per beam for 10 sec. At the position of the calorimeter the four beams are still sperated from each other. Each beam will be stopped by its own V-shaped calorimeter, formed by an arrangement of eight water-cooled panels (two by two on either side, see Fig. 7). The panels are about 20 x 20 cm^2 and identical to the ones developped for ASDEX and WVIIAS LPNI, except for a somewhat different power density profile.

The peak power density at the apex will be about 7 kW/cm^2 perpendicular to the beam axis for a focal length of 8.5 m (see Fig. 10). For an angle of inclination of 15° and 30° for the inner and outer panels respectively and a nominal peak power density of 2.75 kW/cm^2 perpendicular to the panel surface there will be a factor of 1.6 safely margin for the power density (i.e. 11 KW/cm^2 perpendicular to the beam could still be tolerated,

should there be a focal length problem). In addition there is another safety factor of 1.6 for the panels, since the burnout limit is > 4.5 kW/cm², as demonstrated for ASDEX LPNI /6/.

The average power per panel will be below 300 kW, the average power density below 1 kW/cm². The whole calorimeter assembly will consist of four V's, mounted together on a common structure, the overall design very similar to ASDEX and WVIIAS LPNI. The whole assembly will be about 1 m high and 0.8 m wide and can be moved up and down inside the box.

The maximum total ion power that has to be removed per beam occurs for 60 kV hydrogen operation and will be less than 2.3 MW. The maximum ion power at full energy will prevail for the highest proton content that may be present. For safety reasons 95 % H^+ have been assumed. Similar safety considerations for the half and one third energies, in case there should be a species problem, lead to the following individual ion powers, not occuring simultaneously but each of those being a worst case.

E_o (60 keV)	2.2 MW	(95 % H^+)
$E_o/2$ (30 keV)	0.5 MW	(30 % H_2^+)
$E_o/3$ (20 keV)	0.1 MW	(10 % H_3^+)

For the ion removal a 180° reflection magnet with four quadrants has been chosen. The reasons lie in the existing experience at IPP both which the computations and the experimental tests of the magnet performance, and its advantages for the overall beamline design compared to a transmission magnet (more space for calorimeter and for the pumping in PR II, gas load from the ion dumps occuring in PR I). Its possible adverse effect like space charge forces due to the high local ion density at the cross-over point will show up experimentally in the ASDEX and WVIIAS LPNI programme and can be taken into account. The 3D-iron code "PROFI" /7/, which has been used to design the reflection magnet for ASDEX and WVIIAS LPNI is still available at IPP and will be used in the same way in

order to compute the field distribution of the magnet itself and the magnetic shielding of the sources, the neutraliser and PR I (vertical stray field $\lesssim$ 150 G , 350 G , 500 G respectively). Together with a whole package of additional routines already available /8/ ion trajectories and power densities on the pole faces and the ion dump can be worked out. The preliminary design proposed at present foresees an overall length of 0.8 m and a gap width of about 0.25 m. The pole faces should be inclined by $\pm$ 4 in the horizontal plan following more tightly the beam contours in order to reduce the conductance through the magnet. Each quadrant will be about 1.8 m high allowing a radius of curvature of 0.50 m for the 60 keV H^+ ions ($B_o \simeq 0.07$ T).

Since the total ion power for the worst case is equal to the neutral power on the calorimeter for the "worst" case, the overall ion dump design will be similar to the calorimeter design. There will be four individual V-shaped dumps, located as shown in Fig. 7, each made up of eight actively cooled panels like the calorimeters, but completed by large-area inertial parts to cope with the ion power at half and one third energy. The exact dimensions, i.e. the location and orientation of the dump and the inclination of the panel will be subject to the detailed design mentioned above.

2.3.4 Performance and Losses

The loss processes that occur inside the neutral injector are usually divided into four groups: losses in the source and accelerator, transmission losses on all defining apertures like neutralisers,scrapers etc.; neutralisation losses due to non-equilibrium and finally reionisation losses.

For the first type conventional figures are 2 % of the drain power on the grids and 4 % BSE under standard operating conditions /9,2/.

The second type losses are difficult to compute and the figures evaluated under section 2.1, amounting to a few percent only, are by no means adequate since the non-Gaussian part of the beam is neglected. Experience /9,2/ shows that 85 ÷ 90 % of the drain power can be transmitted onto a calorimeter representing the acceptance of the torus porthole. For safety here it is assumed that 85 % of the extracted power (not the drain power) is transmitted.

The third type of losses is caused by the insufficient thickness of the neutraliser target. In section 2.3.2 the neutraliser target was chosen such that 90 % of F_o^∞ for the full energy would be achieved. Finally in section 2.3.2 the reionisation losses have been evaluated as 7 % of the neutral power. The total neutral power transmitted to the torus for 60 kV hydrogen and a species distribution of 85 : 10 : 5 is there (per source):

$$\left.\begin{aligned} P_{E_o} &= 0.76 \\ P_{E_o/2} &= 0.15 \\ P_{E_o/3} &= 0.09 \end{aligned}\right\} \quad \text{x 1.61 MW}$$

For 70 kV deuterium and the same species distribution, assuming that everything else except F_o^∞ will be the same one obtains:

$$\left.\begin{aligned} P_{E_o} &= 0.80 \\ P_{E_o/2} &= 0.13 \\ P_{E_o/3} &= 0.07 \end{aligned}\right\} \quad \text{x 2.26 MW}$$

The three difference curves in Fig. 1 have been obtained using the above mentioned parameters. However in evaluating the energy dependence only the variation of F_o^∞ is taken into account.

2.4 Power Supplies and Cooling System

The power supplies required for the bucket source will be largely identical to the JET power supplies except for a possibly higher arc current should this turn out to be necessary because of the higher current density. The same applies to the decel power supplies, a gradient-grid network will not be needed for the triode system.

The H.V. power supply, that was installed for the ASDEX and WVIIA plasma heating systems, will also be used for ASDEX Upgrade neutral injection. As can be seen from Fig. 2, four modules of 35 kV, 40 A each, will be grouped together in order to produce the required 80 A at 60 kV (on the source). The characteristics plotted in Fig. 2 show that higher currents can be taken out at lower voltage if the total power is constant. (Note: these are voltage regulated power supplies.) The second curve (labelled "No. of HV-modules = 3") e.g. shows that 60 kV, 60 A can be supplied by a group of three modules only. (Note that the voltage U_x in Figs. 1,2,3,5 and 6 is the extraction voltage on the ion source; the corresponding power supplies output is assumed to be 10 kV higher.)

The grouping together of four modules is not yet possible at present and requires some modifications of the control circuits. Also the capability of currents > 50 A per module is strictly valid only for the modules No. 9 ÷ 16. Whether the old modules (No. 1 ÷ 8) could be modified to yield the same characteristics is being investigated at present. The HV modulators will be identical to the ones used in the ASDEX LPNI system except for some upgrading in the grid driver circuits.

The remaining power supplies for the titanium evaporators and the magnets are current-regulated power supplies of standard industrial specifications.

The cooling systems will have to provide high pressure (25 bar) demineralised cooling water for the grids and the panels. A

total flow of around 350 m^3/h will be required. This will be provided by the general cooling system of ASDEX Upgrade, such that only the secondary circuit with the high speed pump need to be installed specifically for neutral injection. The primary circuit, the heat exchanger, the reservoirs etc. will be a common system for all users on ASDEX Upgrade.

2.5 Teststand

The present teststand will have to be replaced by a bigger facility capable of coping with the bigger dimensions, higher power levels, increased gas flows etc. It will consist of a new vacuum tank representing basically one quarter of the actual beamline, except for the calorimeter which will stand both ion and neutral power. It will be equipped with half a magnet, an ion dump and titanium pumps either of the Fontenay-aux-Roses-type (possibly at reduced length) or of the rectangular planar type as used in ASDEX and WVIIAS LPNI. The cooling systems installed on the present teststand (2 x 40 m^3/h, 30 bar and 15 m^3/h, 15 bar) will be sufficient for cooling enough panels and the grids respectively.

The data acquisition and computer system can also be maintained, possibly extended to some degree. The H.V. regulator and the H.V. power supplies will be maintained. For the latter a group of four modules will be required out of the sixteen foreseen for ASDEX Upgrade. This is nevertheless possible by switching power supplies in between shots from the experiments to the teststand and back, a feature which is already available and being used at present. The remaining power supplies and all the control circuit will have to be rebuilt.

2.6 Schedule and Cost

The critical path for the project will be the computations, design, fabrication, assembly and testing of the new beamline. Due to the present engagement of all the experienced staff in ASDEX and WVIIAS LPNI (as well as JET) it is hard to see how the

design could be terminated before early 1987. Allowing about 20 months for fabrication and assembly and another 5 ÷ 6 months for installation on ASDEX Upgrade and commissioning, experiments not could start before early 1989. The power supplies, cooling, control and computer systems,if ordered towards the end of 1986, will all easily be procured and commissioned by end of 1988.

Also the PINIS need to be ordered by the end of 1986, in order to arrive in time to be conditioned on the teststand beginning 1988.

The design of the teststand has to commence rather soon. Since it does not require too much physics design, it can be soon taken over by the engineers, which are not so much of a bottle-neck at present.

The manpower enganged in ASDEX Upgrade will increase steadily, as the work for LPNI ASDEX and WVIIAS is approaching completion. When both LPNI experiments have reached the operation phase, there will be nine professionals (six man years per year) and eight technicians available for ASDEX Upgrade injection.

Of course the progress with the ASDEX and WVIIAS-programmes will determine the transfer of staff to ASDEX Upgrade programme, and the schedule for ASDEX Upgrade mentioned above can only be met if no major hold-ups occur along the former programme.

The cost estimate is based on information by JET concerning the sources and power supplies. The cost for the other comonents are extrapolated from the ASDEX/WVIIAS LPNI systems experience.

Cost Estimate [MDM]

1 complete injector box		7.4
box, stand and shields	1.7	
vacuum equipment	2.0	
internal structures (magnet, calor., dumps etc.)	2.2	
design, assembly and miscell.	1.5	
5 PINIS		4.3
5 PINI-structures	1.6	
5 sets of grids	1.3	
5 plasma generators	1.4	
Power supplies and cooling		8.0
HV-power supplies(modifications, regulators, snubbers etc.)	2.2	
plasma source supplies	4.8	
cooling system	1.0	
Control and data acquisition		2.0
Teststand		5.7
mechanical equipment (box, calor., pumps etc.)	2.8	
power supplies	1.2	
control, diagnostics, etc.	0.7	
install. and miscell.	1.0	
Prototype source and development		1.0
prototype PINI	0.8	
development work	0.2	

Σ = 28.4

References

/1/ T.S.Green, Proc. 13th SOFT, Varese, 1984, p. 693.

/2/ M.Fumelli, ibid, p. 617 and JIDT 4/82-4.

/3/ M.Wutz, Theorie und Praxis der Vakuumtechnik, Vieweg & Sohn, Braunschweig, 1965.

/4/ Fontenay-aux-Roses, JDC-progress report, March 1985.

/5/ Z.Sledziewski, Proc. 13th SOFT, Varese, 1984, p. 343.

/6/ J.H.Feist et al., Jahrestagung der Kerntechnischen Gesellschaft, München, Mai 1985.

/7/ Rented from T.U. Darmstadt.

/8/ P.J.Schneider et al., Proc. 10th Symp. Fus. Eng., Philadelphia, 1983, p. 530.

/9/ PINI-A Data Base, Culham Laboratory, 1983.

Figure Captions

Fig. 1: Computed overall efficiency defined as $P_N/I \cdot U_x$ vs. extraction voltage U_x for different species distributions; P_N = transmitted neutral power, I = drain current; the only energy dependence taken into account is that of the neutralisation fraction.

Fig. 2: Required drain current I_x for a neutral power of 1.5 MW vs. extraction voltage U_x for three different species distributions (labelled "$H^+ : H_2^+ : H_3^+$ = 85 : 10 : 5/70 : 20 : 10/55 : 35 : 10") and maximum possible drain current from the power supply vs. extraction voltage for different numbers of modules grouped together (labelled "number of HV-modules = 3/4"); note that U_x is the extraction voltage on the source, the p.s output is assumed to be 10 kV higher.

Fig. 3: Maximum possible neutral power per source compatible with the power supply vs. extraction voltage for different numbers of modules grouped together; the underlying efficiency is taken from Fig. 1 for $H^+ : H_2^+ : H_3^+$ = 85 : 10 : 5.

Fig. 4: Proposed triode acceleration system as scaled from /2/.

Fig. 5: Perveance-matched ion current for a standard size PINI extraction area (180 x 468 mm²) vs. extraction voltage for different interelectrode spacings d and HV-power supply characteristics as in Fig. 2.

Fig. 6: As in Fig. 5 but for an enlarged PINI extraction area (204 x 490 mm²).

Fig. 7: ASDEX Upgrade beamline concept.

Fig. 8: ASDEX Upgrade torus porthole and interface to injector box.

Fig. 9: Transmission through the porthole vs. injector angle φ for different beamlet $1/e$-divergences; f_v = vertical focal length; f_h = horizontal focal length; ℓ_v, ℓ_h = distance from earth grid to cross-over-point of different beams in the vertical and horizontal planes respectively; R = 0: torus center; B/L = beamline; U = 0: cross-over of beam-line-axis with porthole-axis (R = 2.84 m).

Fig. 10: Peak power density at the apex of the calorimeter vs. focal length for different beamlet $1/e$-divergences.

Fig. 11: Transmission through box exit (ϕ = 800 mm) vs. focal length for different beamlet $1/e$-divergences.

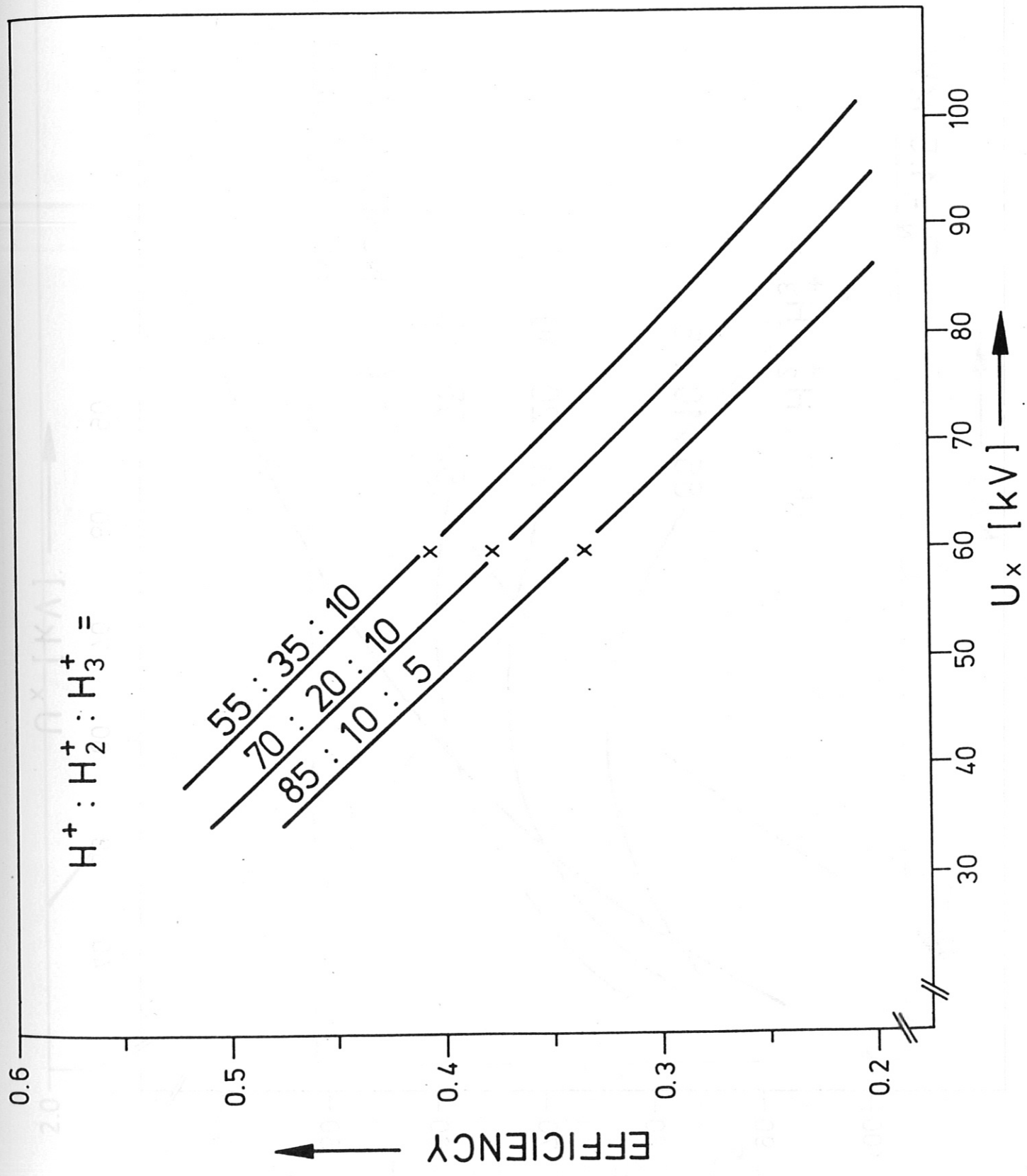
EFFICIENCY
0.6
0.5
0.4
0.3
0.2
30
40
50
60
70
80
90
100
U_x [kV]
$H^+ : H_2^+ : H_3^+$ =
55 : 35 : 10
70 : 20 : 10
85 : 10 : 5

Fig. 1

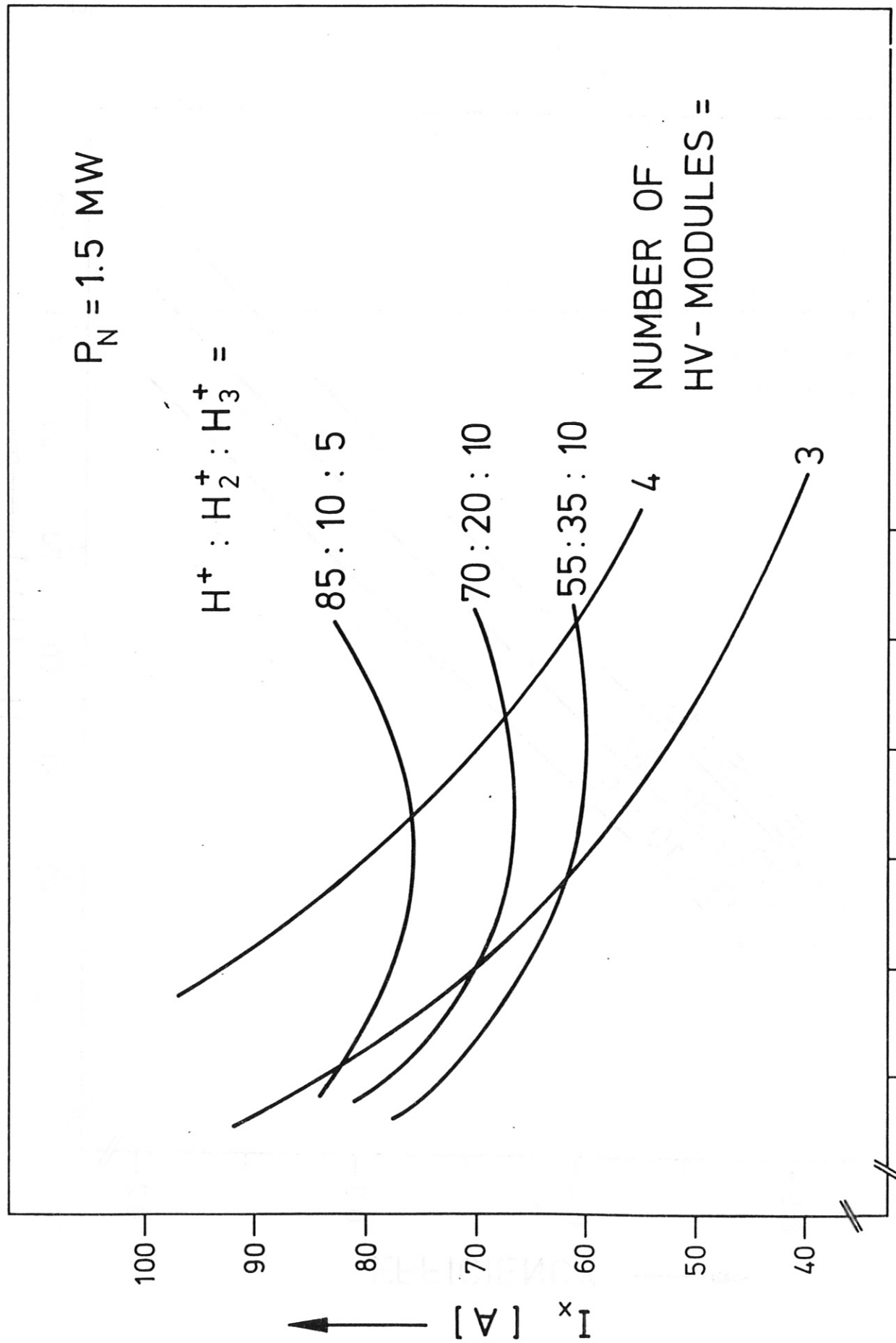
$P_N = 1.5$ MW
$H^+ : H_2^+ : H_3^+ =$
85 : 10 : 5
70 : 20 : 10
55 : 35 : 10
NUMBER OF HV-MODULES =
4
3
I_x [A]
100
90
80
70
60
50
40
40
50
60
70
80
90
U_x [kV]

Fig. 2

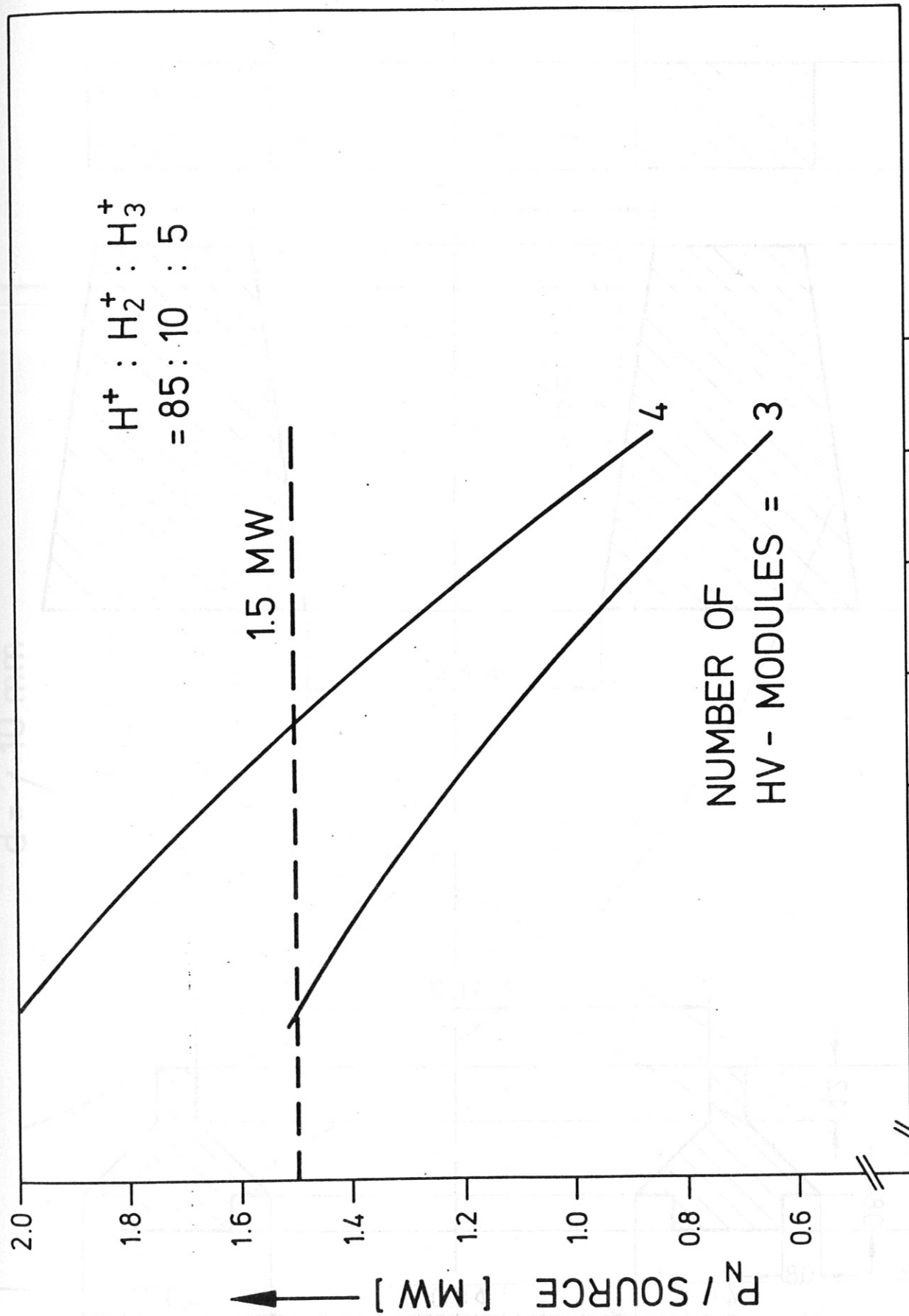
$H^+ : H_2^+ : H_3^+$
= 85 : 10 : 5
1.5 MW
4
3
NUMBER OF
HV - MODULES =
P_N / SOURCE [MW]
U_x [kV]
2.0
1.8
1.6
1.4
1.2
1.0
0.8
0.6
40
50
60
70
80
90
100

Fig. 3

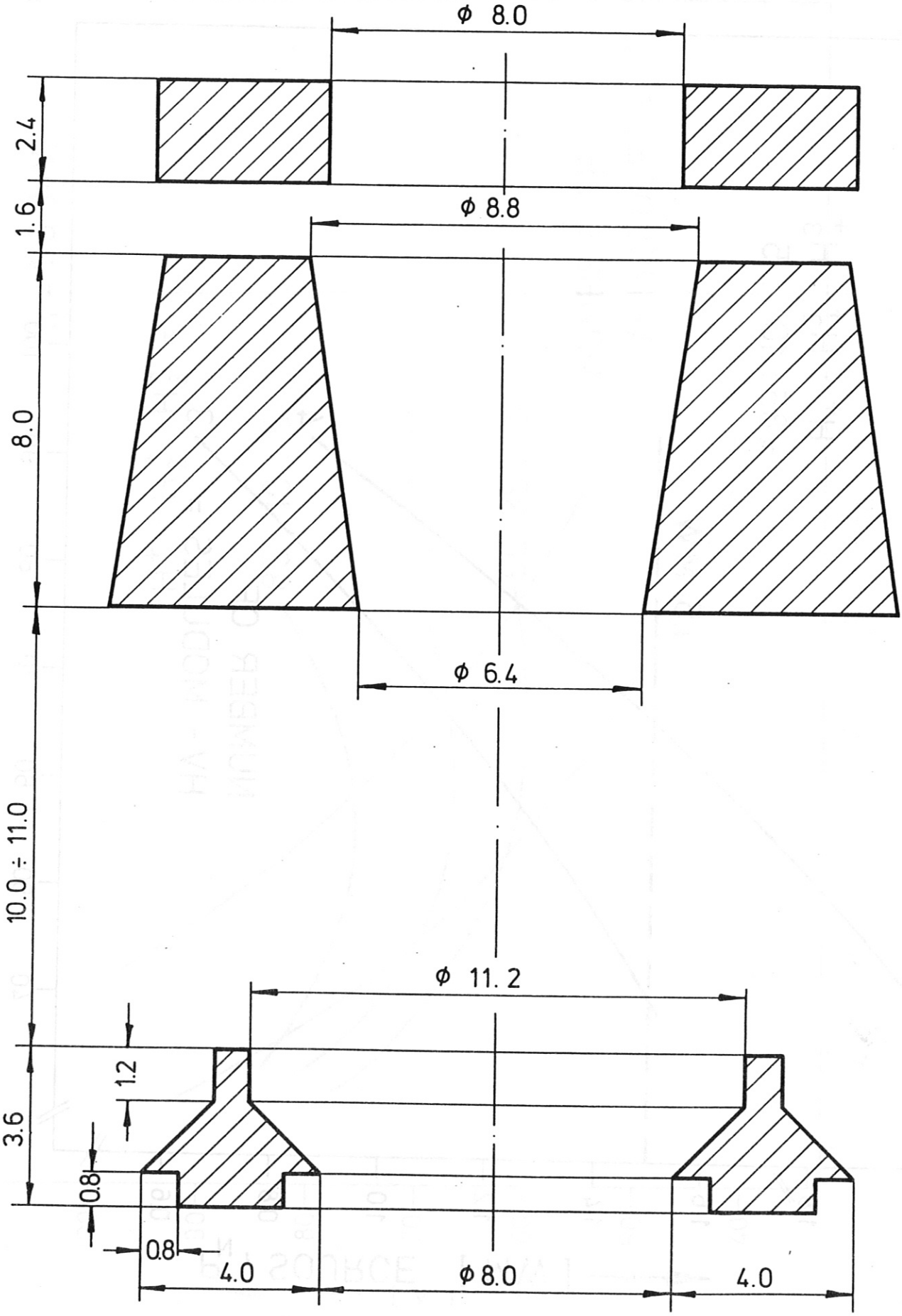

Fig. 4

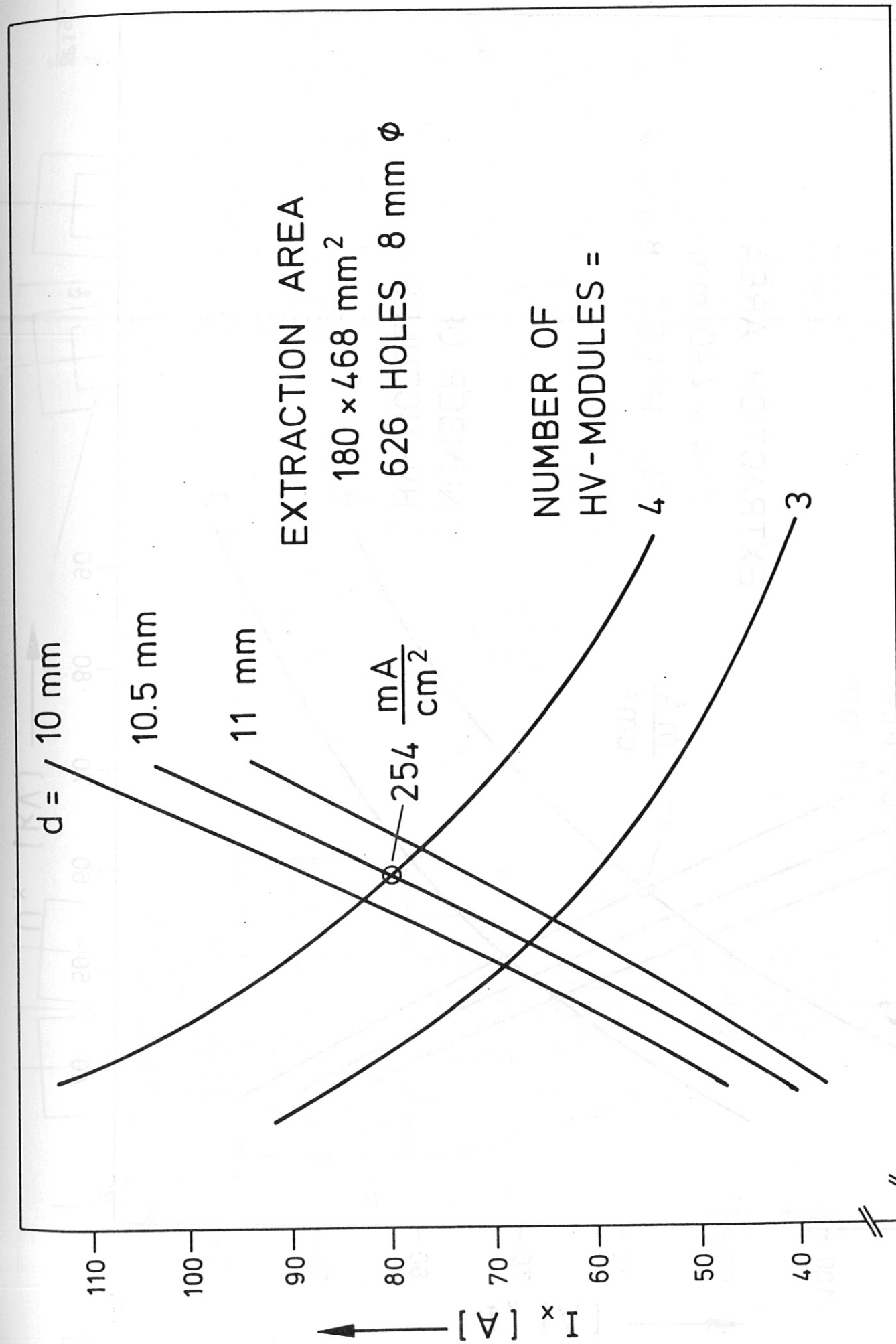
d = 10 mm
10.5 mm
11 mm
254 mA/cm²
EXTRACTION AREA
180 × 468 mm²
626 HOLES 8 mm Φ
NUMBER OF
HV-MODULES =
4
3
110
100
90
80
70
60
50
40
I x [A]
40
50
60
70
80
90
Ux [kV]

Fig. 5

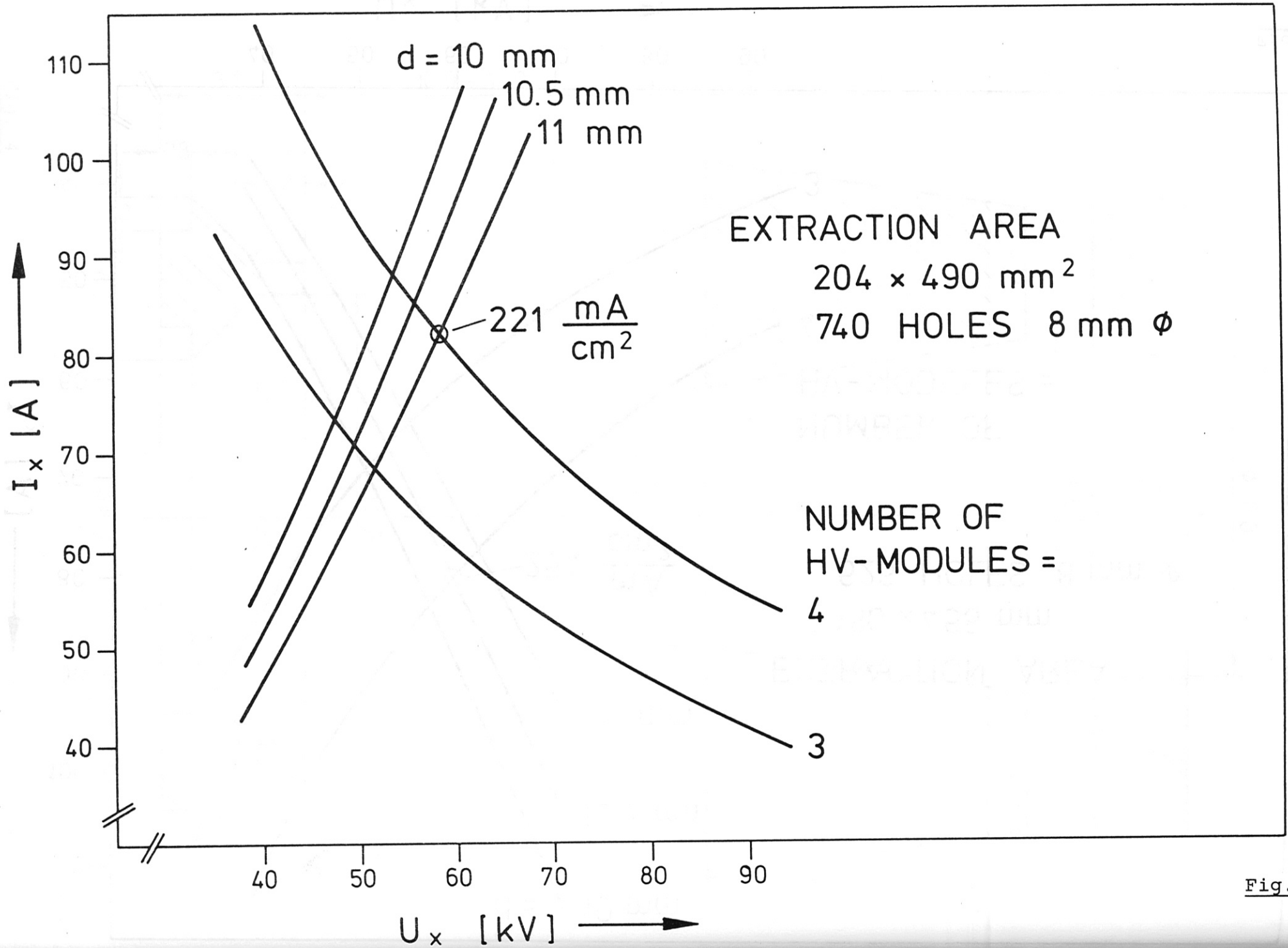
d = 10 mm
10.5 mm
11 mm
221 mA/cm²
EXTRACTION AREA
204 × 490 mm²
740 HOLES 8 mm Φ
NUMBER OF
HV-MODULES =
4
3
110
100
90
80
70
60
50
40
40
50
60
70
80
90
Ix [A]
Ux [kV]

Fig. 6

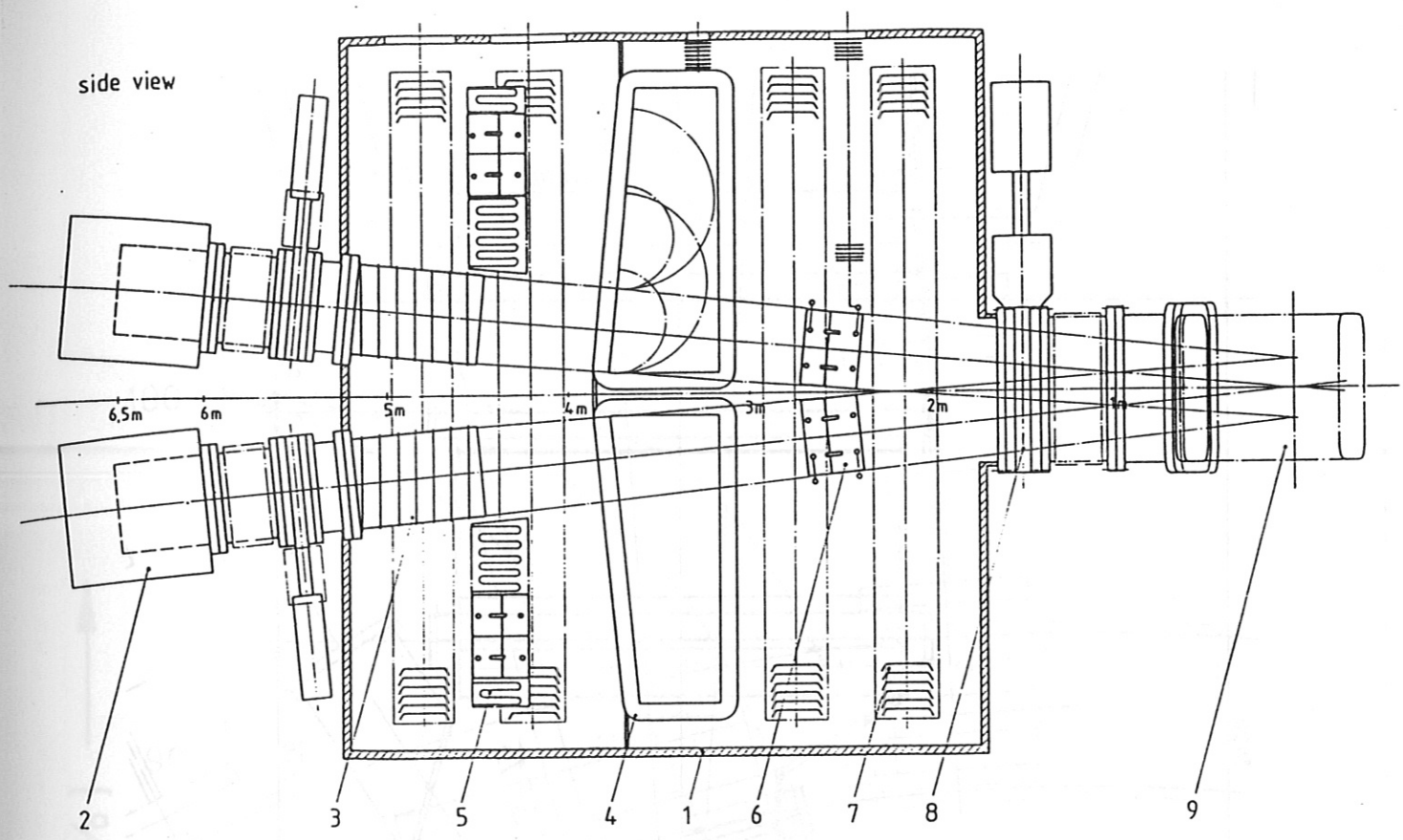

1 Vacuum box
2 PINI
3 Neutralizer
4 Reflexion magnet
5 Ion dump
6 Calorimeter
7 Titanium pump
8 Torus valve
9 Torus porthole
10 PR I
11 PR II

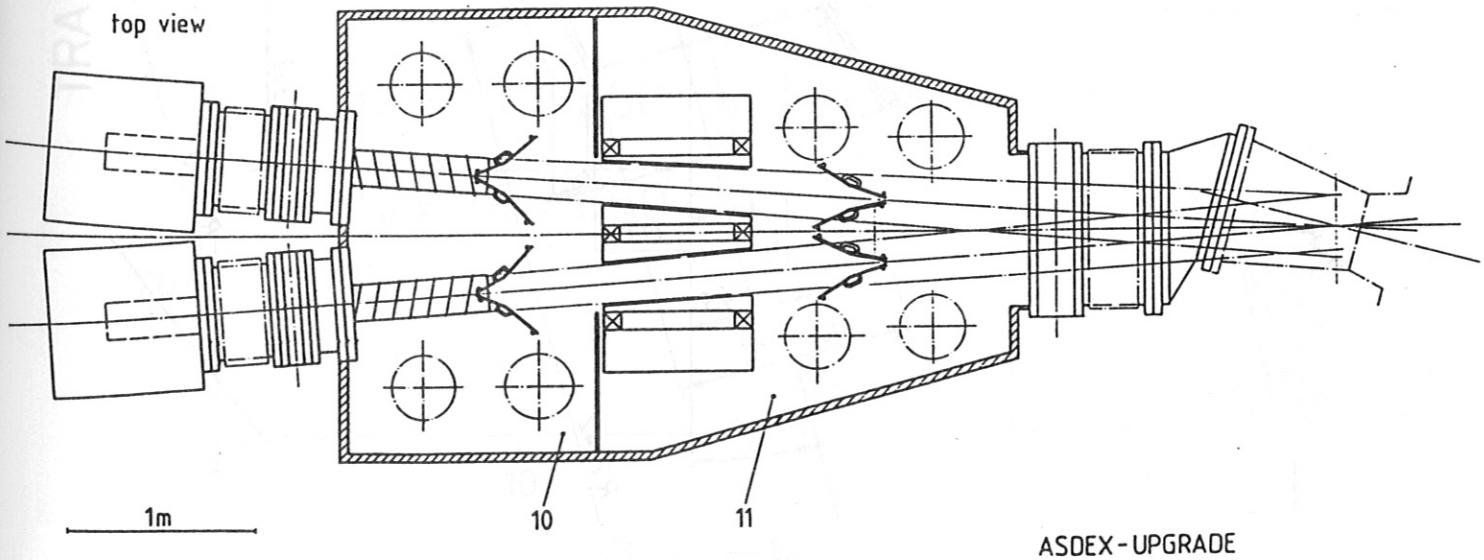

ASDEX-UPGRADE
NEUTRAL INJECTOR

Fig. 7

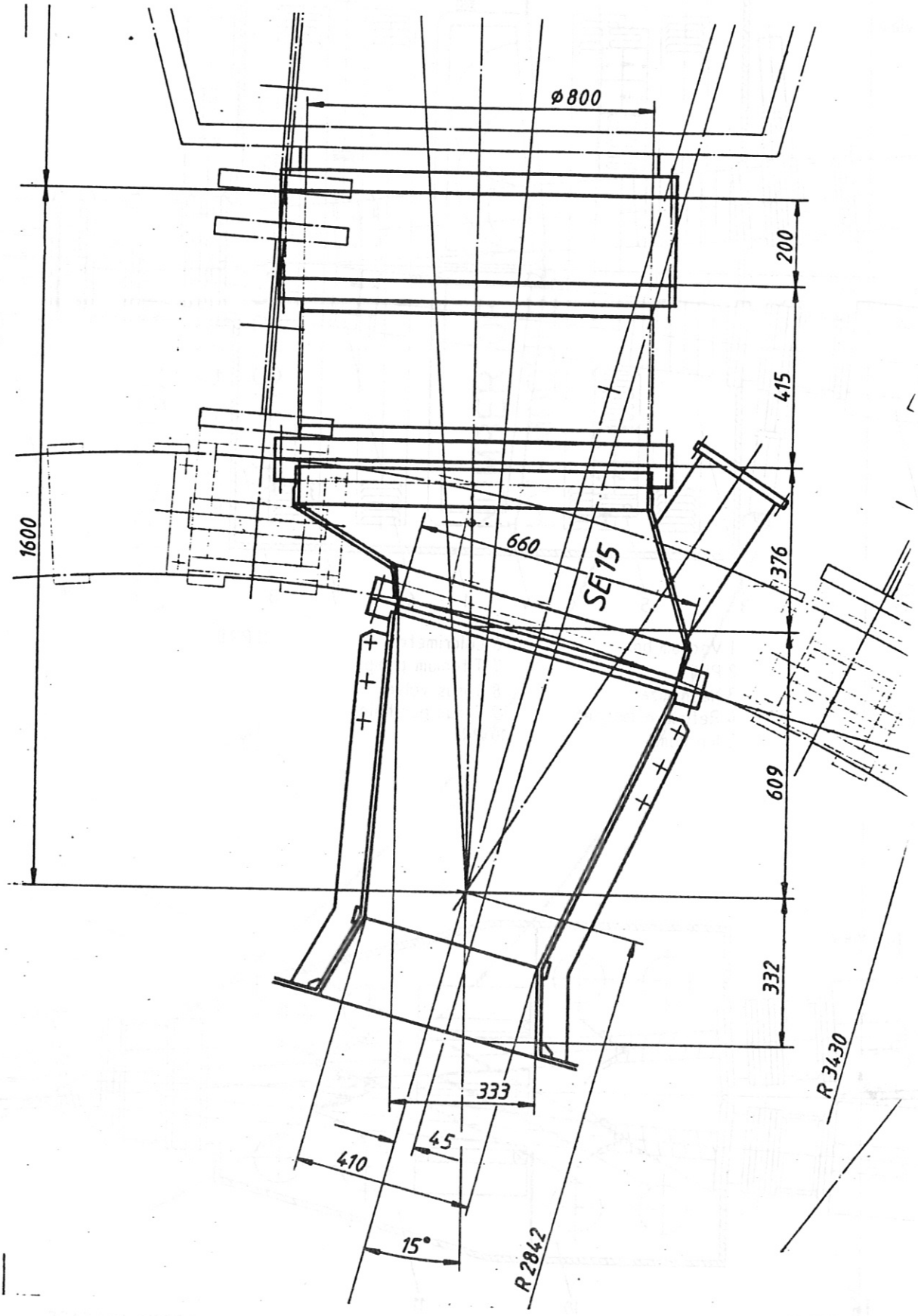
ø800
200
415
1600
660
SE15
376
609
332
R3430
333
45
410
15°
R2842

Fig. 8

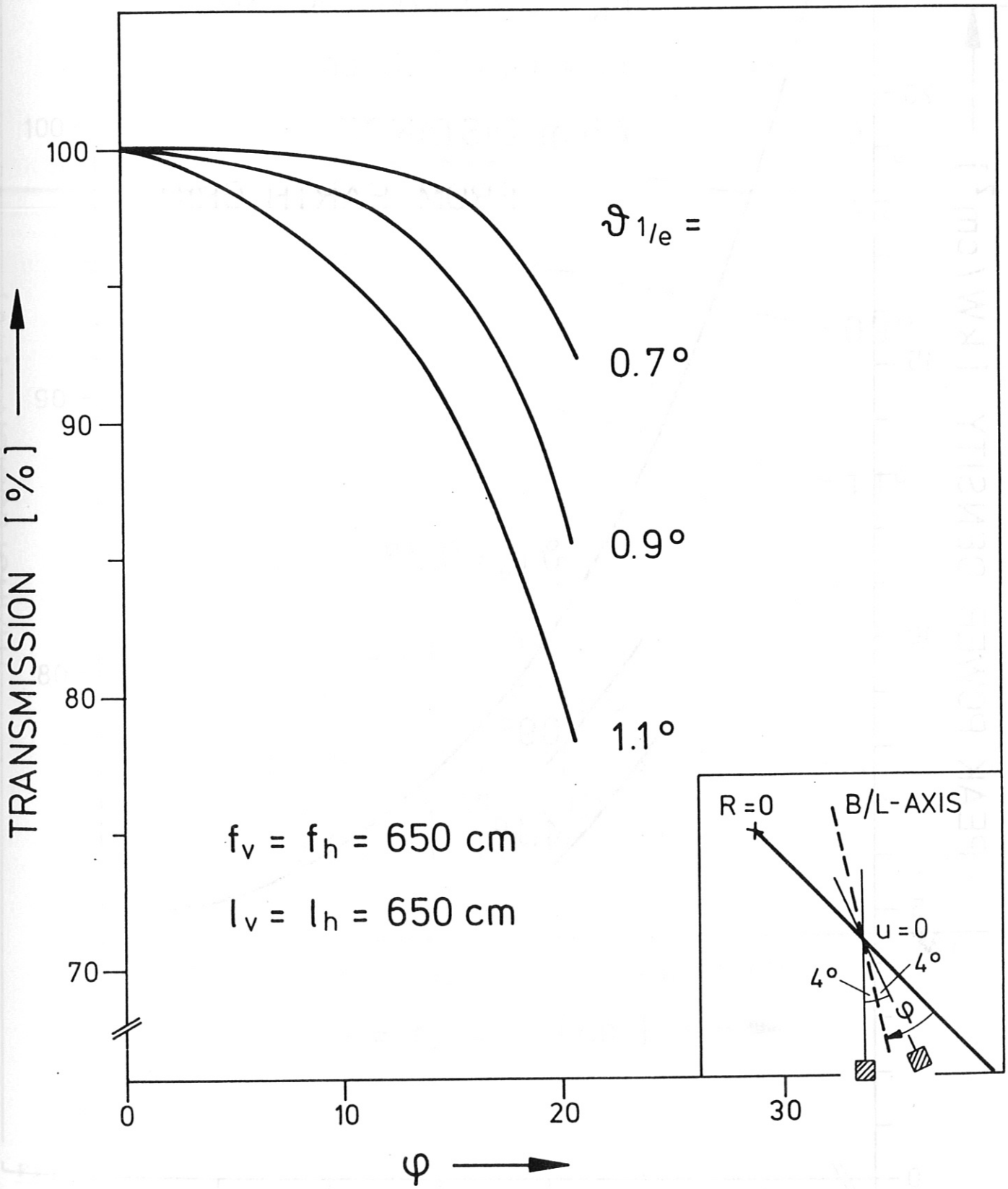
100
90
80
70
TRANSMISSION [%]
$\vartheta_{1/e}$ =
0.7°
0.9°
1.1°
$f_v = f_h = 650$ cm
$l_v = l_h = 650$ cm
R = 0
B/L-AXIS
u = 0
4°
4°
φ
0
10
20
30
φ

Fig. 9

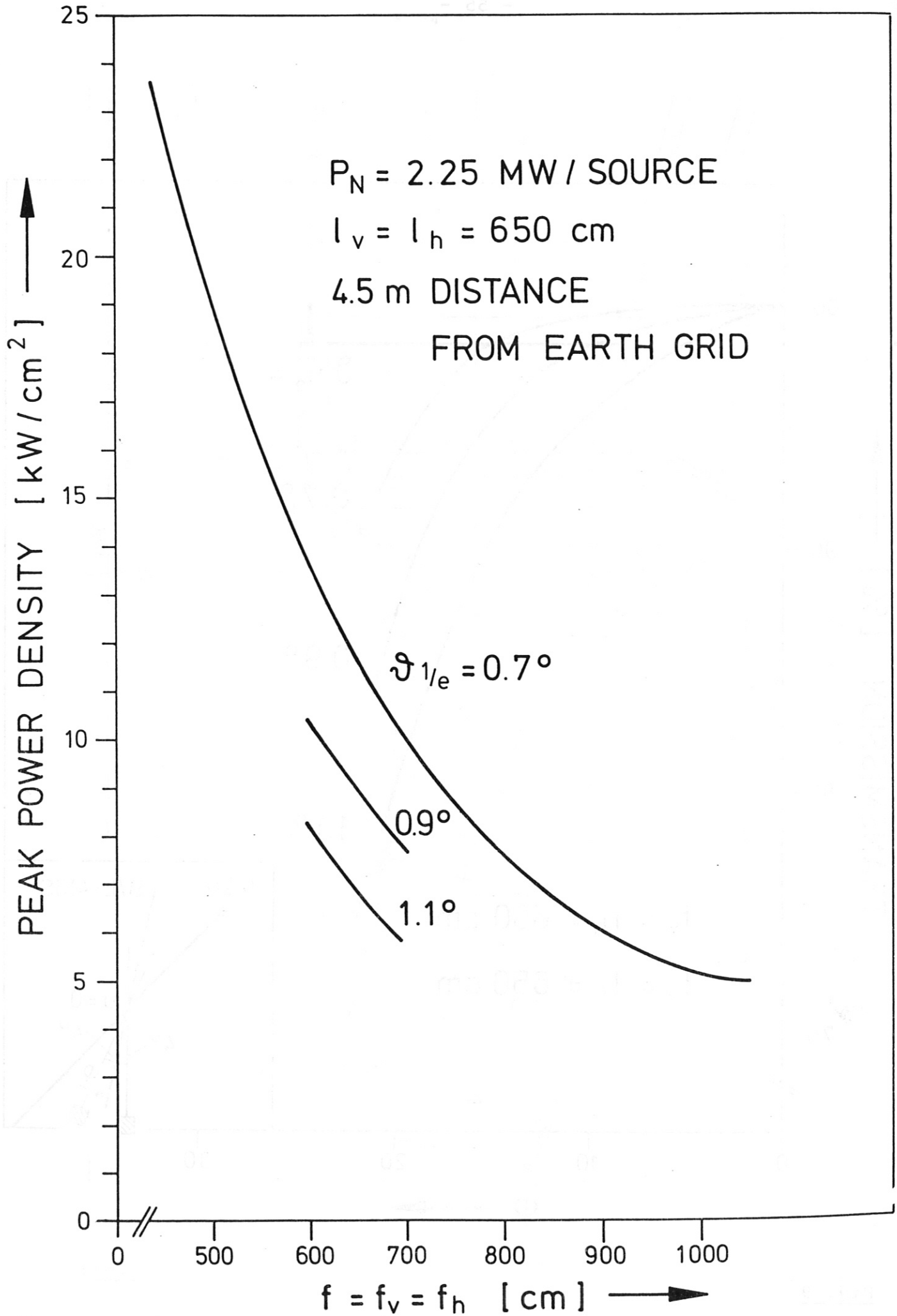
25
20
15
10
5
0
PEAK POWER DENSITY [kW/cm²]
P_N = 2.25 MW / SOURCE
l_v = l_h = 650 cm
4.5 m DISTANCE
FROM EARTH GRID
ϑ 1/e = 0.7°
0.9°
1.1°
0
500
600
700
800
900
1000
f = f_v = f_h [cm]

Fig. 10

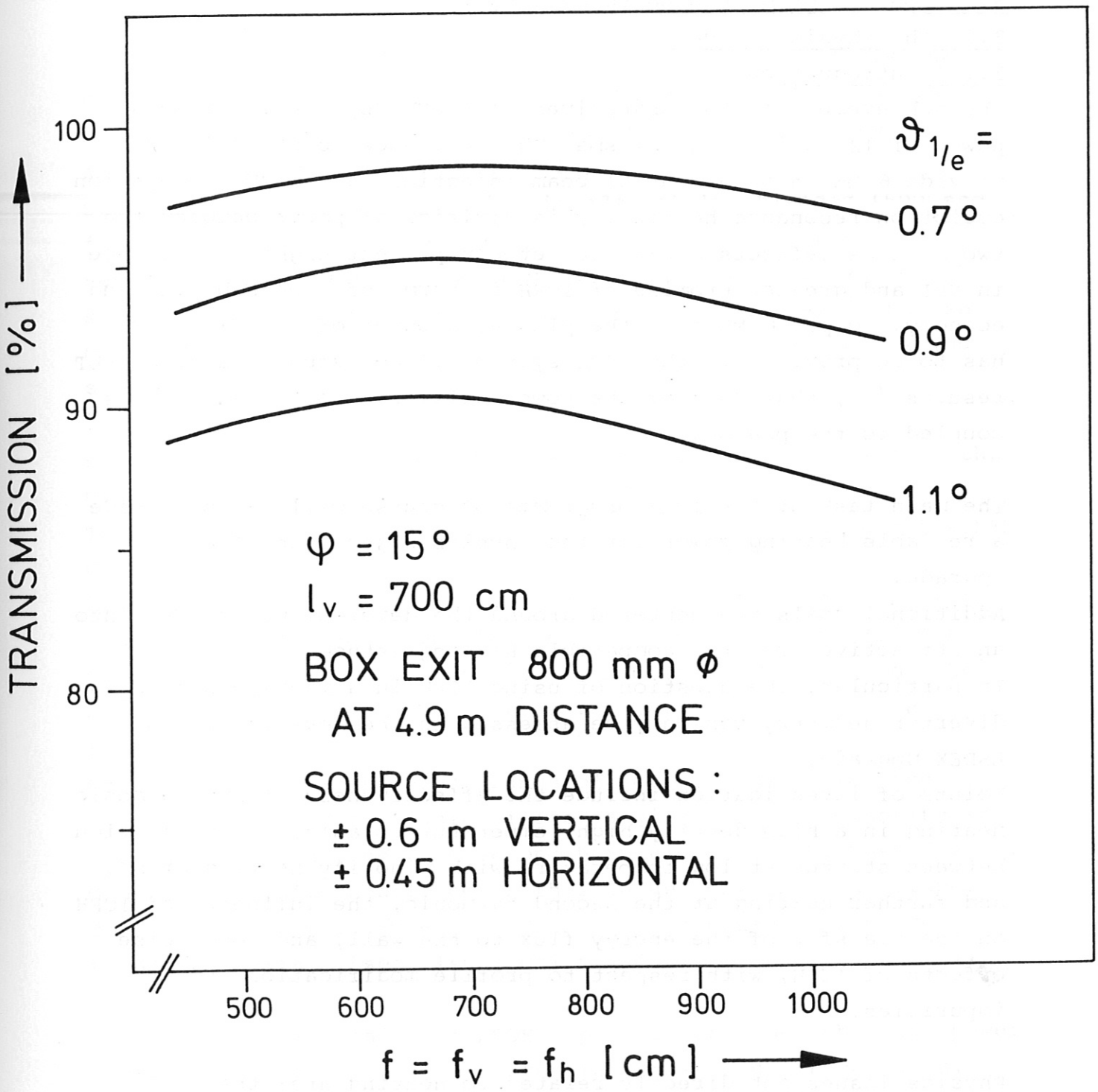
100
90
80
TRANSMISSION [%]
$\vartheta_{1/e}$ =
0.7°
0.9°
1.1°
φ = 15°
l_v = 700 cm
BOX EXIT 800 mm φ
AT 4.9 m DISTANCE
SOURCE LOCATIONS :
± 0.6 m VERTICAL
± 0.45 m HORIZONTAL
500
600
700
800
900
1000
f = f_v = f_h [cm]

Fig. 11

3. Ion Cyclotron Resonance Heating (ICRH)

3.1 The physics concept

3.1.1 Introduction

The achievement of the objectives of ASDEX Upgrade requires a power of 12 MW into the plasma. The reference solution is to provide 6 MW through neutral beam injection, and 6 MW through ion cyclotron resonance heating. This division of power between the two methods reflects a balance between present higher confidence in NBI and greater promise of ICRH in terms of accessibility and economy. To put 6 MW into the plasma, a power of 7.5 MW has to be provided by the ICRH system, if we assume, based on PLT results /1/, that 80 % of the power delivered to the antenna is coupled to the plasma.

The main task of the ICRH programme of course will be to provide a reliable heating power for the physics objectives of ASDEX Upgrade.
Additional goals are centered around the development of ICRH into an attractive, reactor compatible heating method.
In particular, the question of using ICRH in a machine with open divertor geometry can only be assessed in the near future in ASDEX Upgrade.
Points of investigation include the effectiveness of 2nd harmonic heating in a high density high temperature plasma, the transition between startup at low temperature with minority heating or NI, and further heating at the second harmonic, the influence of ICRH on the transfer of the energy flux to the wall, and long pulse effects of ICRH, with respect to profile modification and impurities.

Physics issues not directly related to heating are: the possibility to use ICRH as a current drive method, and the modelling of possible α particle driven instabilities by using a very energetic He^3 minority /2/.

3.1.2 Low field side excitation, choice of method and frequency

Space constraints on the inside of the torus together with the divertor geometry exclude the possibility of using anything but low field side excitation.
Launching the fast wave from the low field side restricts the choice of ICRH methods to minority heating and second harmonic heating. The mode conversion regime, which would require an antenna on the high field side, cannot be used.
Since the ASDEX Upgrade machine is adequately shielded (500 sec full performance shots per year are allowed in D), the restrictions imposed in the original planing on the heating scheme (only second harmonic in H) are no longer valid and use can be made of the minority heating or second harmonic heating scheme in D.

Figure 3.1 shows the frequency requirements as a function of the magnetic field for the different scenarios.
Three magnetic field cases have particular significance for ASDEX Upgrade:
2.7 T reference case for single null (SN) operations, 3.25 T for double null (DN) and pump limiter (LIM) operation and 3.9 T as maximum magnetic field. The figure also shows the range of the magnetic field around its central value for R_o - 1/4a to R_o + 1/4a.
Generators with a frequency range of 30 - 120 MHZ allow the complete spectrum of possibilities ranging from He_3 minority in the SN 2.7T case, up to H second harmonic at the highest fields. Generators, which nearly cover this range, have been developed for ASDEX / W VII, (30 - 115 MHz), and consequently a proven technology exists (see also Section 3.2.3).

Generator studies made for ASDEX Upgrade confirmed the high power capability of the new tetrode generation at high frequencies. Those studies have also shown that it is not until the frequency range is restricted to 80 - 120 MHz that major simplifications are possible in the pre-driver, driver and final stages. Since

this last frequency range would limit the operating scenarios to 2nd harmonic H only it is considered too restrictive. Therefore we decided to take advantage of the industrial development acquired through the work for the ASDEX generators and choose a frequency range of 30 - 120 MHz.

3.1.3 Harmonic cyclotron heating

Harmonic cyclotron heating is the preferred heating method for reactor operation. It is the reference solution for NET and INTOR. In a hot dense enough plasma, absorption of the wave should be particularly effective /3/. Experiments have already been performed in PLT, JFT-2, Alcator C and ASDEX. Results are summarized in Table I. Further experiments are foreseen in D III D, JET, and Tore Supra (Table II).

For ASDEX Upgrade, the dispersion relation in the plasma is shown in Fig. 3.2. The fast wave, which tunnels through the evanescent layer at the plasma edge, propagates to the cyclotron resonance layer.
The form of the dispersion relation depends on $k_{//}$. The figures were drawn for $k_{//} = 8\ m^{-1}$ corresponding to the maximum in the spectrum of the 2x2,(π,π)* antenna defined in Sect. 3.1.7.

---

* Our nomenclature is explained in Sect. 3.1.5.2. A 1 x 2,(0) array consists of two single loops in the poloidal direction, excited in phase. This is commonly called a monopole-dipole antenna in the monopole configuration.
A 2 x 2,(π,π) array consists of an array of four loops (in the toroidal direction two times two loops in the poloidal direction) with difference in phase π both in the toroidal and poloidal direction. This is commonly called dipole-quadrupole antenna in the quadrupole configuration.

Table I Summary of recent experimental results for second harmonic ion cyclotron resonance heating

	I_p(MA)	B(T)	R (m)	a (m)	Volume (m^3)	$\bar{n}_e$ (10^{19} m^{-3})	T_{eo}	ΔT_e	T_{io}	ΔT_i	Frequency (MHz)	Power (MW)	Pulse length (s)	Remarks
PLT [4]	o.2	1.3	1.3	o.4	4.1	3.8			5oo	27oo	42	3.2	o.3	
Alcator C [5]	o.2 - o.35	6	o.64	o.125	o.4			1oo			18o	o.2	o.7	results unclear
JFT-2M [6]	o.18	1.25	1.31	o.35	3.1	3	8oo	4oo	5oo	5oo	38	o.6	o.o5	with NBI (o.5 MW)
ASDEX [7]	o.4	2.2	1.65	o.4	5.2	4.5	63o	1oo	5oo	2oo	67	o.55	1	

Table II Proposed second harmonic experiments

	I_p (MA)	R (m)	a (m)	b (m)	Volume (m^3)	B_{max} (T)	$\Delta\Phi$ (Vs)	Frequency range (MHz)	Generator output power (MW)	Pulse length (s)	Operation date
JET [8]	4.8	2.96	1.25	2.1o	153	3.45	34	25 - 55	up to 30 MW	2o	85
D-III-D [9]	5	1.67	o.67	1.4o	31	2.2	1o.5	3o - 6o + 8o	9 MW	1o	86-88
Tore Supra [10]	1.7	2.38	o.85	o.85	34	4.5	21	35 - 65 + 12o	9 MW	30	87
ASDEX UG	2	1.65	o.5	o.8	13	4	9.5	3o - 12o	7.5 MW	1o	88

Results from ray-tracing calculations using the RAYIC code (12), which take into account the complete antenna spectrum, predict for an 1 x 2,(0) antenna array a single pass absorption of around 40 %. Typical variations with density and temperature are shown in Fig. 3.3 and 3.4. Single pass absorption increases both with temperature and density.
For a 2 x 2,(π,π) antenna array the $k_{//}$ spectrum of the radiated waves can be better adapted to the dependence of the absorption on $k_{//}$ (see also Sect. 3.1.7). Therefore the single pass absorption can increase to around 55 % for those antennas.

3.1.4 Minority heating regime

The presence of two species in a plasma introduces, between the cyclotron resonance layers of each species, a resonance-cut off pair.

The pure minority heating regime occurs when the concentration of the minority is sufficiently low (the $k_{//}$ or the temperature sufficiently high) that the doppler broadening of the cyclotron resonance layer masks the mode conversion and ion-ion hybrid resonance layer.

For higher minority concentration one has two different cases. If the cyclotron resonance of the minority is higher than the cyclotron resonance of the majority ions (as for He^3 or H in D) a wave launched from the low field side will first encounter the cyclotron resonance of the minority ions, then the cut off, before eventually tunelling to the ion-ion resonance layer. Depending on the type of minority species, on the temperature and density of majority and minority ions, and on the wave vectors /11/ more or less power will be given to the minority ions, or to the electrons through mode conversion at the ion-ion hybride resonance layer.
Figure 3.5a shows for H minority in D, a pure minority case (n_H/n_D = 0.02, $k_{//}$ = 8 m^{-1}). Figure 3.5b shows the reappearance of

the cut-off at higher minority concentration (n_H/n_D = 0.04, $k_{//}$ = 8 m^{-1}). Fig. 3.6a and Fig. 3.6b present similar cases for a He^3 minority in D. Note that cut-off region is narrower than for the H minority.
In the case that the cyclotron resonance of the minority is lower than the cyclotron resonance of the majority (as for He^3 or D in H) a wave from the low field side would first encounter the cut-off before it could eventually tunnel through to the ion-ion hybrid resonance layer and the minority cyclotron resonance layer.
This last regime is thus not suited for a machine with antenna on the low-field side.
Both H minority and He^3 minority regimes in D have shown promising results in other machines, the best results have been obtained with He^3 minority in PLT.

There are several other reasons to prefer He^3 in comparison to H, as minority species.
With H as minority it may be difficult to achieve the conditions of pure minority heating since ASDEX Upgrade has extensive graphite coverage on the walls. This can act as a hydrogen reservoir and make control of the H minority, especially at low concentration very difficult. This problem does not occur with He^3 which recycles completely at the wall, so that its concentration can be better controlled.
Charge exchange losses of the high energy minority species is also markedly lower in the case of He^3 minority than in the case of H minority.
All in all, the efficiency achieved in the He^3 minority heating regime equals the efficiency observed in the best experiments with second harmonic heating. Its use as a heating method for ASDEX Upgrade is therefore proposed although it requires to extend the frequencies to lower ranges.

3.1.5 The Antennas

3.1.5.1 Calculation and optimization procedure

The antennas have been mainly calculated and optimized for the second harmonic case.

Antenna coupling programs (2D and 3D) /13/ were used to compute the power coupled to the plasma. The antenna coupling calculation can say something about the voltage needed to radiate a given amount of power to the plasma but provide no information on how much of this power is absorbed in the plasma. Ray tracing calculations were therefore made to give some guidance about the "quality" of the power radiated by the antenna. Those calculations can tell us how much power is absorbed in a first pass through the plasma. Thus for different antenna geometries we could compare not only the required coupling voltage but also the power absorbed in single pass. Maximum electric fields on the antenna and the line were calculated, and taken into account when choosing the antenna geometry. In the optimization procedure we have also kept in mind that we want to minimize "parasitic power" (coax modes and surface waves) which can propagate at the plasma boundary and in the region between plasma boundary and vessel.

3.1.5.2 Nomenclature

In order to define unequivocally the antenna configuration we will be using a nomenclature similar to the one in use for lower hybrid grills.

To define the geometry the number of loops in the array in the toroidal direction (ν) and in the poloidal direction (μ) are counted. The notation is then an $\nu \times \mu$ array.

To define the electrical connection two numbers are sufficient if the change in phase between adjacent loops in the toroidal ($\Delta\alpha$) and poloidal direction ($\Delta\beta$) is periodic. We write them down as $(\Delta\alpha, \Delta\beta)$.

The complete definition includes then both the geometry and the electrical connection in the form $\nu \times \mu$, $(\Delta\alpha, \Delta\beta)$

For non periodic phase arrangement the complete matrix should be given.

Some examples are shown in Fig. 3.7.

3.1.5.3 Antenna Types, $k_{//}$ Shaping and Coaxial Modes

An antenna array of the 1 x 2,(0) type has the advantage of being simple and having, for limited geometrical extend, a rather large power coupling capability. However, it has disadvantages.
The $k_{//}$ spectrum of such an antenna array is peaked at $k_{//} = 0$ (curve a of Fig. 3.20). This spectrum has in a twofold sense negative effects: the preferred excitation of fast waves with small $k_{//}$ which are weakly damped by the plasma (the absorption increases with increasing $k_{//}$); the excitation of the so called coaxial modes which are characterized by the dispersion relation $k_{//}^2 + k_y^2 = k_o^2$ and which propagate between the plasma boundary and the wall.
There are some experimental indications that the impurity production may be related to these waves. Antenna configuration with a $k_{//}$ spectrum where the peak is removed from $k_{//} = 0$ are therefore an interesting alternative to the 2 x 1,(0) antennas. This can be achieved with 2 x 2, (π,π) antenna arrays.
Both array types have been investigated and optimized. It is expected that the choice between the two array types can be made prior to the time of installation in ASDEX Upgrade, based on experimental results from JET and maybe ASDEX.

3.1.6 Type 1 x 2,(0) Antenna Array

3.1.6.1 General Considerations

With a 2D program a systematic study was made of the maximum voltage needed to couple a given amount of power into the plasma. The antenna width and the distance central conductor - return conductor was varied in a wide range, the plasma parameters being kept constant. The results are summarized in Table III.
The maximum voltage on the line decreases strongly with increasing width w_z and, to much lower extend with increasing distance central - return conductor distance d. The small decrease of V_{max} with increasing d results from the fact that the electrical length of the antennas was kept constant at $\lambda/4$. The resonant $\lambda/4$ condition for different antenna configurations (with

Table III V_{max} for $\lambda/4$ antennas versus d and $2w_z$ for 1 MW of power per antenna array (1x2)

Distance central conductor - return conductor (cm)	Antenna width (cm) 4	8	16	32
22.6	25.41	19.46	14.11	9.97
16	26.13	19.91	14.33	10.06
11.3	27.2	20.53	14.60	10.16
8	28.64	21.29	14.90	10.27
5.6	30.51	22.19	15.21	10.39
4	32.76	23.19	15.50	10.48

Frequency 76 MHz, corresponding to $2\omega_{CH}$ on the magnetic axis at
R = 1.79 m for 2.7 T at R = 1.65 m
Electrical length $\lambda/4$ = 0.45 m
$n_{eo} = 1 \times 10^{20}\ m^{-3}$ distance central conductor - separatrix 8 cm,
distance to plasma edge 4.5 m
Characteristic impedance of the transmission line 30 Ω

different d and w_z) are obtained by varying the capacitance of the antenna. This was done numerically by the variation of s, the distance between central conductor and Faraday screen. An example is shown in Fig.3.8. For some antennas with broad central conductors and small distances between central conductor and return conductor, the value of s is small (in the range of some mm) and this could, even with the use of additional capacitive loading, cause considerable difficulties in building such antennas.

The influence of the antenna width and the distance central conductor - return conductor on the first pass absorption were investigated with RAYIC /12/, keeping the plasma parameters constant. The form of the flux surfaces is shown in Fig. 3.9. Plasma parameters and profiles are given in Fig. 3.10.

The general tendency is that increasing the width of the antenna decreases the single pass absorption (a negative effect, as opposed to the decreasing voltage by increasing width, obtained from the coupling calculations), Fig. 3.11. Increasing the distance central conductor - return conductor also decreases the single pass absorption (again a negative tendency with respect to the reduction in voltage), Fig. 3.12.

Note that the counteracting tendencies (coupling voltage, absorption) are dominated by the voltage effect. This can be shown by transforming the voltage required per MW of coupled power to voltage required per MW absorbed power.
Table IV presents this for four special cases. If one only cares about maximising absorbed power for a given maximum voltage, one should choose antennas as wide as possible, a similar result as when one maximises the coupled power only.

Table IV V_{max} for $\lambda/4$, calculated per 1 MW of power absorbed in single pass

Distance central conductor - return conductor (cm) \ Width (cm)	4	32
22.6	$25.4 \times \sqrt{\frac{1}{0.377}} = 41.4\,kV$	$9.9 \times \sqrt{\frac{1}{0.305}} = 17.9\,kV$
4	$32.8 \times \sqrt{\frac{1}{0.433}} = 49.8\,kV$	$10.5 \times \sqrt{\frac{1}{0.341}} = 18.0\,kV$

3.1.6.2 Optimization

Let us now investigate trade-offs and optimization within the geometrical constraints for ASDEX Upgrade. The space available for a simple antenna array is 44 cm between protection limiters. To reduce the influence of the proximity of limiters on the antenna impedance it is necessary that the distance central conductor - limiter should not be smaller than the distance central conductor - return conductor. This means that, in our optimization procedure, when we vary the width of the antenna we have to fulfill the constraint $2d + 2w_z = \text{const} = 44$ cm (Fig. 3.13). Keeping this constraint in mind the voltage per MW coupled was again calculated with 2D and 3D programs.
With the ray tracing program the percentage of power absorbed in single pass was calculated. From both we have computed the voltage needed per MW absorbed. Results are shown in Fig. 3.14. With this voltage (per MW absorbed) we have calculated (Fig. 3.15) the maximum electric field on the transmission line (for a 30Ω, 6 1/8" line, the choice of 30Ω will be justified later) and the maximum electric field //B in the antenna (assuming distance central conductor - limiter to be equal to d, $E_{max} = V_{max} / d$, keeping $2d + 2w_z = 44$ cm). The rise of E_{max} on the line with smaller width reflects the increase in V_{max} per absorbed power for smaller antennas. The increase of E_{max}//B for small width is the same effect as for the maximum field on the line. The increase at larger width reflects the decreasing central conductor - limiter distance.

Choosing an optimum configuration now means a trade off between several tendencies. We want to minimize voltage per MW absorbed, but we also want to maximize the single pass absorption (Fig. 3.14), since the power not absorbed in the first pass may be a cause of impurities. We want to minimize the electric field on the line and in the antenna (Fig. 3.15). We have to keep in mind the caveat mentioned in 3.1.6.1 and Fig. 3.8, that it is increasingly difficult to make wide antennas $\lambda/4$ long, and have to consider the production of coaxial modes.

Taking all this into account, we have chosen the width of the central conductor to be 16 cm (central conductor - return conductor distance = 14 cm). Indeed going to higher width, although it further reduces the voltage and electric field on the line, reduces the single pass absorption markedly and results in increasing E fields on the antenna. Going to smaller width does not bring any significant increase in single pass absorption, but is penalized by a sharp increase in voltage, a sharp increase in E on the line and on the antenna.

For the chosen geometry the achievement of $\lambda/4$ length is possible. The central conductor - Faraday screen distance would be 2 cm, with an additional capacitance at 2 cm.
The power P_{CM} going into the coaxial mode can be expressed by an effective resistivity R_{CM} and the squared antenna current.
The effective resistivity R_{CM} of the chosen antenna array is shown in Fig. 3.16. For operating frequencies below 80 MHz the power going into the coaxial mode is less than 50 kW per 1 MW radiated fast wave power. At frequencies between 80 and 120 MHz P_{CM} is considerably higher. Especially for ICRF heating experiments in this frequency range 2 x 2,(π,π) antenna array with $k_{//}$ spectra peaked at $k \neq 0$ are an interesting alternative.

3.1.7 Type 2 x 2,(π,π) Antenna Array

3.1.7.1 Limited width

Simply replacing the central conductor in the previous configuration in order to change the 1 x 2 array to a 2 x 2 array does not provide sufficient power handling capability of the array. For a 2 x 2 array with dimension as defined in Fig. 3.18, the $k_{//}$ spectrum peaks at 12 m^{-1} (Fig. 3.19). The maximum voltage, calculated with a 2D coupling code, per 1 MW radiated power, would be V_{max} = 22.5 kV. The single pass absorption (from RAYIC) reaches 60 %, giving a voltage per MW absorbed in single pass of 29.0 kV. This would result in a maximum electric field (per MW absorbed) on the line of 6.8 kV/cm and, along B, on the antenna

of 9.7kV/cm (from $E_{max} = 2\ V_{max}/\varepsilon$). The corresponding value for the 1 x 2 array are 4.8 kV and 1.6 kV. Thus, even assuming optimistically that the line is the critical component, the power handling capability of the 2 x 2 array is at least a factor 2 lower then of the 1 x 2 array.

3.1.7.2 Extended Width

In order to obtain for a 2 x 2 array a power handling capability similar to the 1 x 2 array, we have to go to larger overall width. Because of geometrical constraint, the antenna width can only be extended on one side yielding a more complex antenna, asymmetric with respect to its feed points. The maximum width available between protection limiters is then limited to 70 cm (if we limit the size of the return conductor to what can pass in one piece through an A port).

For different 2 x 2 array configurations the antenna impedance and the maximum voltage on the line was again calculated using a 2D program. Figure 3.18 shows a poloidal cross section of the array. The width $2w_z$, the gap ε between the two conductors and the distance d between conductor edge and lateral antenna frame are connected by $4w_z + 2d + \varepsilon = 70$ cm. Within this constraint and for a given distance central conductor - return conductor (0.14 m, same as for the 1 x 2 array) we have varied the distance ε between the two central conductors. The $k_{//}$-spectra for the radiated active power /13/ are shown in Fig. 3.20 for three 2 x 2 arrays and for comparison for the 1 x 2 array of maximum width ($2w_z = 42$ cm, d = 14 cm). Note that the k -spectra in Fig. 3.20 are not normalized to equal amounts of radiated power. The location of the maximum lies in the range of $k_{//} = 8\ m^{-1}$. The differences on the position of the maximum are small and in the range of $/k_{//}/ \simeq 1\ m^{-1}$.
Larger differences are found with respect to the maximum voltage V_{max} in a 30Ω coax line (see Fig. 3.21). The dependence of V_{max} on ε is essentially dominated by the variation of the conductor width $2w_z$.

Calculations were also performed in order to obtain the percentage of power absorbed in single pass for the 2 x 2 antennas. The single pass absorption is about 55 %. Results are shown in Fig. 3.21, as a function of the inter-conductor distance In accordance with the small change in the maximum of the $k_{//}$-spectrum with ε, the variation in absorbed power is also small.

It is also interesting to note that, for this extended width array, if we consider voltage per MW absorbed, it is possible to find 2 x 2,(π,π) configurations which have lower voltages than the corresponding 1 x 2,(0) array which would fit in the same space.

Calculating again the maximum electric field on the line, and E_{max}// B (from $E_{max} = 2V_{max}/\varepsilon$) on the antenna we obtain Fig. 3.22. If we accept on the line a slightly larger electric field than on the antenna, the favoured solution would have ε = 14 cm. The maximum electric field in the line (per MW absorbed) would be 3.3 kV/cm and on the antenna 2.2 kV/cm.
The corresponding values for the 1 x 2(0) array of same total width ($2w_z$ = 42 cm) would be 3.4 kV/cm and 1.2 kV/cm.

3.2 Technical Description

3.2.1 Introduction

This part describes in more detail the RF technical arrangements and solutions proposed to fulfill the aims discussed in the previous sections. It is foreseen to provide the 7.5 MW through 4 ICRF generators, each generator feeding one antenna array. A single 6 1/8" transmission line goes from each generator to two stub tuners, before splitting into separate 9" lines to feed different parts in the antenna array. On the vacuum side of the feedthrough the transmission line goes again to 6 1/8". Bellows in inner and outer conductor of the transmission line are at present the favoured solution to take up the thermal expansion of

the vacuum chamber. A stub near the antenna will reduce the VSWR in the 9" line and allow at the same time the introduction of coolant.

3.2.2 Layout

Fig. 3.23 shows the general layout of the ICRH system in the southern part of the L6 hall. The antennas will be distributed evenly around the torus (Fig. 3.24). The transmission lines leave the shielded area in direction north through channels in the platform and under the shielding wall(Fig. 3.25). By appropriate choice of the geometry, by filling the channels with polyethylene balls and an additional shielding wall the cumulative dosis can be kept below 150 mrem/a, outside the shielding house. The four generators are situated north of the shielded area of ASDEX Upgrade and provision is made to further add four generators. The ICRH control room will be situated directly in the neighbourhood of the generators. The possibility of remote control from the machine control room with additional local control panels near the generators is an alternative being discussed.

3.2.3. RF Generators

3.2.3.1 General remarks

The RF generators are the most expensive and - besides the antennas - the most critical components of the technical ICRH system. Moreover, the requirements of ASDEX Upgrade - high frequency operation and a large frequency range - are limited by the generator technology and by the characteristics of power tetrodes.

Second harmonic heating of hydrogen for the major operation regimes of ASDEX Upgrade requires high RF power up to 100 - 120 MHz, where the output of power tetrodes is already reduced by RF losses. To allow heating of a deuterium plasma via

H or He minorities, calls for a frequency range beginning at about 30 MHz (see Sect. 3.1.2). Since it is the most economic way to produce as much RF power as possible with one generator and since the power tetrode is the limiting element, the real limitation of tetrodes at high frequencies and the possibilities of further development have to be checked carefully.

The successful development of the generators for ASDEX / W VII (Fig. 3.26, Table V), tunable between 30 and 115 MHz and with an output power of 1.5 MW up to 80 MHz, showed that a generator with a frequency range of 30 to 120 MHz can be built. The high frequency power limitation has been investigated by study contracts.

Table V Operational Generators for ASDEX/WVII

Frequency range	30 - 115 MHz
12 frequencies preprogrammable	
Output power	
30 - 80 MHz	1.5 MW
100 MHz	1.0 MW
115 MHz	0.54 MW
Pulse length	max. 10 s
Time between pulses with max.power	5 min
Average power	max. 50 kW
Rise time with automatic regulator	≈ 1 ms
with pin modulator (for conditioning purpose)	≈ 10 µs
Bandwidth at 67 MHz	200 kHz
Efficiency at 80 MHz	> 65%
Output impedance	50 Ω

3.2.3.2 Study contracts

Study contracts including theoretical investigations and (as far as possible) practical tests have been placed with two manufacturers of generators and four tube manufacturers in order to

- clear the limitations of existing tetrodes
- investigate the necessities and possibilities of further developments in order to meet the requirements of ASDEX Upgrade (at least 1.5 MW up to 100 MHz)
- give the output limits of such a tetrode at and below 60 MHz and at 120 MHz
- study possible generator designs based on the results of the tetrode investigations.

The results of the studies can be summarized as follows:

- A new generation of larger power tetrodes is necessary to meet the high frequency requirements
- The first type of this generation is the one developed for ASDEX/W VII by BBC. Other companies have in the meantime also started development work. Table VI gives the data of these tetrodes.
- Besides calculations the power limitation of the ASDEX/W VII power tetrode has been investigated by tests up to 115 MHz. Table VII gives the results of these tests.
- The studies were requested for a tunable range between 60 and 120 MHz, the frequency range originally envisaged. They confirmed that even up to 120 MHz a coaxial design design similar to ASDEX/W VII generators is suitable. A comparison with the generator design of ASDEX/W VII shows that an extension to the low frequency range between 30 and 120 MHz will be also possible.

Thus the studies showed that frequency range and power demands for ASDEX Upgrade are realistic. In case of the same manufacturer the principle design of the ASDEX/W VII generators has to be only slightly changed.

Table VI Technical data of possible power tetrodes for ASDEX Upgrade

		BBC CQK 650/2	Philips OZ 237	Thomson TH 525	Siemens RS 2086 SK
Frequency	MHz	115	120	120	120
Output power	MW	1.2	1.5	1.0	1.25
Anode voltage	kV	14	22	14.7	14.3
Max. anode voltage	kV	24	24		22
Anode surface	cm^2	2500	1060	1000	1400
Active length	cm	26	11	13	20
Max. anode loss	kW	1250	1000	1200	1000
Max. screen grid loss	kW	15	9	10	12
Anode screen grid capacity	pF	185			140
Cathode design		parallel wire cath. (low resistance)	mesh cathode (high resistance)	mesh cathode (high resistance)	straight mesh cathode (low resistance)
Status		operational	design	design	design

All 4 tetrodes should allow an output power of 2 MW at 60 - 80 MHz(for the BBC tetrode this value has been tested) at anode voltages of about 22.5 kV and anode currents of about 120 A.

Table VII: Test results for the BBC tetrode CQK 650/2

Frequency	MHz	60	80	100	115
Output power	MW	2.0	2.0	1.5	1.2
Pulse length	s	2.3	2.3	2.3	2.3

The pulse length was limited by the power supply.

3.2.3.3 Generator concept

The required 6 MW in the plasma can (within some frequency range) be provided by 4 generators, with each generator connected to one antenna array (Sect. 3.2.7). A full power of 8 MW will be available up to 80 MHz. A power reduction at higher frequencies seems unavoidable (6 MW at 100 MHz, 4.8 at 120 MHz; see Table VI, VII).

Each generator is composed of an amplifier chain with its own oscillator, power regulator and phase shifter (see Fig. 3.27). Alternatively, all generators can be driven by one common oscillator with adjustable phases. The power delivered to the load (forward power or alternatively forward minus reflected power) is feedback controlled, the nominal value of this power being prescribed as an arbitrary analog time function. The RF power radiated to the plasma can thus be integrated in a closed feedback loop regulating the plasma temperature ASDEX Upgrade.

Although continuous tuning of the frequency will be possible, a certain number of discrete frequencies will be preprogramable. The coaxial design has proved to be insensitive to uncontrolled oscillations, but a few small forbidden frequency bands could be allowed, if they can not be totally avoided.

Each generator will get its own control system including the power feedback system and allsupervision functions and switching off-equipments necessary for a self-protecting operation. Remote operation from the ASDEX Upgrade control room will be possible, too, if advantageous. For test and tuning operation each generator can be switched on a dedicated dummy load.

The technical data of the generators are summarized in Table VIII.

Table VIII Technical data of RF generators for ASDEX-Upgrade

Frequency range	30 - 120 MHz
about 12 frequencies preprogrammable	
Output power	
30 - 80 MHz	2.0 MW
100 MHz	1.5 MW
120 MHz	1.2 MW
Pulse length	max. 10 s
Time between pulses with max.power	5 min
Average power	70 kW
Rise time normal mode	1 ms
for conditioning	10 s
Efficiency up to 80 MHz	60 %

3.2.4 High voltage power supply

At IPP a high voltage DC power supply system is already available with 16 more or less equal modules. Since the modules can be operated in series or in parallel, this system can serve as power supply system for neutral beam injection and all rf heating methods. However, as it was originally built for neutral injection with several voltage levels between 35 and 105 kV, it is not really adapted to ICRH generators, especially to the high

frequency generators for ASDEX Upgrade, whose tetrodes will be designed for low voltage (below 20 kV at high frequencies) and high currents. The power needed for the planned 6 MW neutral injection correspond to the total dc power of the already available modules. So, for the additional high voltage supply units needed, it seems reasonable and economic to install special units better adapted to ICRH requirement. Each module shall supply the dc power for one generator. With a generator effectivity larger than 60 % the dc power of one module should be larger than 3.4 MW for 2 MW RF power. With regard to the tetrode characteristics in the frequency range envisaged, one module should have the following main data (Table IX).

Table IX

Nominal power	3.5 MW
Pulse length	10 s every 5 min
Current	160 A above a voltage of 14 kV

The modules will be powered by one of the flywheel generators of the IPP with about 100 Hz. To give maximum flexibility in case of faults, each module can be switched to each generator. The rectifier modules will be equiped with a control and supervision system guaranteeing a self-protecting operation. In order to reduce interface problems, e.g. in the field of control and supervision, the manufacturer of the dc supply should either be subcontractor of the rf generator-manufacturer or at least be required to adapt its design to that of the rf generator. The safety equipment (crowbar system to protect the power tetrode in the case of arcing) should also preferably be built by the manufacturer of the RF generator.

3.2.5 Transmission line system

The transmission line system has to transport the rf power to the antennas and to match the antenna impedance to that of the generator. The choice of the transmission line is essentially a

choice of matching methods, characteristic impedance and of diameter.
Geometrical constraints, and constraints on the maximimum electric field are the main considerations dictating the choice.

3.2.5.1 Matching

Large VSWR values (i.e. high voltage) occur in the antenna and the unmatched part of the line system. In principle there are 3 possibilities to match the load:

- a resonant antenna allows feeding at a point with impedances equal to the line impedance. High voltage is limited to the antenna itself. With variable frequencies the electric length of the antenna has to be varied, e.g. by means of adjustable capacitances at the antenna ends (within the vacuum vessel!).Such antenna is envisaged for Big D. Because of the large frequency range this method is not considered for ASDEX Upgrade.

- a system with two tuners outside the vessel allows matching in the neighbourhood of the antenna. The long transmission line to the generator is then matched with resulting low voltage level. This method is used for ASDEX/W VII, TEXTOR, TFR etc.

- since the electrical length between antenna and tuners acts as impedance transformer, a variation in frequency also allows matching. If the line length is long compared to λ, i.e. if the one tuner necessary in this case is installed at the generator site, this matching can be effectively done by a small frequency change within the bandwidth of the generator. This method is used by JET. The advantage of this matching system is that automatic matching by a feedback loop can be done relatively easily. A disadvantage is the high voltage level on the total length of the line, calling for a larger diameter of the coax lines. It can be reduced by a second tuner

directly at the antenna feeder, which may be needed to introduce the coolant for the vacuum feeding line anyhow. Another disadvantage is that, if upper and lower antennas have different impedance as in the case of ASDEX Upgrade the power balance between the two antennas may change during matching.

The decision over the matching method for ASDEX Upgrade has not yet been made. Since the double tuner system requires the most space in the experimental area, we can cover all the possibilities by choosing presently this system as reference design (Sect. 3.2.5.2, Fig. 3.28). In this case additional matching by frequency variation would be possible to some extent in the upper frequency region.

The final design will be made based on
- the calculation of the voltage level in both cases and
- the investigation of the possibilities for both cases to improve the matching within a shot in case of antenna coupling variations caused by varying plasma parameters (e.g. n, T, displacements).

These investigations have been started, but are not yet finished.

3.2.5.2 Reference design

For the reference case the transmission line consists for each generator of a 6 1/8", 30Ω line from the generator to the experimental area. Depending on location the length of this matched part varies between 25 m and 50 m (see Figs.3.24 - 25). In the experimental area (Figs. 3.28 - 30) a first stub (9" or even larger as the 12" for ASDEX) is followed by 9" extension υ and a second tuner (9"). The extension υ allows to change the distance between the two tuners. After the second tuner the transmission line splits in two 9" feeding lines for the upper and lower antenna. Each one of the two lines has again an extension in order to be able to choose the phase of each two antennas independently, and to position a voltage maximum at the

junction D (this minimizes the sensitivity of the power distribution between the two antennas to small impedance variations).
A final stub in each line near the antenna is required for introduction of coolant but can also be used to reduce the VSWR in the line between B and D (Figs. 3.28, 3.30) and in order to equalize the impedance seen in D of both antennas (note that with its single null geometry the top and bottom antennas of ASDEX Upgrade are not similar and have an inherent difference in impedance).
Reflectometers, voltage and current probes at different points of the line system and at the antenna input allows measuring the standing wave forward and reflected power as well as the active power delivered to the antenna (see also Sect. 3.2.8.3).

3.2.5.3 Choice of the line impedance

The present choice of 30Ω for all parts is based on the following considerations /14/:

For a transmission line with inner radius b and outer radius a, the characteristic impedance is given by

$$Z_c = 377\Omega \frac{1}{2\pi} \log_e \frac{a}{b}$$

If the line is terminated on an impedance Z_A the net power is related to the maximum voltage on the line through

$$P = \frac{1}{2}\frac{1}{Z_c}\frac{1-|R|}{1+|R|}|V_{max}|^2$$

where /R/ is the reflection coefficient

$$|R| = \left|\frac{Z_A - Z_c}{Z_A + Z_c}\right|$$

The maximum voltage can be expressed in terms of the maximum electric field occuring on the inner conductor through

$$E_{max} = \frac{V_{max}}{b \log_e \frac{a}{b}}$$

This gives

$$P = \frac{1}{377\Omega} \pi a^2 |E_{max}|^2 \left\{ \left(\frac{b}{a}\right)^2 \frac{1-|R|}{1+|R|} \log_e \frac{a}{b} \right\}$$

For a given power and a given outer conductor diameter (cost or geometrical constraints) the electric field will be minimum when

$$\Psi = \left(\frac{b}{a}\right)^2 \frac{1-|R|}{1+|R|} \log_e \frac{b}{a} = e^{-Z_c/30\Omega} \frac{Z_c}{60\Omega} \frac{1-|R|}{1+|R|}$$

is maximum.

When /R/ = 0 (a matched line) it is easy to show that Ψ is maximum for Z_C = 30Ω, which justifies the choice of 30Ω for the line between stubs and generators.
We have investigated the variations of Ψ also for the section AB. Then Ψ will not only depend on Z_C, the characteristic impedance, but also on the frequency (through /R/ the reflection coefficient which varies with the antenna impedance, which itself depends on frequency). Using the 1 x 2,(0) antenna array, with values for the impedance shown in Fig. 3.17, the variation of Ψ with characteristic impedance and frequency is shown in Fig. 3.31.

Although in the region 40 - 100 MHz the value of Ψ is larger for 50Ω than for 30Ω presently preference is given to 30Ω because of its better power handling capabilities in the critical high and low frequency region and the flatter curve. Detailed 3-D antenna calculations will be carried out to further refine the analysis.

3.2.6 Interface

3.2.6.1 Concept

In addition to connecting the antenna to the transmission line, the interface has two major tasks: to take up the thermal expansion between the vacuum chamber and the fixed transmission line, and to provide the separation between the vacuum of the torus and the controlled atmosphere of the transmission line (Fig. 3.32).

3.2.6.2 Solutions to take up the thermal expansion

The vacuum chamber has a radial thermal expansion of 8 mm and a change in height of 3.0 mm for the top antenna port (B_o) and 4.5 mm for the bottom antenna port (B_u).
Two solutions can be envisaged.
The most commonly used is the one with sliding contacts in inner and outer conductor. It has been used in TEXTOR and ASDEX.
It could also be incorporated in ASDEX Upgrade (Fig. 3.33).
However, those sliding contacts are not yet tested up to high power and long pulses, and can occasionally give arcing problems.
It is also easier to cool the center conductor internally if it is continuous.
Therefore we have also investigated the possibility to use bellows in inner and outer conductor (Fig. 3.34 - 35). Offers have been received and some prototypes will be ordered to test the voltage that can be withstood, to measure what their characteristic impedance is, and to ascertain whether they have to be mounted separately, as shown in Fig. 3.32, or can be combined in the same section, as in Fig. 3.34.

3.2.6.3 Feedthrough

The torus vacuum will extend up to the first stub near the antenna (Fig. 3.30, 3.32). This vacuum will be additionally pumped through direct connection with the large torus pumps.
A feedthrough between this T pieces and the stub itself will allow the stub to be operated under pressurized dry air

atmosphere. A similar feedthrough in the descending part of the transmission line will disconnect the vacuum of the torus from the atmosphere chosen for the rest of the transmission line.

The choice of vacuum feedthrough has not been made yet. A demountable, simple feedthrough is being developed in house (Fig. 3.36). It has the advantage of low cost, compactness and demountability and will be used if high power tests are succesful (up to now it could only be tested for short pulses up to 600 A, 50 ms and 30 kV, 10 ms).
An alternative is to use the feedthrough developed by Oak Ridge National Lab. (Fig. 3.37). This feedthrough has achieved impressive results on the teststand (600 A, 1 s; 75 kV, 5s) and is being used in TEXTOR. Both feedthroughs have the advantage that a natural transition from 6 1/8" vacuum to 9" pressurized side can be achieved.

3.2.7 The Antenna Array

3.2.7.1 Introduction

As already discussed in the physics sections, two types of antennas have been investigated: the 1 x 2 antenna array and the 2 x 2 antenna array configuration. The choice between both will be made in the light of results from JET, and possibly ASDEX.

In principle only four antennas will be installed, but four additional sectors could be fitted with antennas for a possible extension. The torus sector in which the antennas are installed is shown in Fig. 3.38.

3.2.7.2 Supporting structure

Each of the 8 planes has, as part of the vacuum vessel, a rectangular box. Four bushings with tapped holes, whose locations are precisely defined with respect to a reference plane are

welded onto each side of the box. The return conductor is bolted onto those bushings and thus firmely attached to the vacuum chamber. The return conductor then serves as the structural base on which the other parts of the antenna can be mounted (side pieces with limiter and Faraday screen).
Two types of return conductor are foreseen: the single flat type, 60 cm wide, suitable for the 1 x 2 antenna array, and the wider curved type, 78 cm (the limit being the width of the access ports $\lesssim$ 80 cm) suitable for the 2 x 2 configuration.

3.2.7.3 The two configurations

The 1 x 2 antenna array has a total width (with protection limiters) of 60 cm. The central conductor is 16 cm wide along its whole length and in the equatorial plane the distance between central conductor and return conductor is 14 cm (Fig. 3.40). The central conductor will be of the folded (trombone-JET) type (Fig. 3.41), or simply straigth (Fig. 3.42) with feedpoint top and bottom and short circuit in the equatorial plane. Those different shapes have been investigated /15/. Best results were obtained with "trombone shaped" loops (like the JET antenna). Model experiments together with further computer calculations will be used to finalize the choice and refine the geometry (distance to Faraday screen $\simeq$ 2 cm, capacitive loading required, distance $\simeq$ 2 cm).
The second configuration would be a 2 x 2 antenna array (Fig. 3.43). Because of its extended width in the toroidal direction, the return conductor is curved as is the central conductor and the Faraday screen. In addition, the width of the components is no longer constant, their boundary being defined by radial plane through the tokamak center. The connection for the 2 x 2 antenna array would be the same as the JET 2x2 array (Fig. 3.44). The feed point would be near the center, with short circuit top and bottom.

3.2.7.4 Faraday screen and side limiters

For the Faraday screen a solution similar to the one being constructed for the cooled ASDEX Faraday screen will be used. Tubes from stainless steel are coated with 20 μm Cu to reduce the rf losses, and further coated with 6 μm TiC to obtain a more plasma compatible surface.
For the side limiters too, the solution used on ASDEX has proved up to now effective. C blocks are soldered, with a Mo interlayer to a copper block which is bolted onto a cooled copper substrate. A slight modification was foreseen with respect to the ASDEX design. In our solution a stainless steel piece holds the bolts in place, while for ASDEX the bolts were attached with threads in the copper itself (Fig. 3.45)

3.2.7.5 Adaption to different plasma geometry.

ASDEX Upgrade has the possibility to experiment with three basic geometries: the single null geometry, double null geometry and limiter geometry. Because of the increasing cost and complexing of cooled antennas there is a strong incentive to be able to use the same antenna for more than one geometry. It did not seem practical to make an antenna that was moveable, or that could be adapted remotedly to the different geometries. However, a solution was found where the antenna adapted to one geometry could be changed to an antenna adapted to a second geometry without the need for new major components.

It consists of the following: in all cases the return conductor, at the same time the structural base is kept unchanged. The protection limiters and the Faraday screen are mounted on side pieces. By making limiters and screen each in two pieces (split in the equatorial plane) and by proper choice of the radius of curvature and the position of the center of the curvature the antenna can be adapted to the different geometries by changing only the side pieces on which the screen and the limiters are mounted (see Figs. 3.46 - 48).

If the central conductor is of the folded type (Fig. 3.41) it too must be changed. A conductor of the straight type (Fig. 3.42) may be adaptable to the different geometries.

3.2.7.6 Tests on ASDEX

Three types of investigations, directly related to the antenna, are in preparation. Their results could have an influence on the design of the ASDEX Upgrade antenna.

1. In the near future (May 1985) the Faraday screen of one ASDEX antenna (Fig. 3.49) will be exchanged for a different type. The present screen is almost optically closed to plasma particles (Fig. 3.50). It will be replaced by a screen of much simpler geometry transparent for plasma particle (Fig. 3.51). If the test proves succesful, the configuration of cooled Faraday screen for ASDEX Upgrade could be considerably simplified.

2. In the summer of this year one of the ASDEX antennas may be reconfigured into a 2 x 1,(π) array. This would provide additional information on the desirability of $k_{//}$ shaping and thus on the necessity to use a 2 x 2,(π,π) array on ASDEX Upgrade.

3. An optically closed, cooled Faraday screen for ASDEX will be installed in ASDEX in 1986. Experience on its construction and information on its behavior in the machine should be transferable to ASDEX Upgrade.

3.2.8 Control, data acquisition and diagnostics

3.2.8.1 General organization of the control system

The general organization of the control system for ICRH will be similar to that for ASDEX, which has proven effective.

The main parts are:
- the central control unit
- eventually a remote control unit
- the rf generator control system.

Central and generator control systems will be situated in direct neighbourhood of the generators. These main control units are connected with all ICRH components, supply systems and with the experiment controls.

The central control unit controls the whole system and mutually interlocks the different components of the system in order to prevent dangerous conditions. The central unit controls directly the tuning network, the coax switching system and the dummy load. It processes error indications of the protection system and starts automatically the needed reactions. It contains signal lamps of important operating states and failures of the ICRH system itself, of the power supply, crowbar and cooling systems and of the experiment.
There is an option, as developped for the ASDEX / W VII system, that the ICRH system can also be operated by a remote control unit situated directly in the machine control room. All commands, signals, measured values and error indications necessary to judge the operating conditions and to operate the system would be available once more at this remote unit.
The rf generator control system directly controls the rf power generator, which thereby can be operated independently or remote by the ICRH control. It contains an interlocking and protection system guaranteeing safe operation with respect to internal or external fault conditions. This system will be included in the order of the generator system.

3.2.8.2 Nominal value, operation modes

The rf output power (either the forward power or the net power delivered to the load ($P_{net} = P_{forward} - P_{reflected}$) can be

determined as nominal value at the generator control or at the remote control unit. The control deviation is limited to less than 5 % by means of a feedback system which is integrated in the generator control (Fig. 3.27). The nominal value can be set as square pulse at the generator control or as an arbitrary time function within safe limits at the central or remote ICRH control unit, or provided by the ASDEX Upgrade control system (feedback regulation of the plasma temperature).

In the case arcing in the antennas or lines is detected by directional couplers, the RF power is switched off, the generator control falls back into a stand-by state and tries to switch on the power again up to five times.

Besides the single pulse mode for heating purpose, triggered by the experiment timers, the generator control also allows a repeating mode with short pulses and adjustable high repetition rate and a continuous mode with the amplitude limited to 50 kW. These operation modes serve for antenna conditioning and for tuning purposes.

3.2.8.3 Diagnostics, data acquisition

The rf output power of the generator and return power, which is reflected to the generator by mismatched tuners or by arcing in the lines, are permanently checked by means of directional couplers at the generator output, the measured values being automatically processed by the protection system and the generator control for safety purpose.

Further directional couplers will be installed in each line in front of the matching network. Measuring line segments with voltage probes will be installed in each branch of the feeding line to detect the standing wave pattern. This information could allow the adjustment of the tuners step by step between the shots, as the RF power is being slowly increased. If reproducible

plasma and rf conditions can be achieved, an automatic tuning procedure may be performed by means of a closed feedforward loop, where a computer learns from the last shot how to improve the tuning for the next one. For long pulses it may even be possible to correct the tuning automatically within a shot by a feedback loop.

Voltage probes will be installed or high loaded parts of the system to detect overvoltages or arcing, with faults leading to an automatic shut down of the RF power by the safety system.

To supervise the antennas, temperature probes will be inserted and also a visual observation of the antennas will be envisaged. Further a set of field measuring probes within the torus could be helpful for a critical examination of the heating result.

The incorporation of a microwave reflectometer in the antenna, to measure the density variation directly in front of the antenna, could help in understanding the results and may even be incorporated in the automatic tuning system (as the antenna impedance is particularly sensitive to changing density and density gradients in front of the antenna).

The acquisition and processing of the measured data will be performed by means of the data acquisition system of the ASDEX Upgrade.

3.2.9 Manpower

The ICRH system will be developed, built and operated by the ICRH group of the IPP. The tasks of this groups are:

- ICRH experiments at ASDEX, W VII and, later ASDEX-Upgrade
- Antenna development for ASDEX, W VII and ASDEX-Upgrade
- Planning and installation of the ICRH-RF-system for ASDEX-Upgrade

Table X shows the major tasks and the staff of the ICRH group. For developing and building the ICRH system for ASDEX-Upgrade, one scientist, two engineers and 2 technicians are needed in addition to the existing staff.

3.2.10 Cost estimate and time schedule

(included in chapter 1)

Acknowledgements

It is a pleasure to acknowledge the design and drafting skills of A. Akbulut, H. Kötterl, J. Leinthaler, P. Schiller, Mrs. E. Sombach, R. Zickert, and the secretarial help of Mrs. Steppi, Mrs. Kraft and Mrs. Alberter.

Table X MANPOWER REQUIREMENT

	Professional	Ing.grad.	Technician
1) General Coordination	1	1/3	
2) ASDEX Heating experiments	1		
3) W VII Heating experiments	1	1	1
4) Generators Operation ASDEX/W VII			
Planning for ASDEX Upgrade	1	1/2	
5) Antenna calculations			
absorption calculation	1		1/2
design, development	1	1/3	
6) Coax. Comp. Planning for ASDEX Upgrade			
Operation ASDEX/W VII		1	
Development of special components	1	1/3	
RF tests		1	1
7) Control / Measurement			
RF diagnostic ASDEX/W VII		1	1
Control)			
RF diagnostic)ASDEX Upgrade	1		
Data processing)		1/2	1/2
8) ICRH theory	1		
Total	8 + 1 N.N.	4 + 2 N.N.	2 + 2 N.N.

References

/1/ E. Mazzucato et al.
Plasma Physics and Controlled Nuclear Fusion Research
(Thenth Int.Conf., London 1984), paper CN-44/F-I-2.

/2/ J. Post, D. Hwang et al.
Princeton Plasma Physics Laboratory Report,
PPPL-1966, December 1982.

/3/ R.R. Weynants
Phys.Rev.Lett. 33 (1974) 78.

/4/ D. Hwang et al.
Phy.Rev.Lett. 51 (1983) 1865.

/5/ M. Porkolab et al.
Plasma Physics and Controlled Nuclear Fusion Research.
(Thenth Int.Conf., London 1984) paper CN-44/F-II-1.

/6/ K. Odajima, H. Matsumoto, H. Kimura et al.
Heating in Torodal Plasmas (Proc. 4th Int.Symp., Rome 1984)
Vol. 1 (1984) 243.

/7/ IPP-Jahresbericht 1984

/8/ JET Joint Undertaking
Progress Reoport 1983

/9/ J. Luxon et al.
Controlled Fusion and Plasma Physics
(11th European Conf., Aachen 1983)
European Physical Society, 1983, Vol 1, 99.

/10/ J. Adam et al.
Implementation of Additional Heating on Tore Supra
Report Association Euratom- CEA, May 1983.

/11/ H. Takahashi
J.Phys., Col. c6, 38 C6-171 (1977)

/12/ M. Brambilla
IPP Report 4/216, Max-Planck-Institut für Plasmaphysik,
February 1984

/13/ M. Söll, E. Springmann
IPP Report 4/215, Max-Planck-Institut für Plasmaphysik,
February 1984.

/14/ K. Theilhaber, J. Jacquinot
Nuclear Fusion, 24. (1984) 541.

/15/ M. Söll, F. Wesner
Fusion Engineering (10th Symp., Philadelphia, 1983)
IEEE, New York 1983, Vol.1,600.

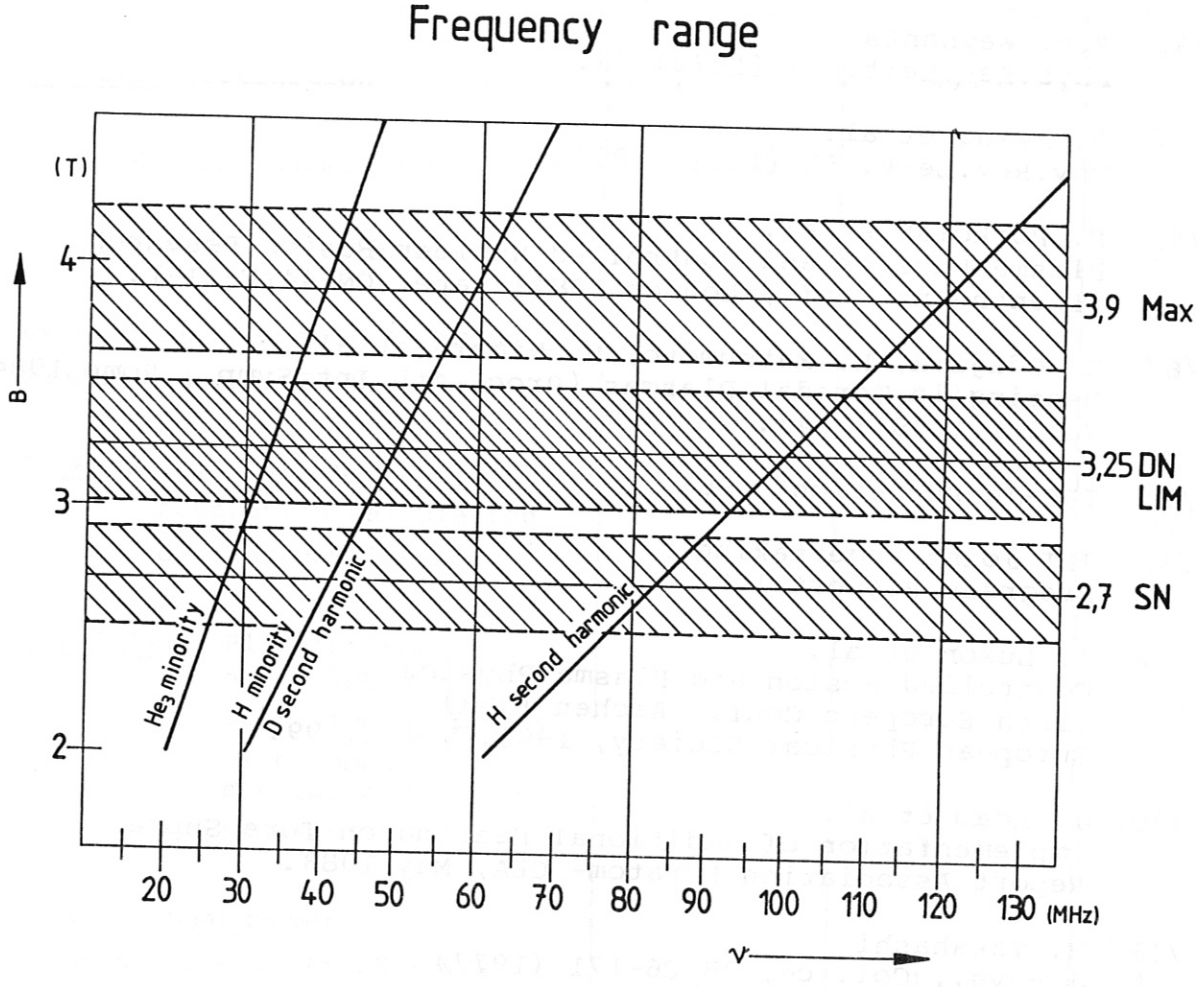

Fig. 3.1: Relation between frequency and magnetic field for the cyclotron resonances of H, D, He^3

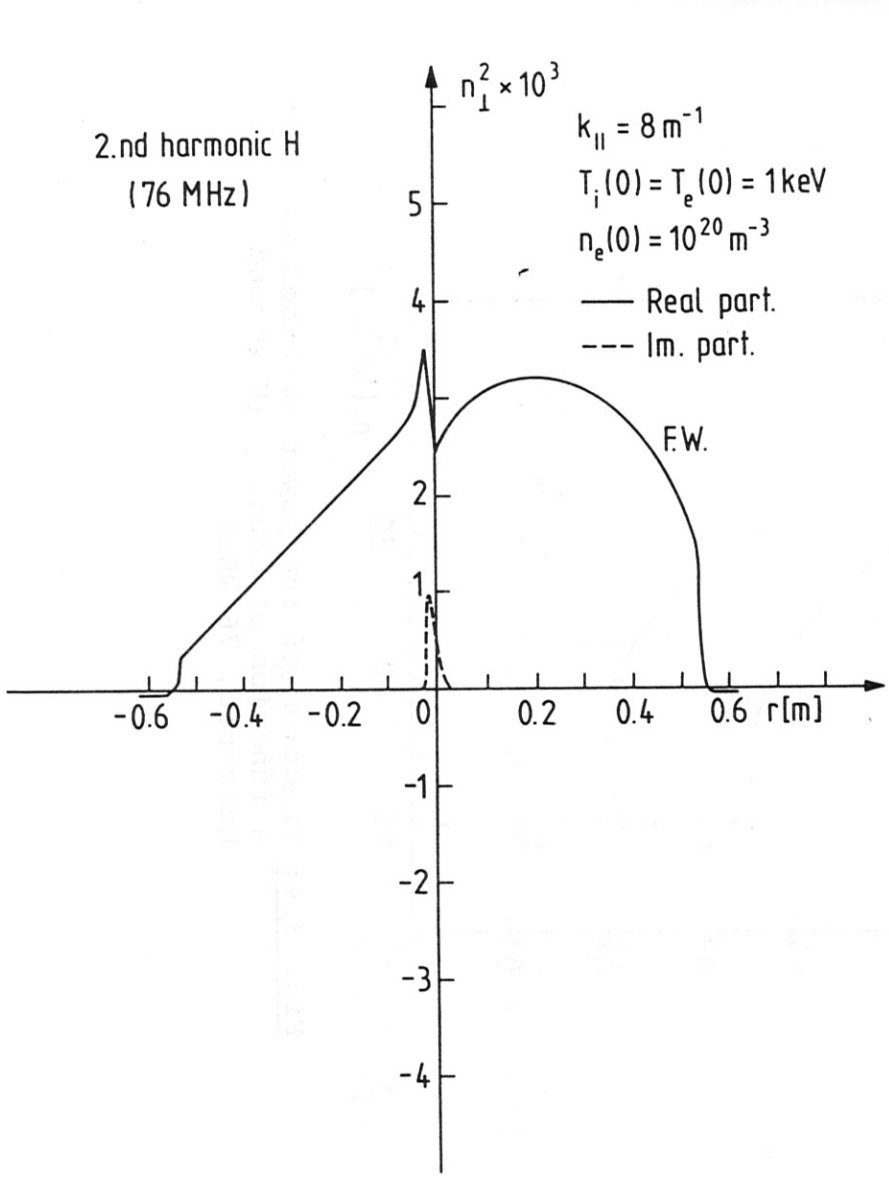

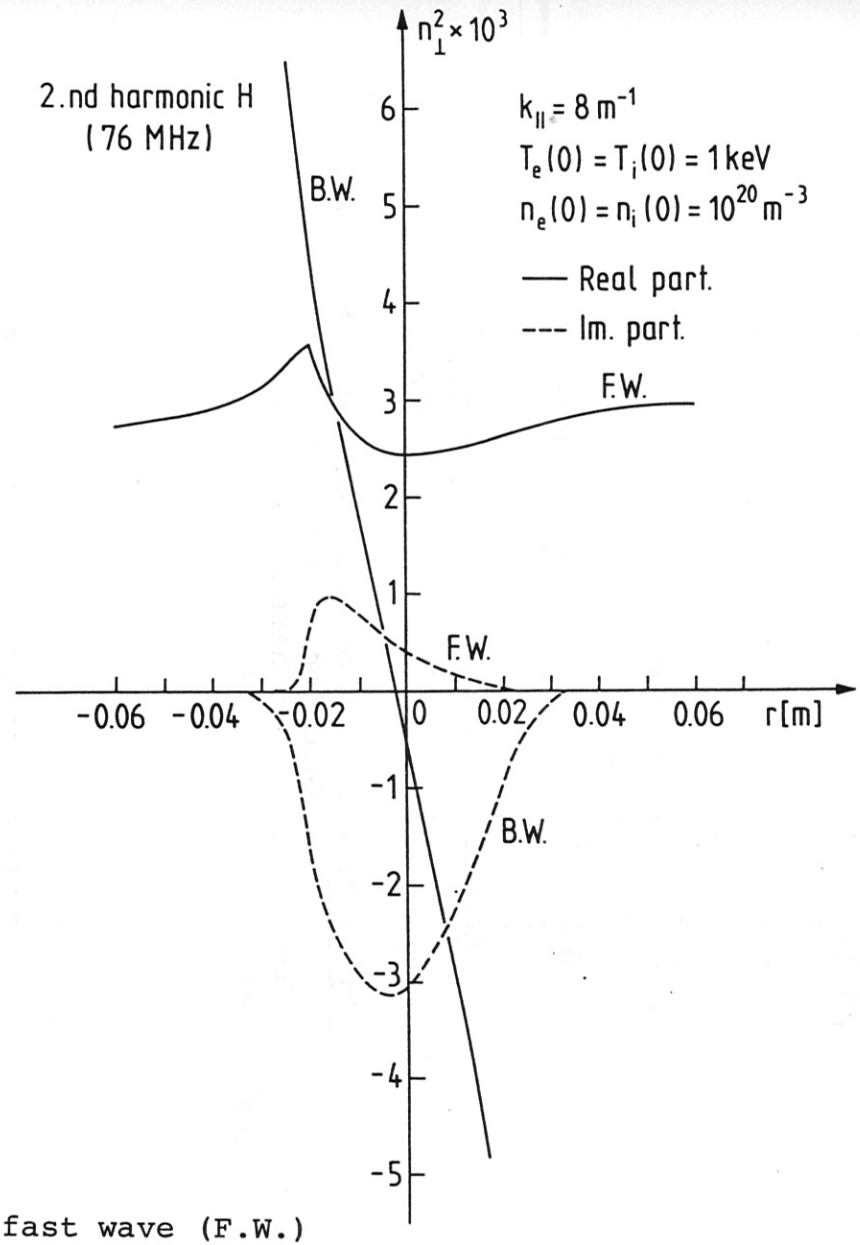

Fig. 3.2: a) Dispersion relation of the fast wave (F.W.)

b) Dispersion relation of the fast wave and the ion bernstein wave (B.W.) near the plasma axis

Density and temperature profiles according to Fig. 3.10

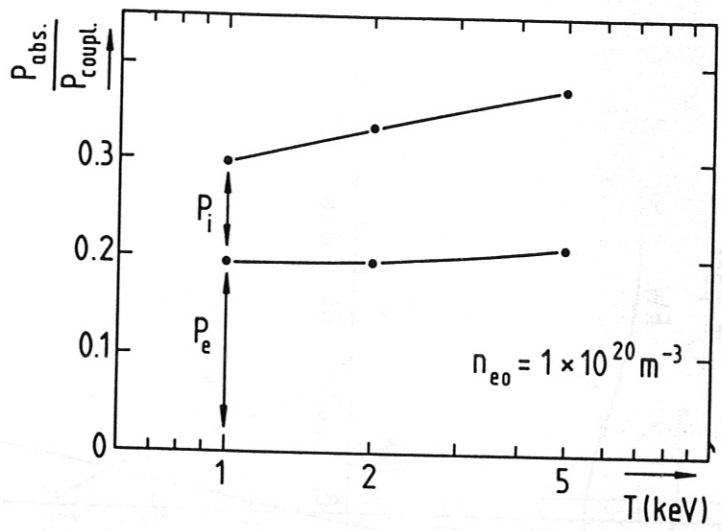

Fig. 3.3: Fraction of the power absorbed as a function of temperature (H second harmonic 76 MHz)

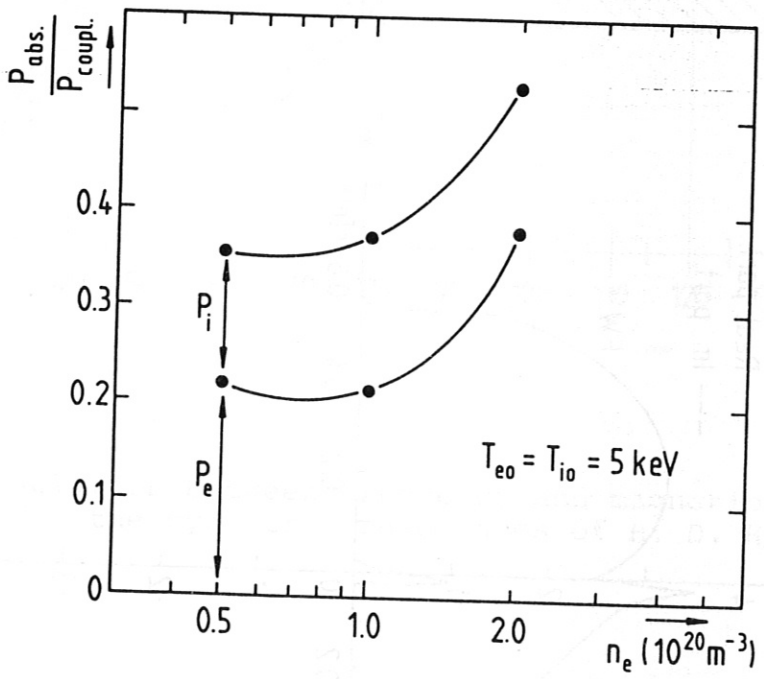

Fig. 3.4: Fraction of the power absorbed as a function of density (H second harmonic, 76 MHz)

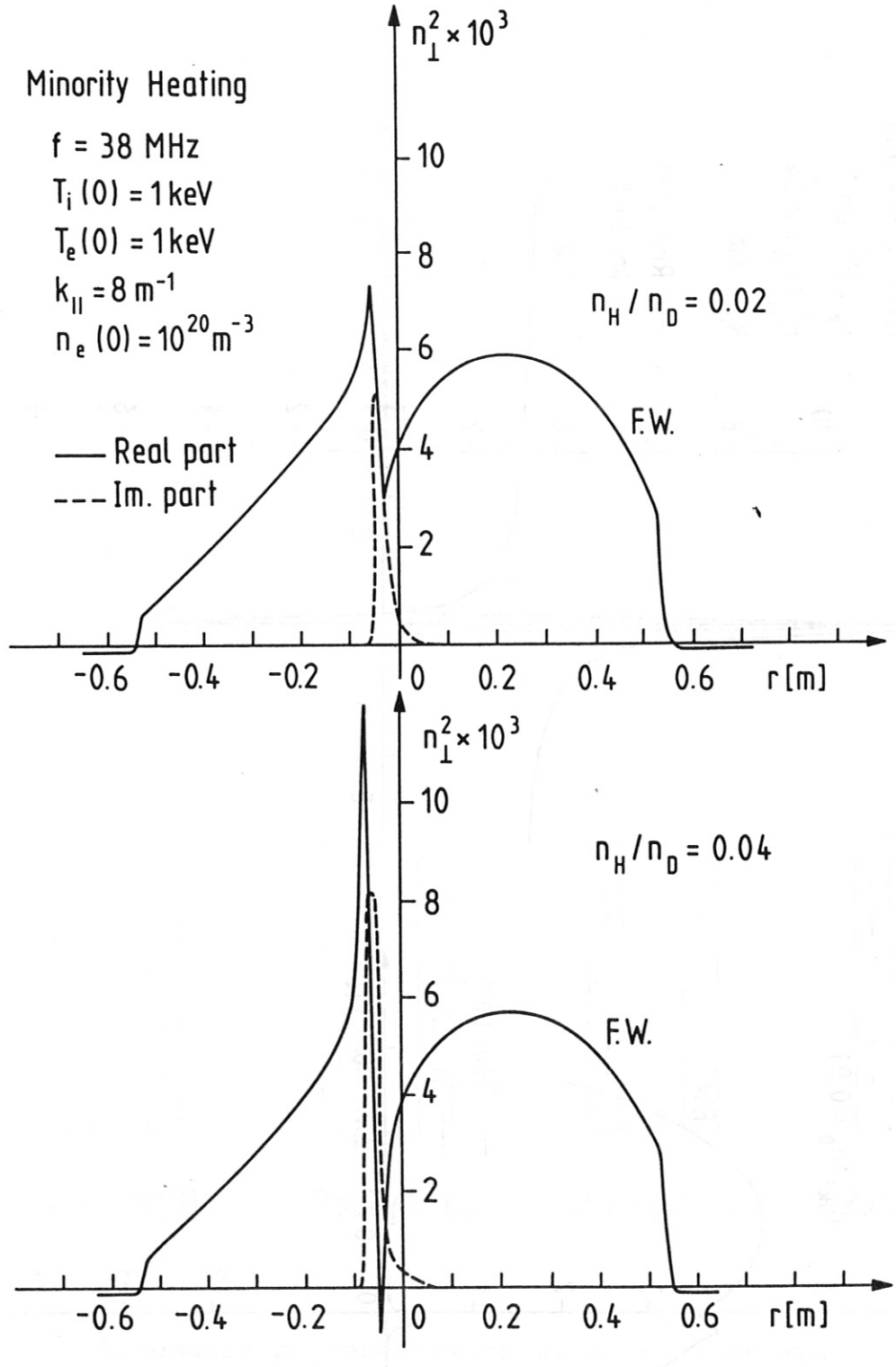

Fig. 3.5: a) Dispersion relation of the fast wave for a hydrogen minority concentration of 2 %

b) Idem for a concentration of 4 %

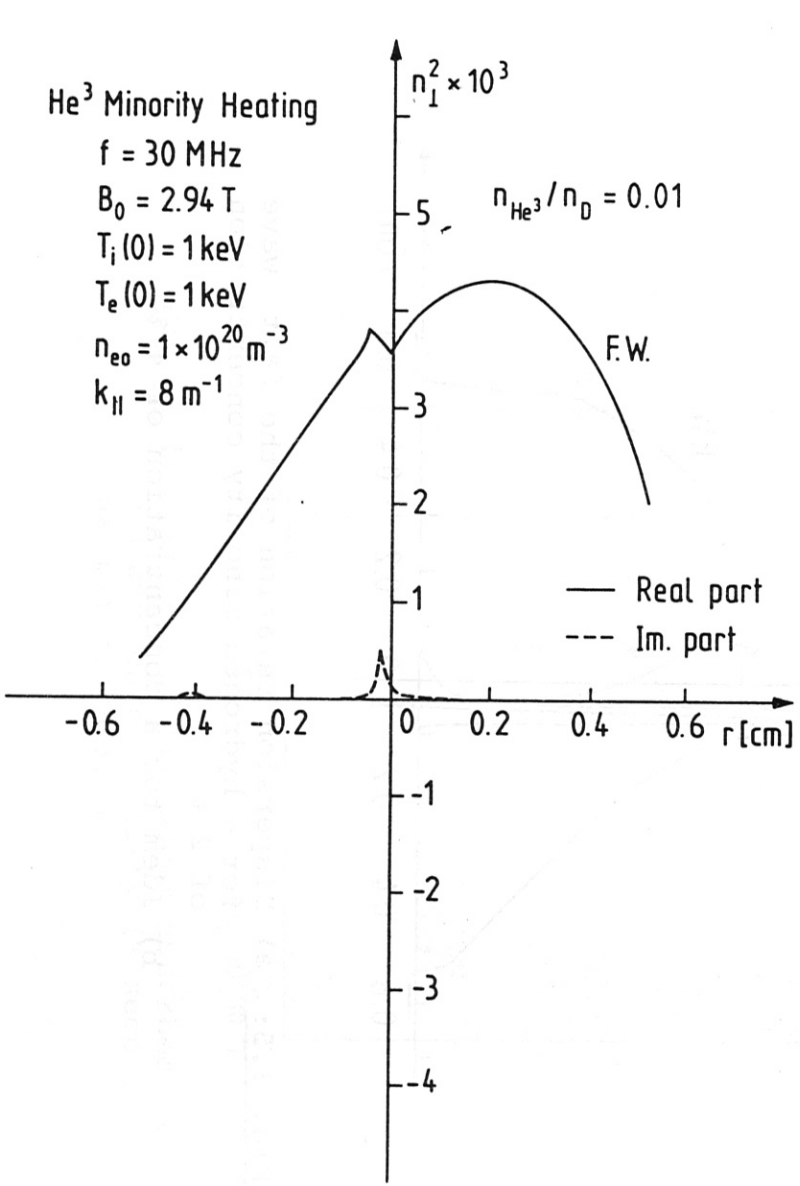

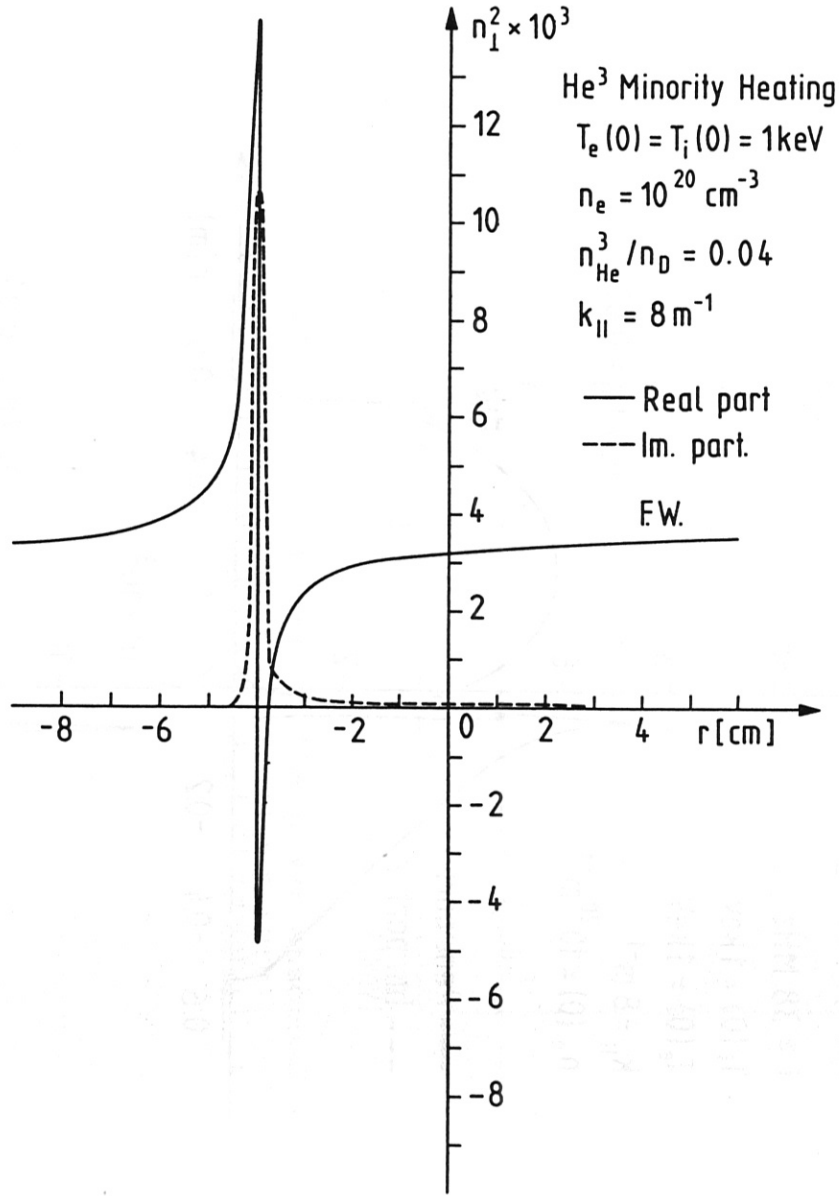

Fig. 3.6: a) Dispersion relation of the fast wave for a H_e^3 minority concentration of 1 %

b) Idem for a concentration of 4 %

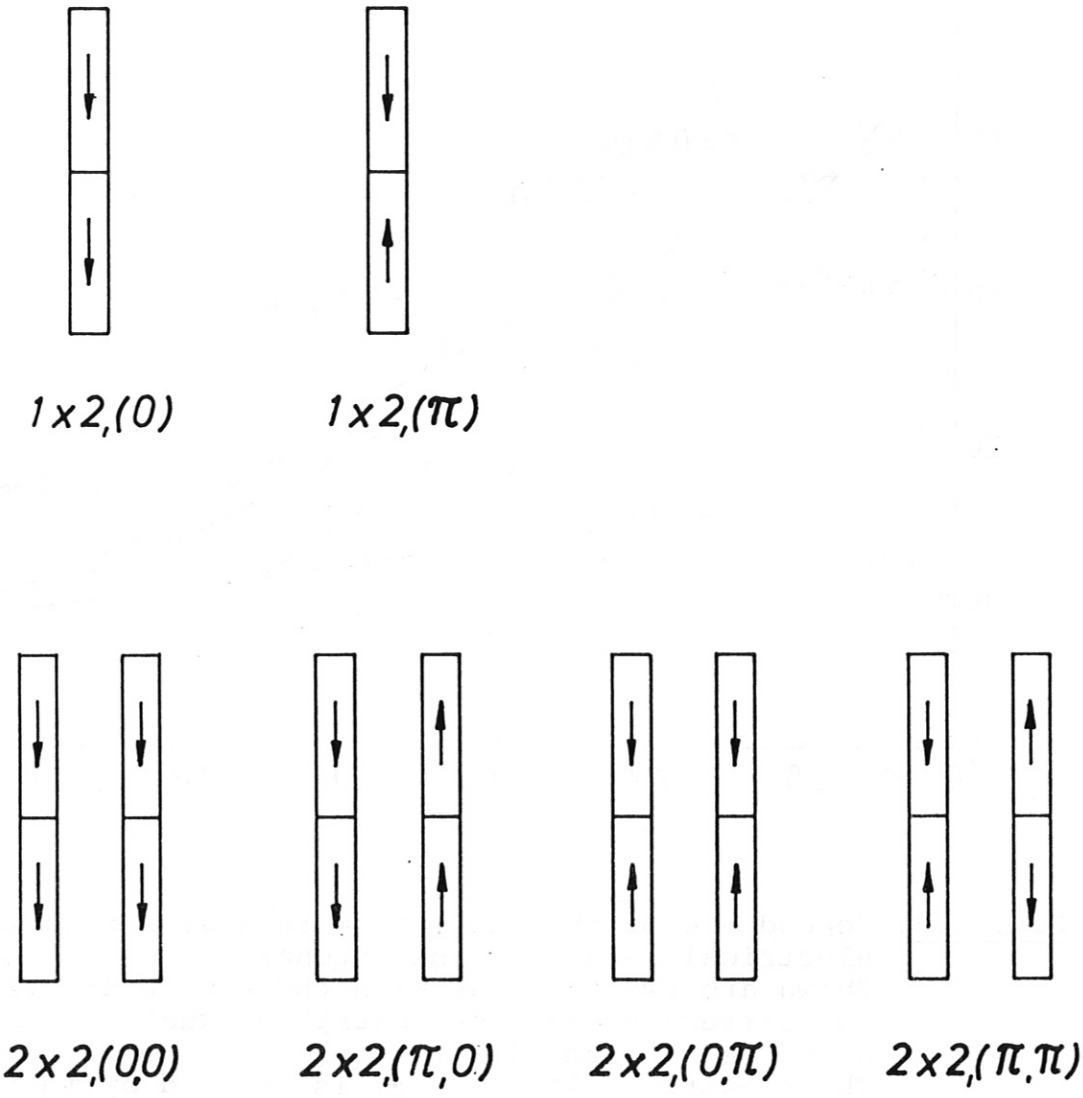

Fig. 3.7: Schematic representation of antenna arrays with corresponding notation

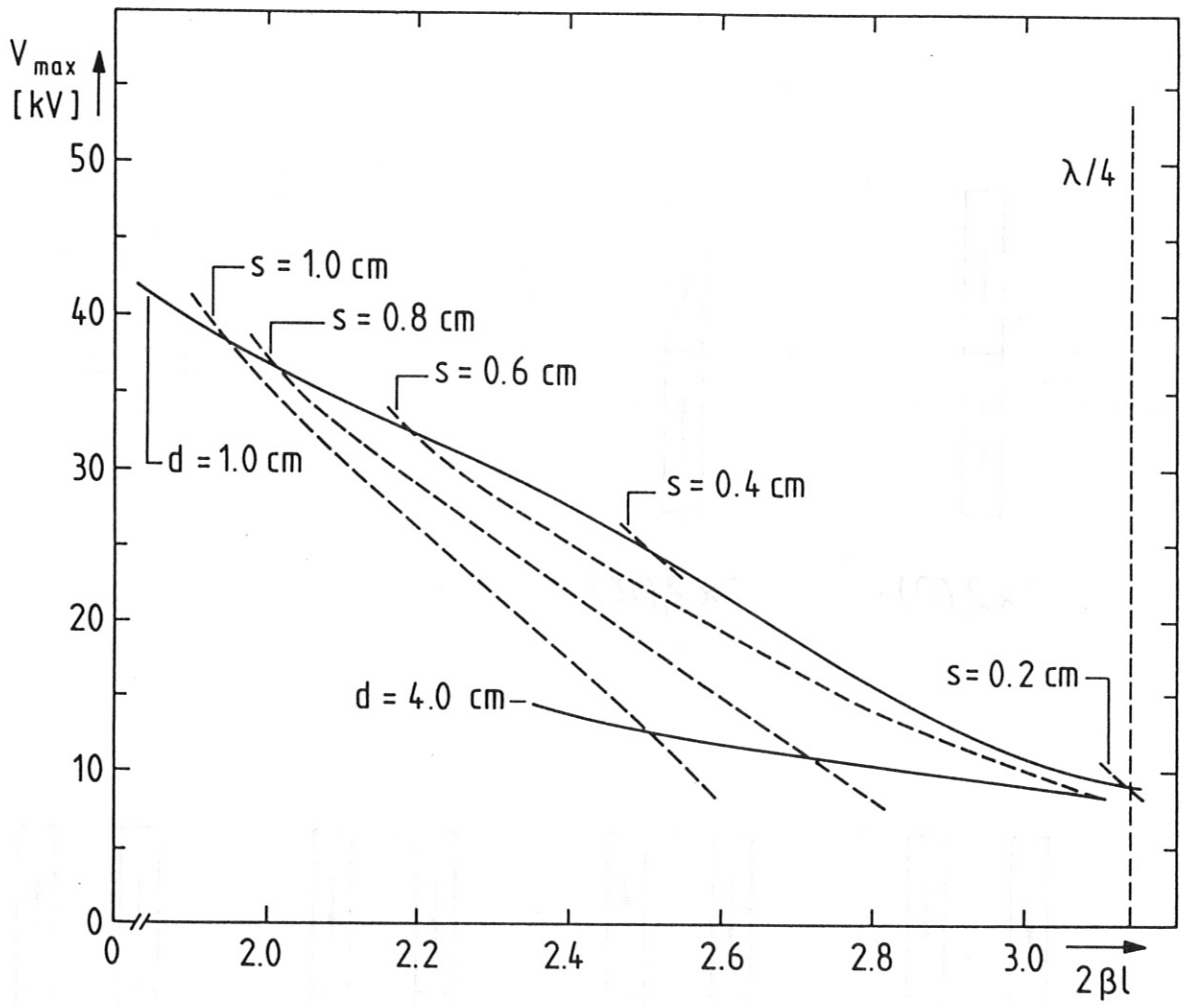

Fig. 3.8: Dependence of the maximum voltage as a function of electrical length of the antenna.
Shown are two antennas with the same width ($2 w_z$ = 42 cm) but different distance central conductor - return conductor (d = 1 cm, 4 cm).
The electrical length $2 \beta l$ is changed by moving the Faraday screen nearer to the central conductor (s = 1 cm — 0.2 cm)

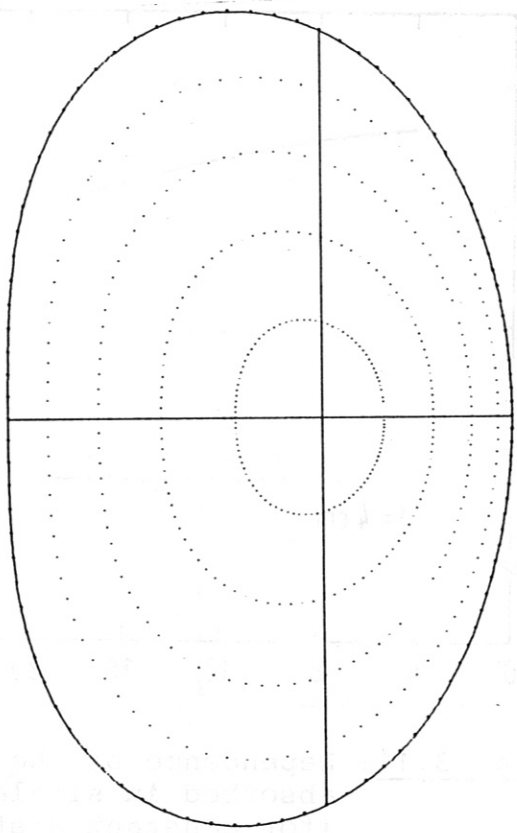

Fig. 3.9: Flux surface plot used with the ray tracing program RAYIC

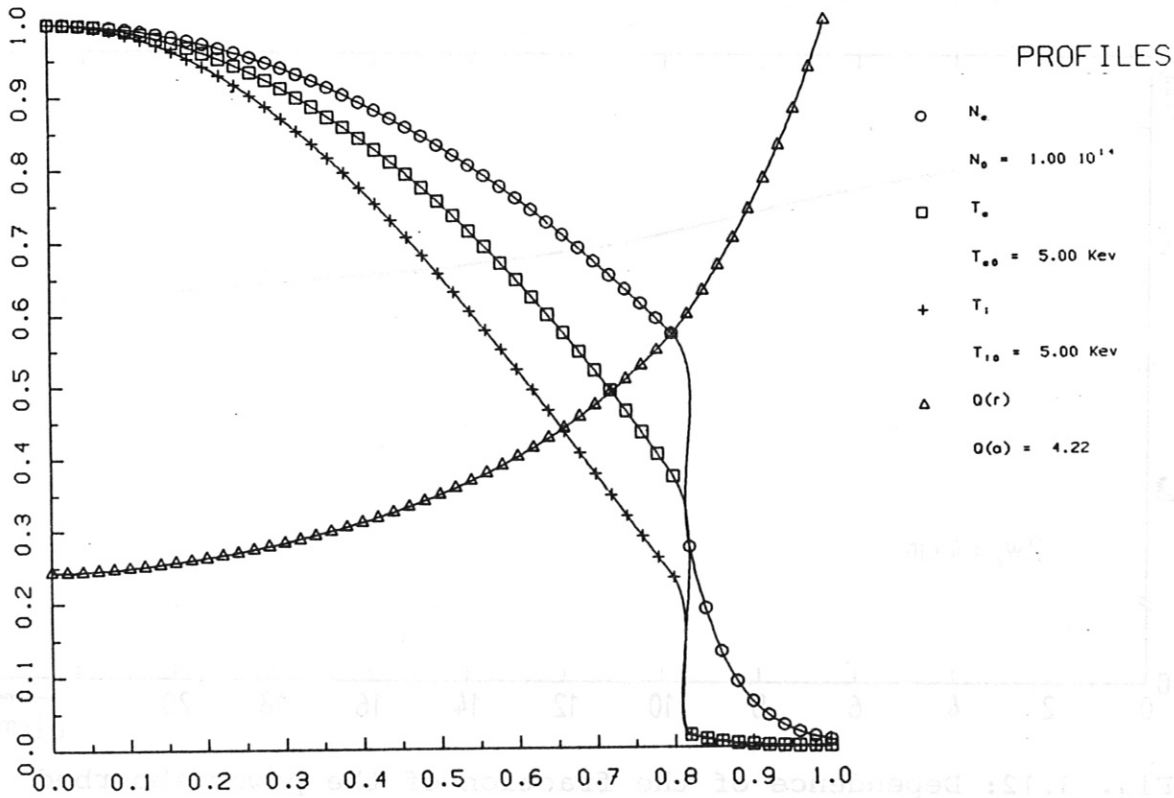

Fig. 3.10: Profiles of n_e, T_e, T_i and q used for the program RAYIC

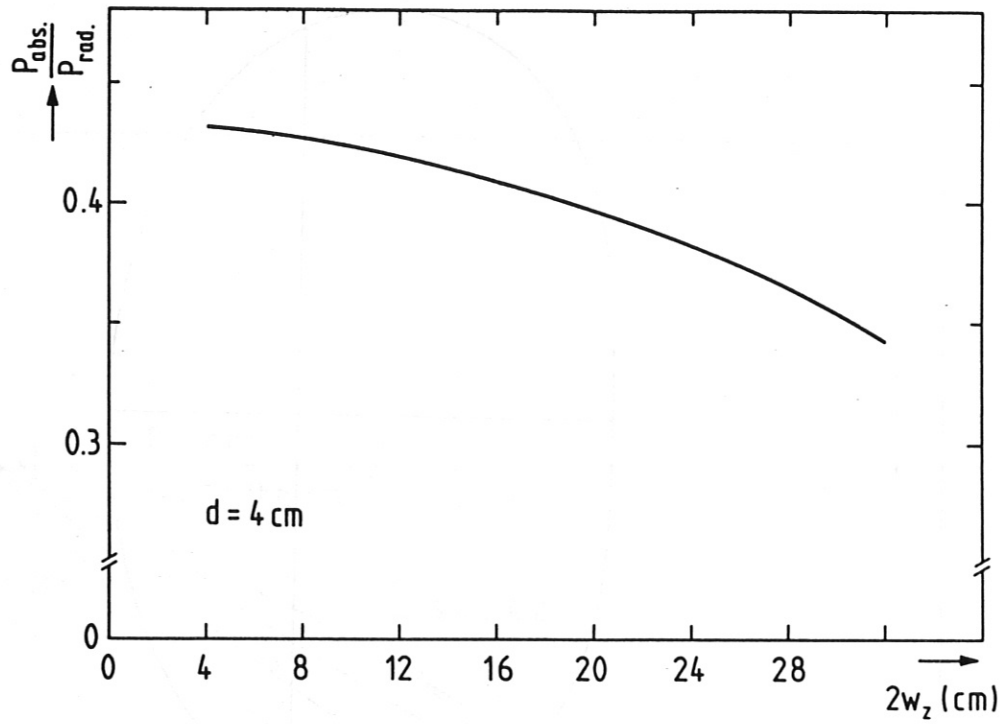

Fig. 3.11: Dependence of the fraction of the power absorbed in single pass on antenna width (for constant distance central conductor - return conductor d = 4 cm)

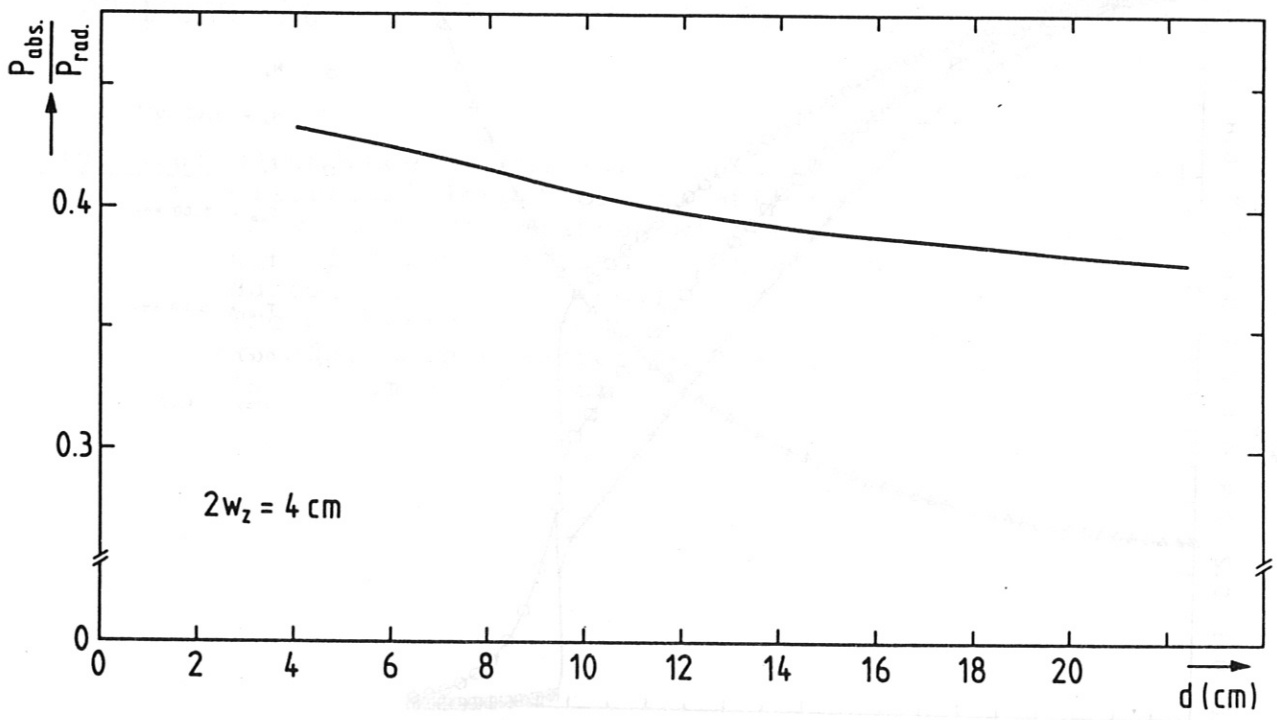

Fig. 3.12: Dependence of the fraction of the power abosrbed in single pass on the distance central conductor - return conductor (for constant width 2 w_z = 4 cm)

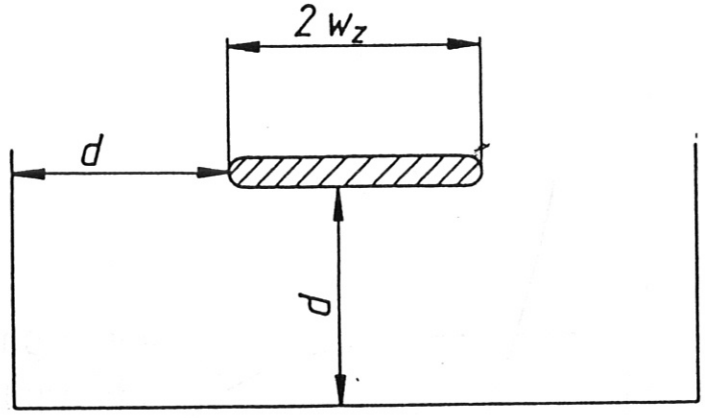

$$2 w_z + 2d = c^{te}$$

Fig. 3.13: Relation between the antenna width (2 w_z) and the distance central conductor - return conductor (d) by given constraint on the total width

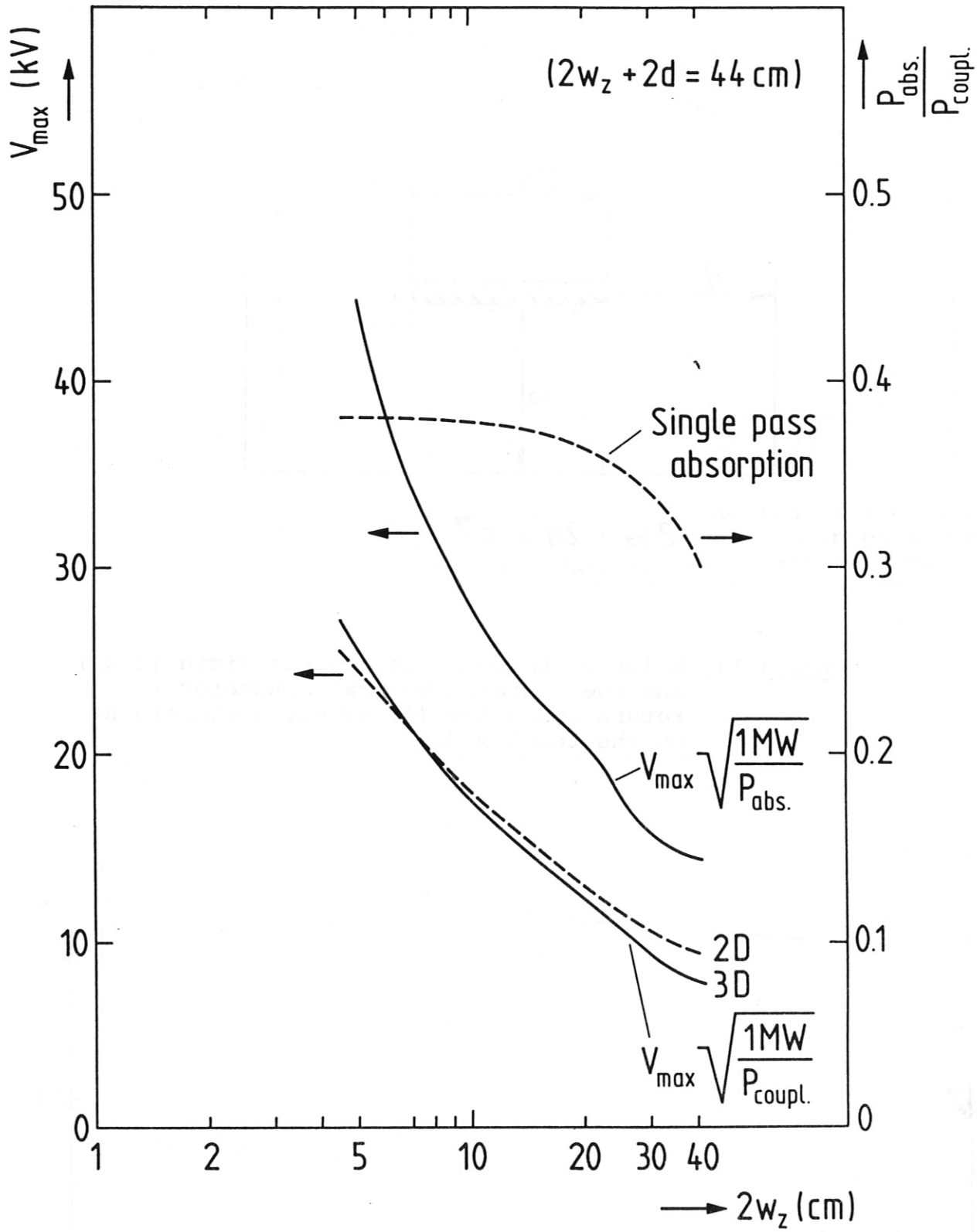

Fig. 3.14: Maximum voltage per MW coupled and per MW absorbed in single pass as a function of the antenna width w_z (varying at the same time d so that 2 w_z + 2d = 44 cm)
Fraction of the power absorbed as a function of the antenna width.
Second harmonic H, ν = 76 MHz

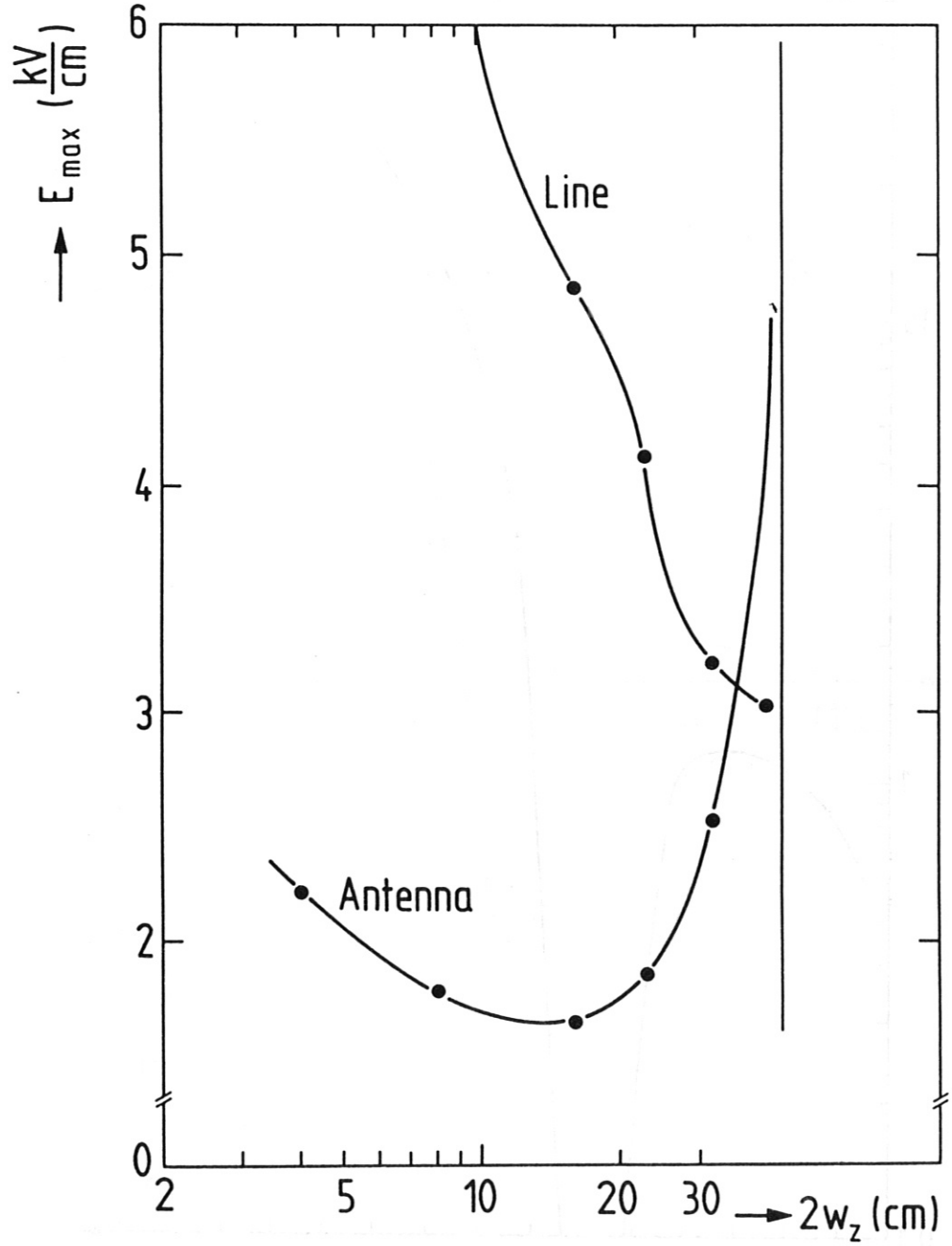

Fig. 3.15: Maximum field in the antenna // B, and in the line per MW absorbed in single pass as a function of the antenna width (and keeping $2\ w_z + 2d = 44$ cm)

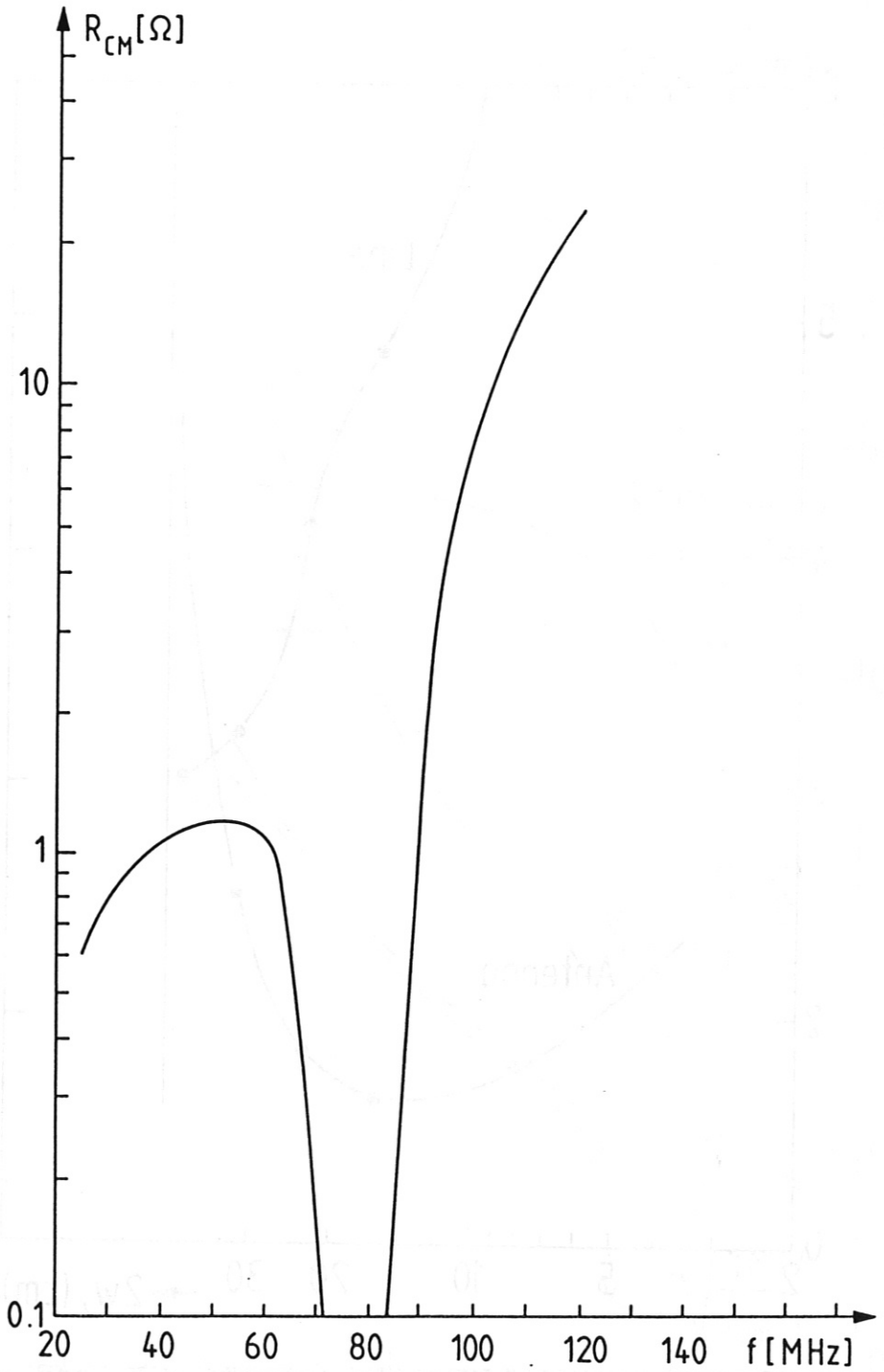

Fig. 3.16: The power going into coaxial modes for a 1x2,(0) antenna is given by $P_{CM}=R_{CM}.I^2$ where R_{CM} is shown in the figure as a function of frequency and I is the antenna current

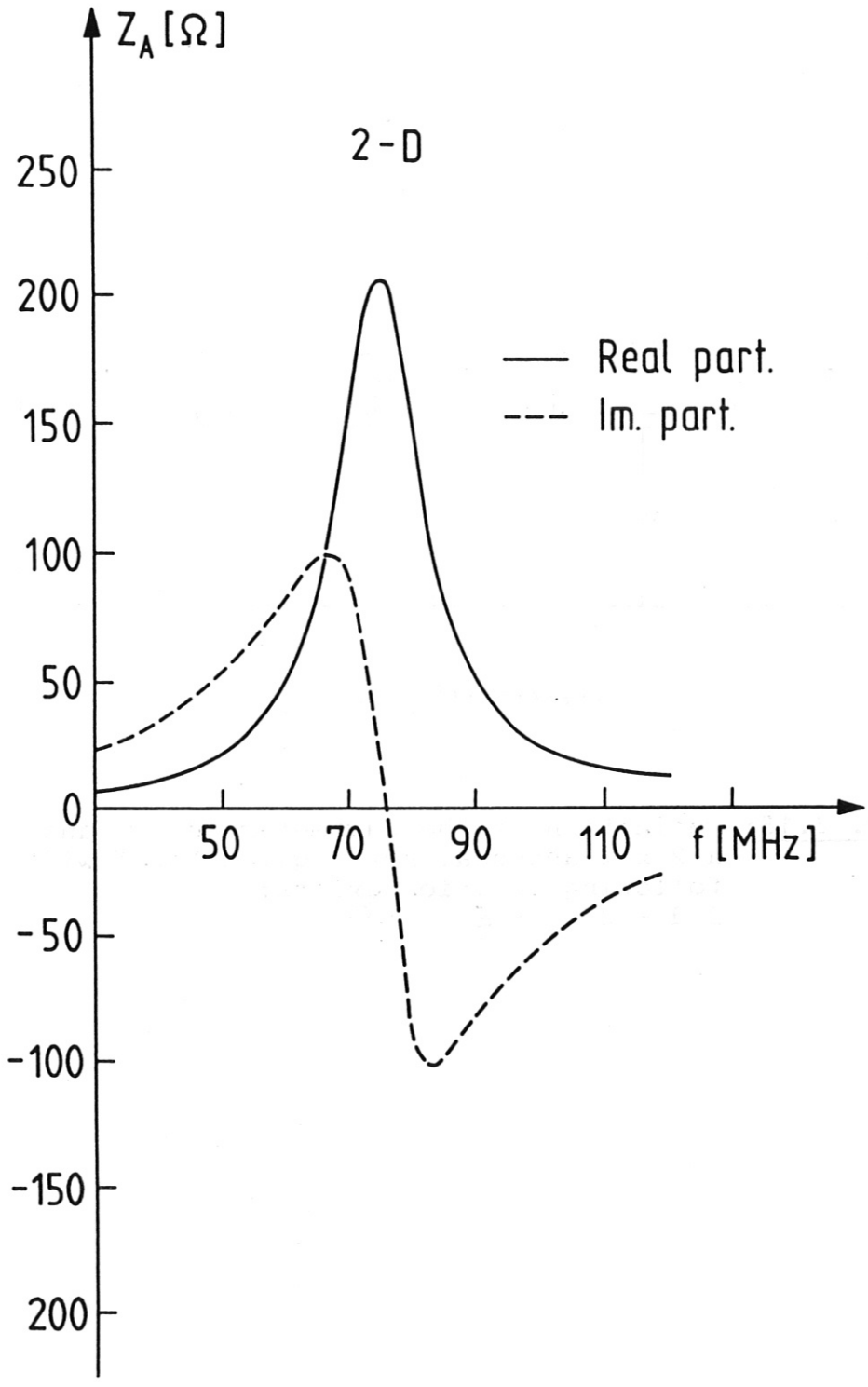

Fig. 3.17: Real and imaginary part of the antenna impedance. The resonance is at 76 MHz.

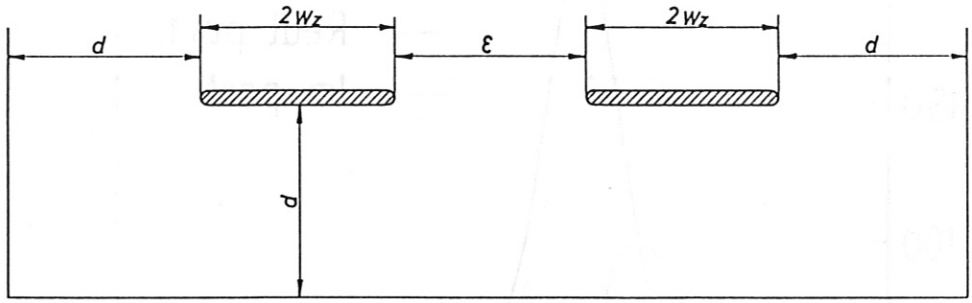

$$2W_z + 2d + \varepsilon = c^{te}$$

Fig. 3.18: Definition of the parameters d, w_z and for a 2 x 2 antenna. For a given total width following relation exists:
2 d + 2 w_z + ε = c^{te}.

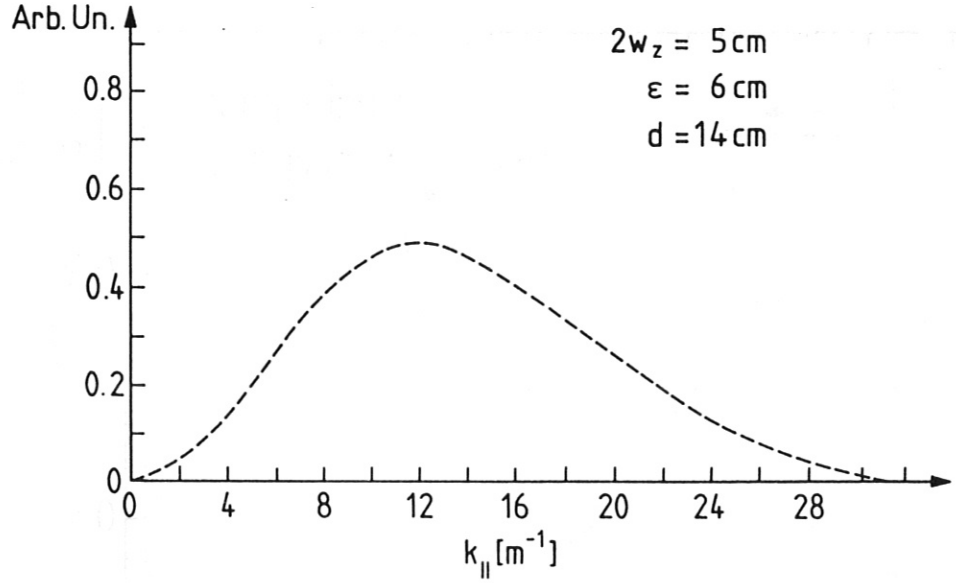

Fig. 3.19: $k_{\parallel}$ spectrum of the power radiated by a 2 x 2, (π, π) antenna with 2 w_z = 5 cm, ε = 6 cm, d = 14 cm
The spectrum is symmetric with respect to $k_{\parallel}$ = o

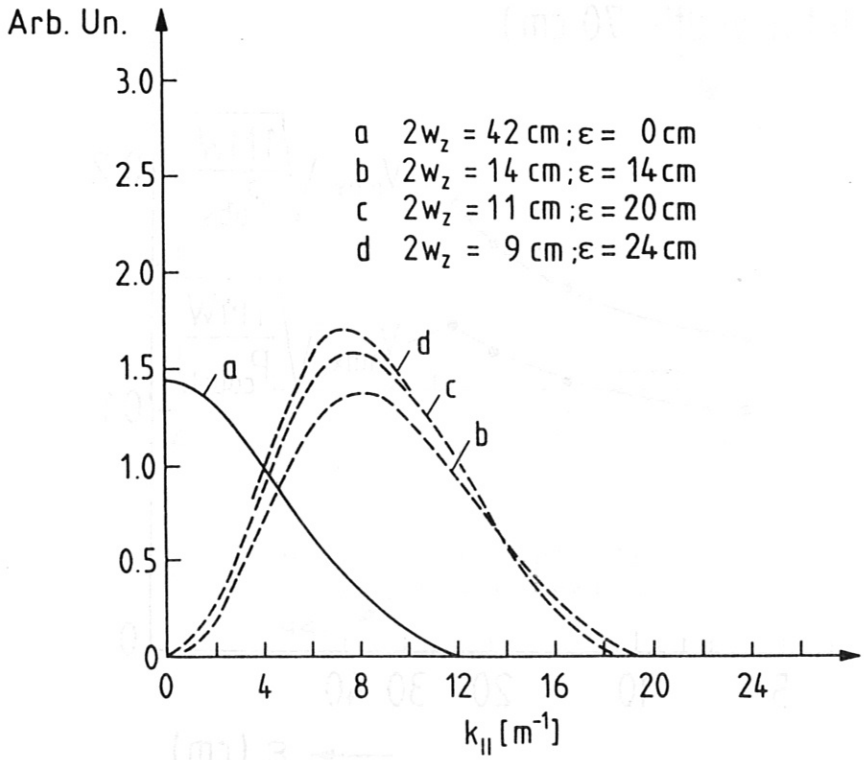

Fig. 3.20: $k_{\parallel}$ spectrum of the power radiated by different antenna configurations.
The curve a corresponds to a 1x2 (0) antenna array, the curves b, c, d are for 2x2, (π, π) antenna arrays
The spectra are symmetric with respect to $k_{\parallel}$ = o

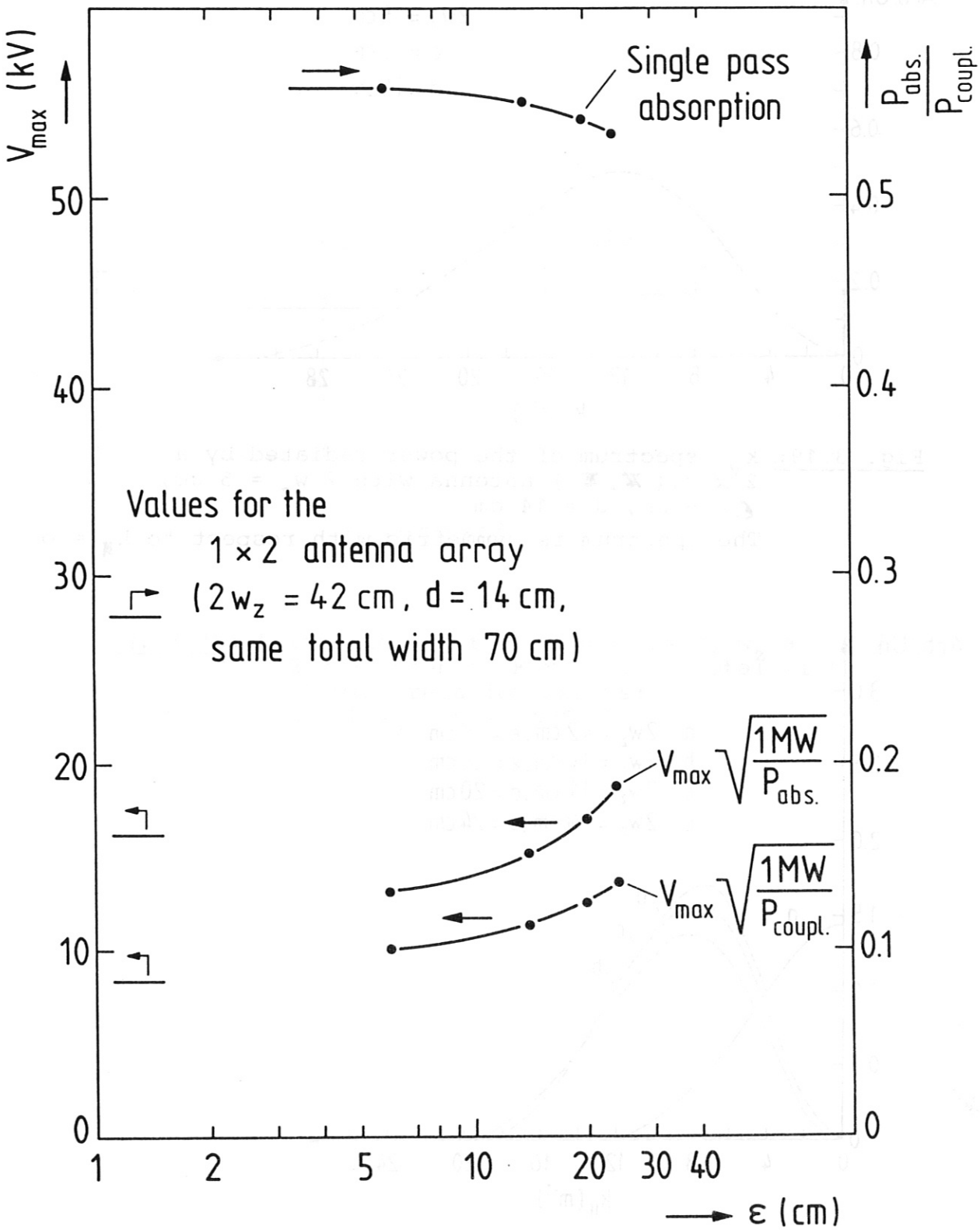

Fig. 3.21: Maximum voltage per MW coupled and per MW absorbed in single pass as a function of the gap ε between the two central conductors of a 2x2 (π,π) array (keeping 2 w_z + 2d + ε = 70 cm and d = 14 cm). Fraction of the power absorbed in single pass. Second harmonic ν = 76 MHz.

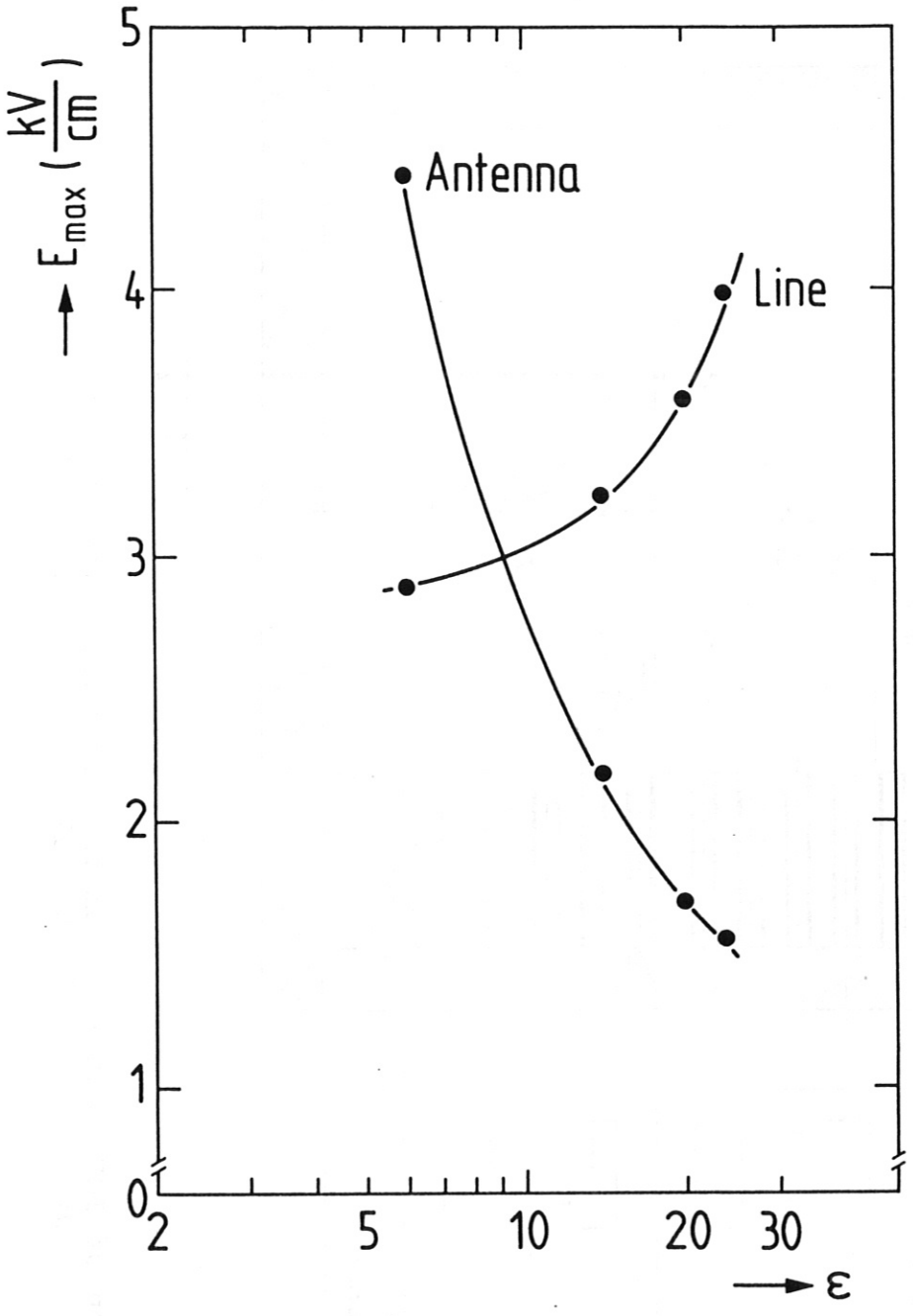

Fig. 3.22: Maximum electric field in the antenna // B, and in the transmission line as a function of the gap e .

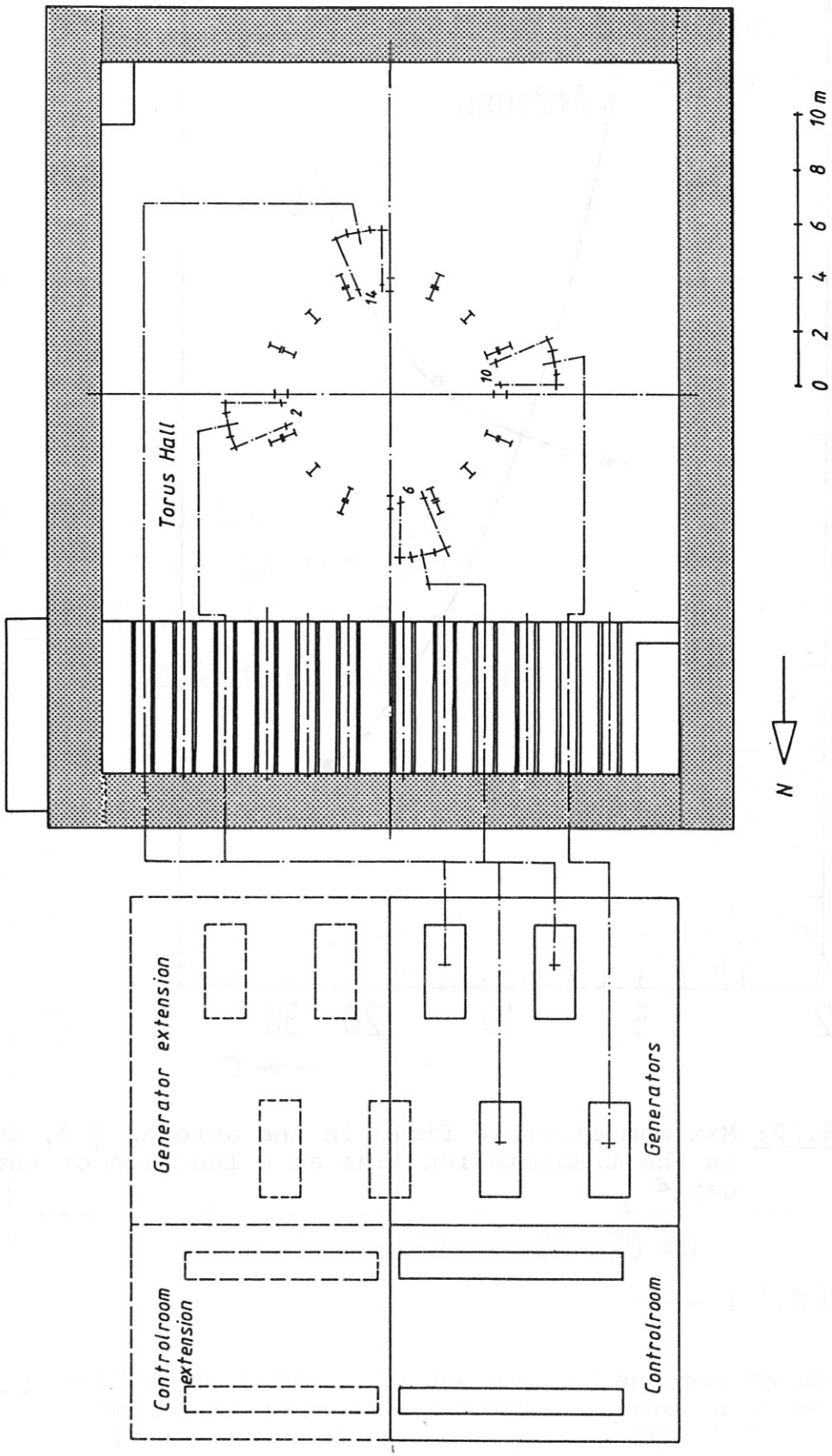

Fig. 3.23: Location of ICRH control room and generator with respect to the experiment with its shielding wall

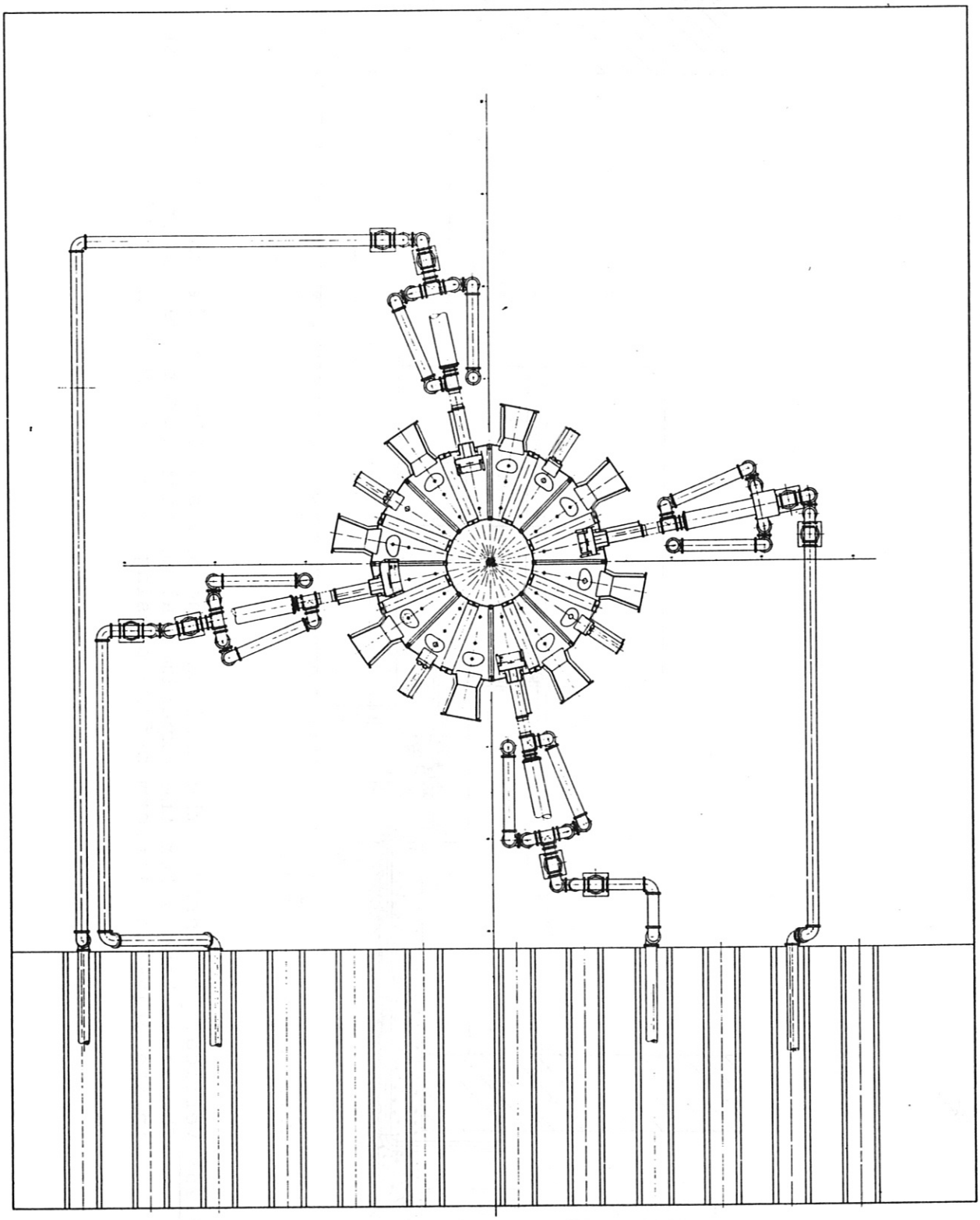

Fig. 3.24: Position of the antennas and the transmission lines with regard to the ASDEX Upgrade

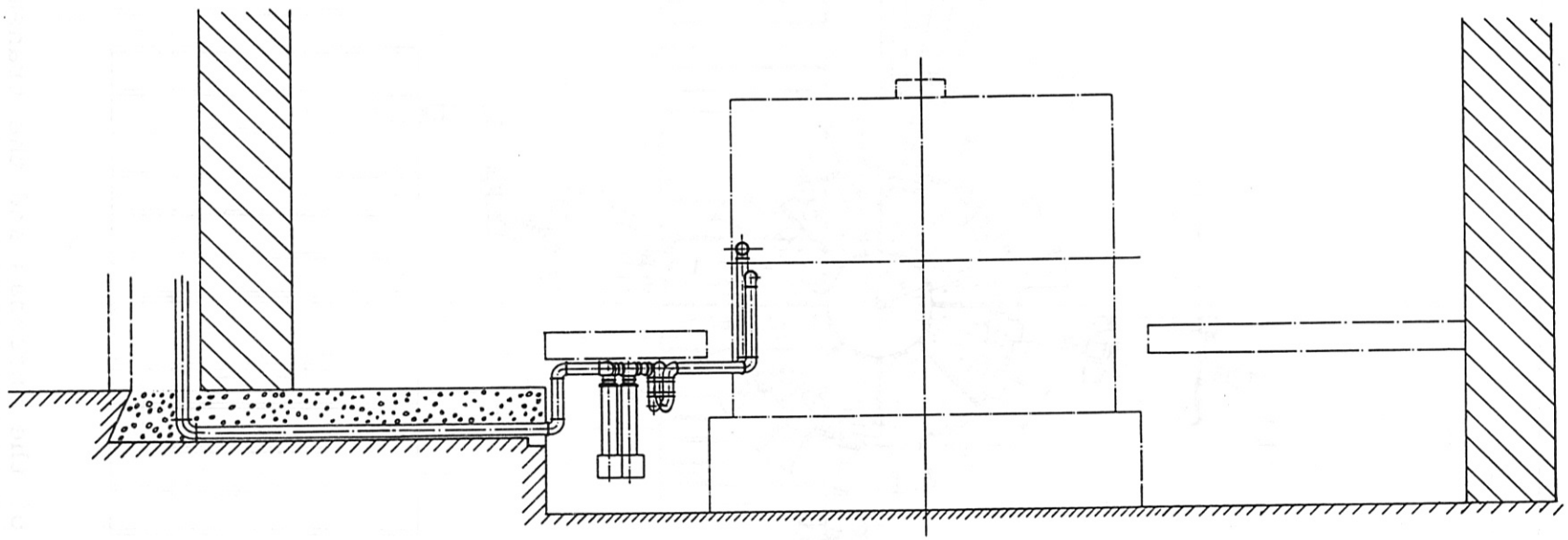

Fig. 3.25: Vertical cut through the hall showing the position of the transmission lines. The lines hang under the experimental platform, continue their way in channels in the drive-in platform before passing under the shielding wall

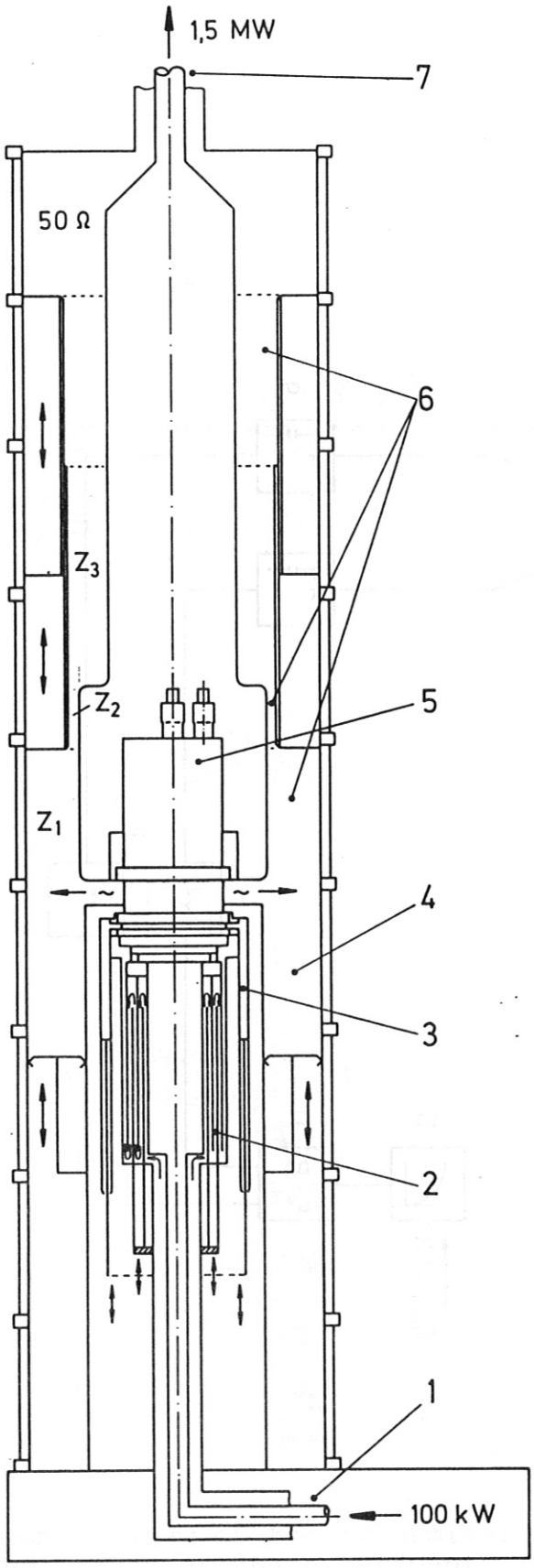

Fig. 3.26: Coaxial final amplifier stage of the ASDEX / W VII generators

1 power input, 2 $\lambda/4$ input transformer,
3 grid-screen grid circuit (adjustable $\lambda/2$ line)
4 adjustable short circuited line (inductance)
5 power tetrode (BBC 650-2), 6 output line transformer (lines of adjustable length)
7 output line

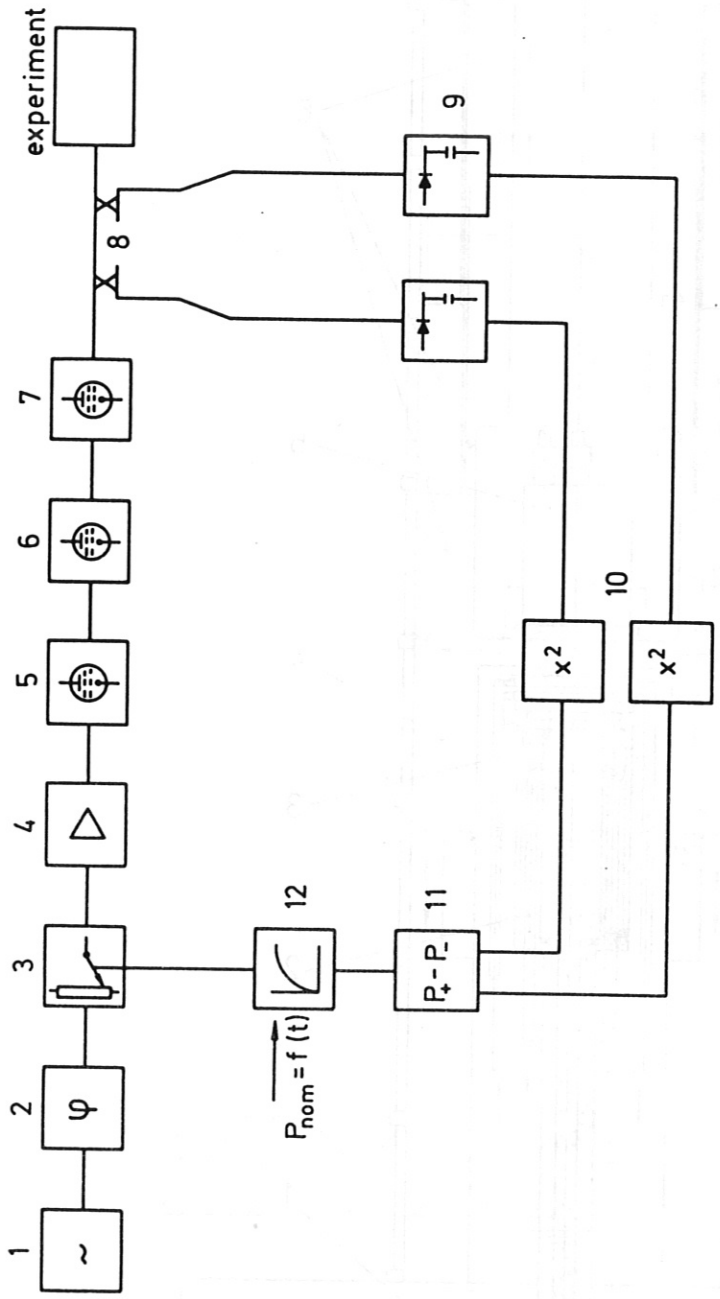

Fig. 3.27: Block diagram of the ICRH generator and the feedback control

1 oscillator, 2 phase shifter, 3 attenuator,
4 wideband amplifier, 5-7 predriver, driver and final amplifier stages,
8 directional couplers (foreward and reflected power), 9 detectors,
10 squaring, 11 subtractor, 12 regulator

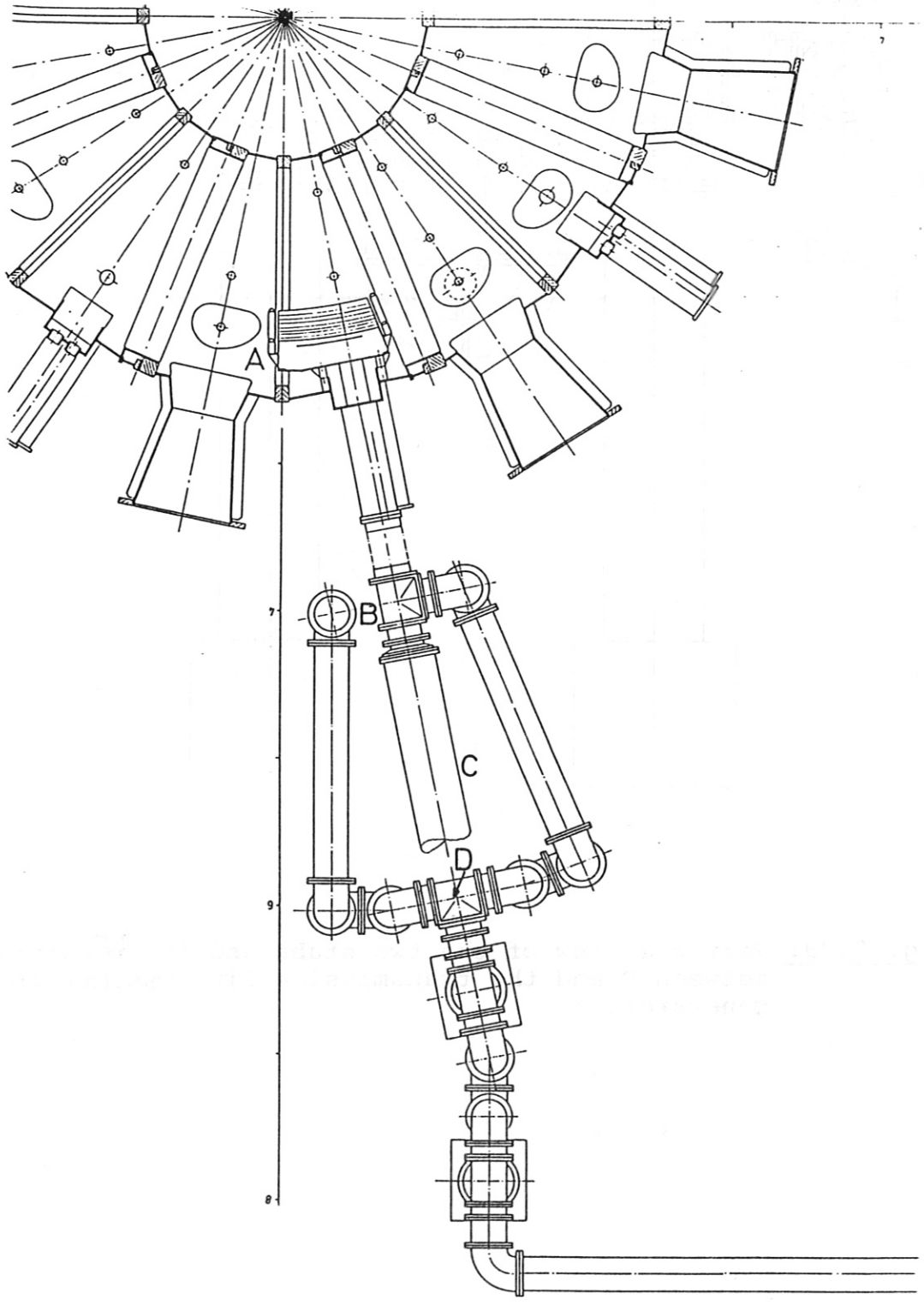

Fig. 3.28: Horizontal view of the transmission line in the neighbourhood of the experiment. The antenna is located in A. The machine vacuum extends to B. Between B and C we have a tuning stub. The two lines feeding the antennas through top and bottom port join in D. Two further stubs and a U extension are located between D and the transmission line leading to the generator.

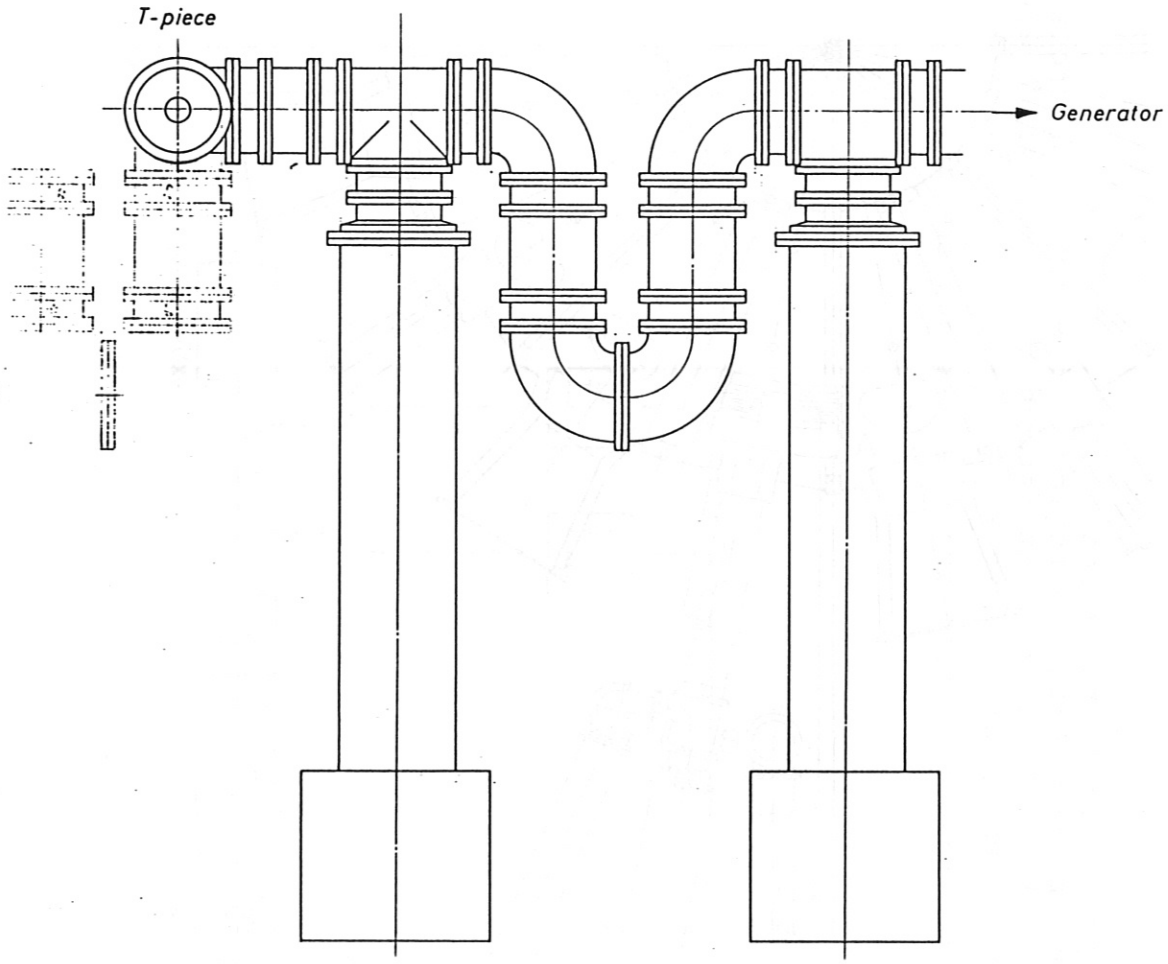

Fig. 3.29: Vertical view of the two stubs and the U extension between D and the transmission line leading to the generator.

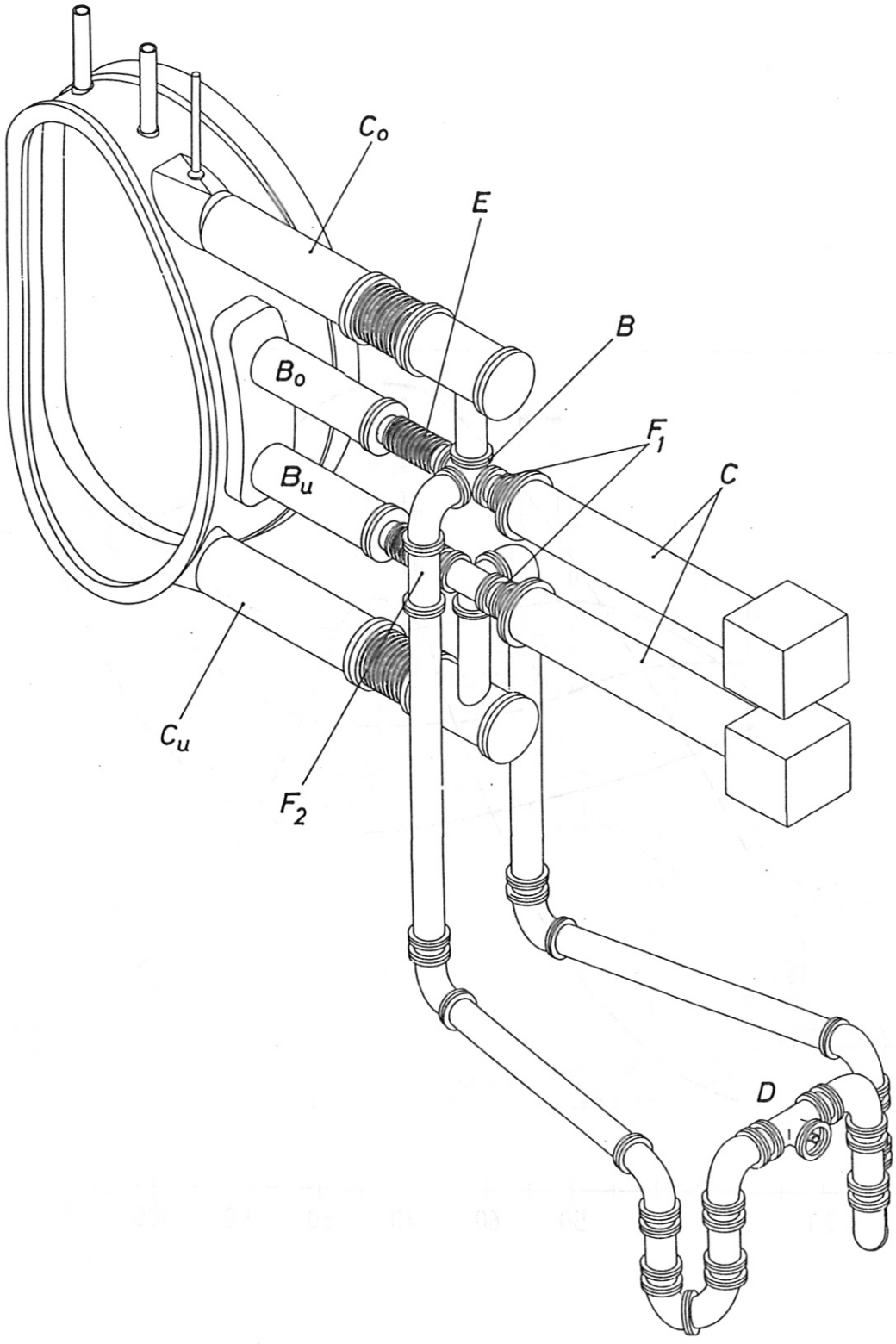

Fig. 3.30: Perspective view of the transmission line in the neighbourhood of the experiment. B_o and B_u are the antenna ports, C_o and C_u the vacuum ports. At the junction B, the transmission line vacuum is connected to the torus vacuum pumps. In E bellows take up the thermal expansion of the chamber. Feed-throughs are foreseen in F_1 and F_2. Stub tuners in C allow some matching and the introduction of coolant. The two feeding lines join in D.

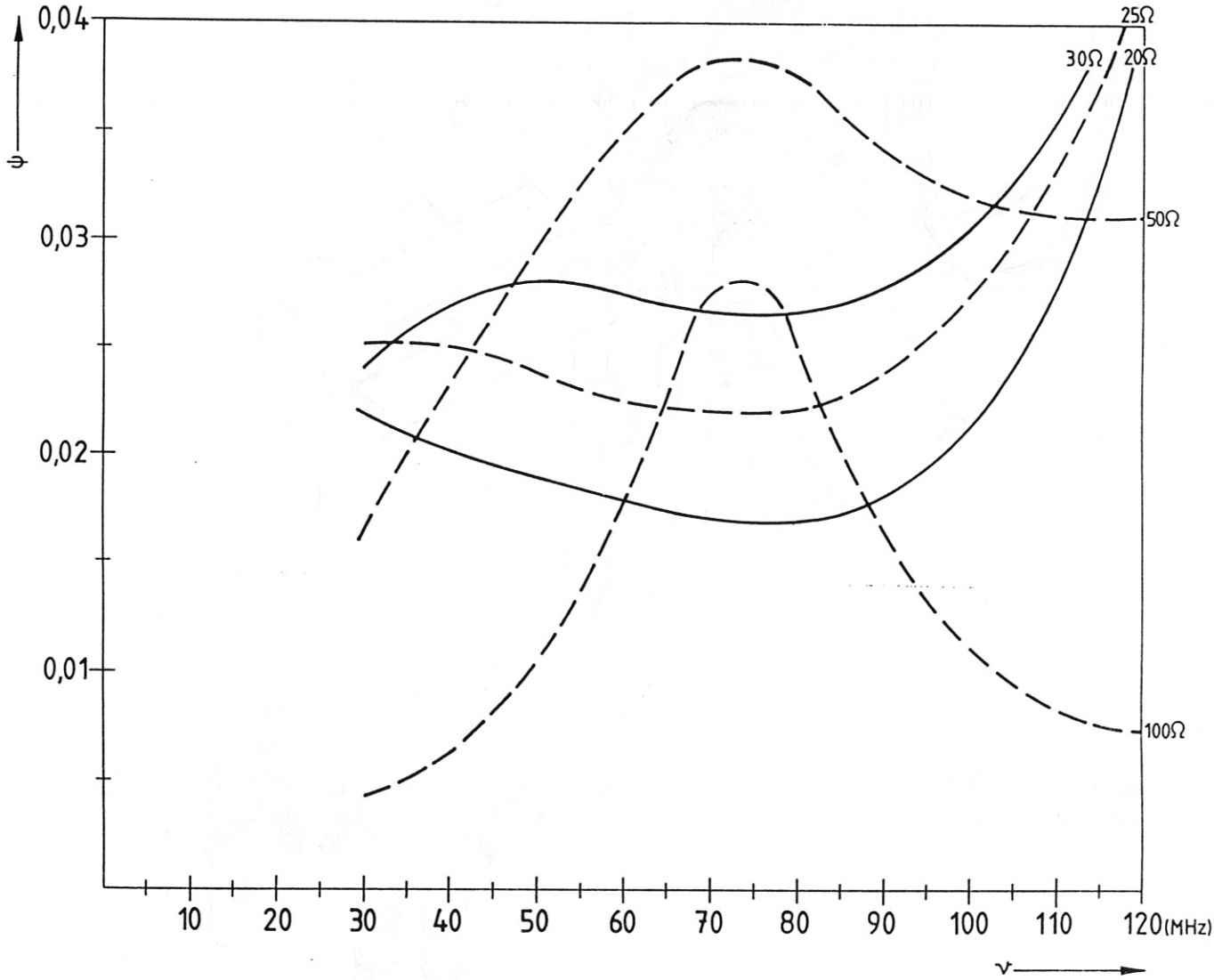

Fig. 3.31: The factor Ψ as a function of frequency for different values of characteristic impedances.

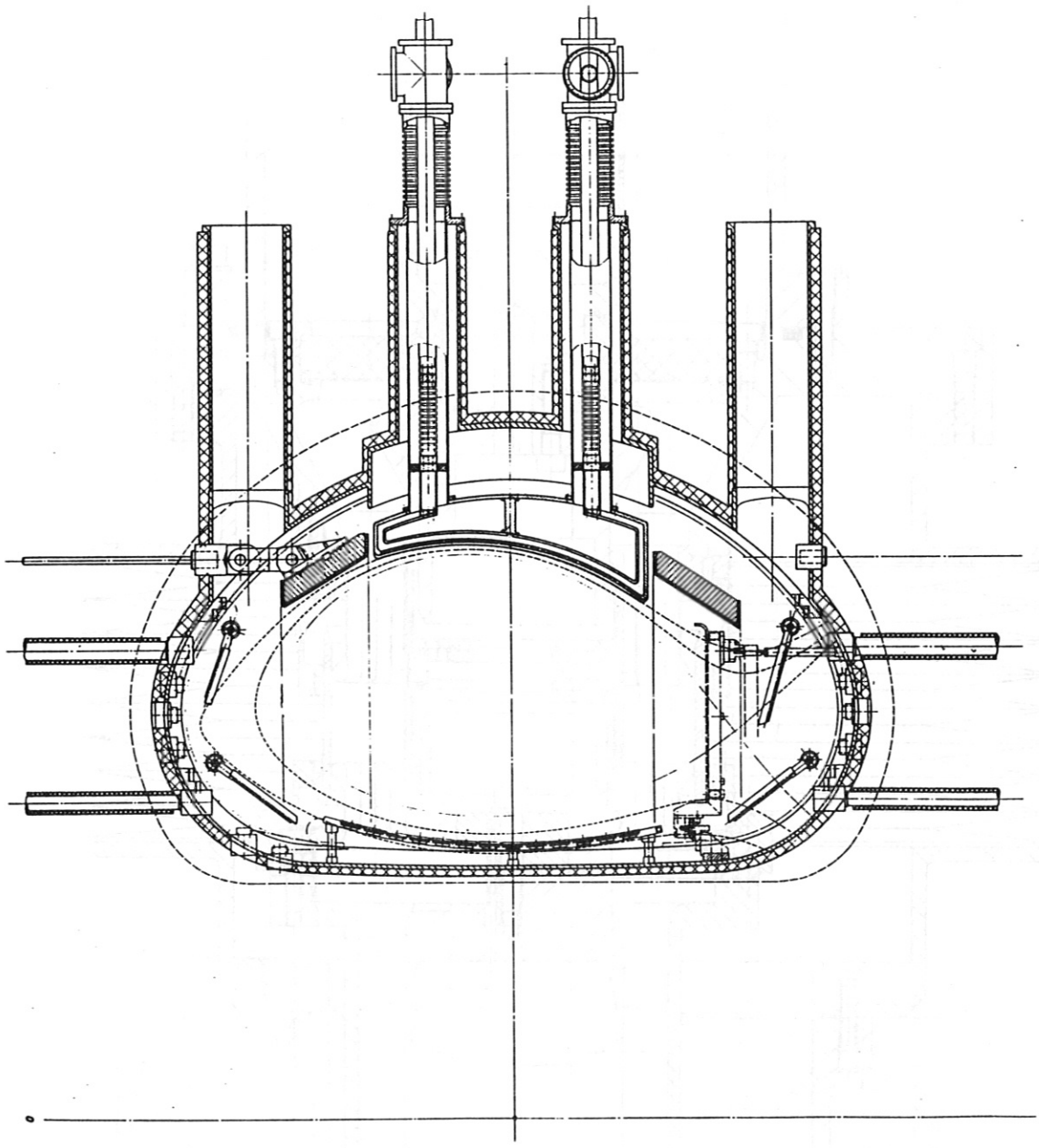

Fig. 3.32: Vertical cut through the antenna sector

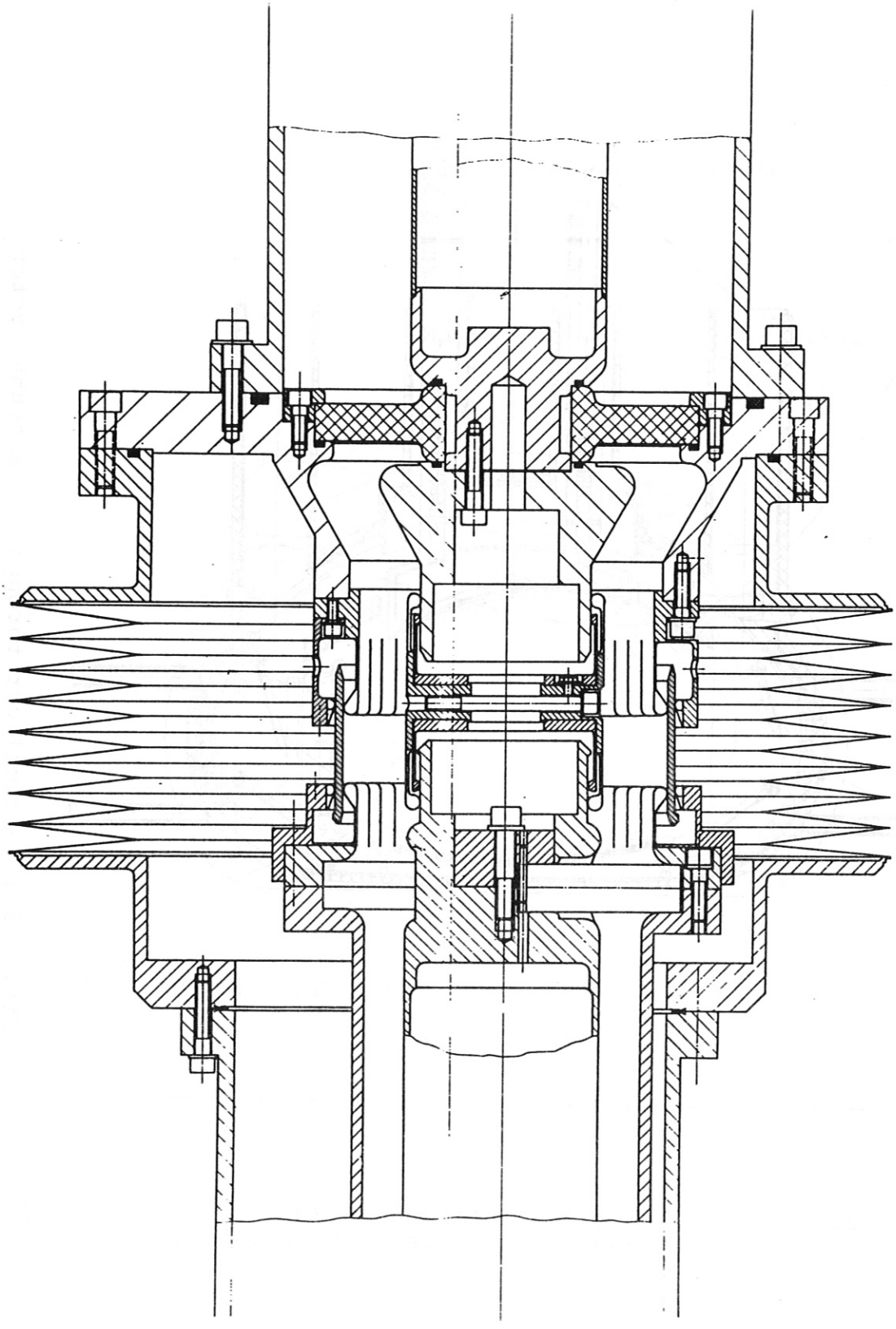

Fig. 3.33: Sliding contacts to take up the thermal expansion.

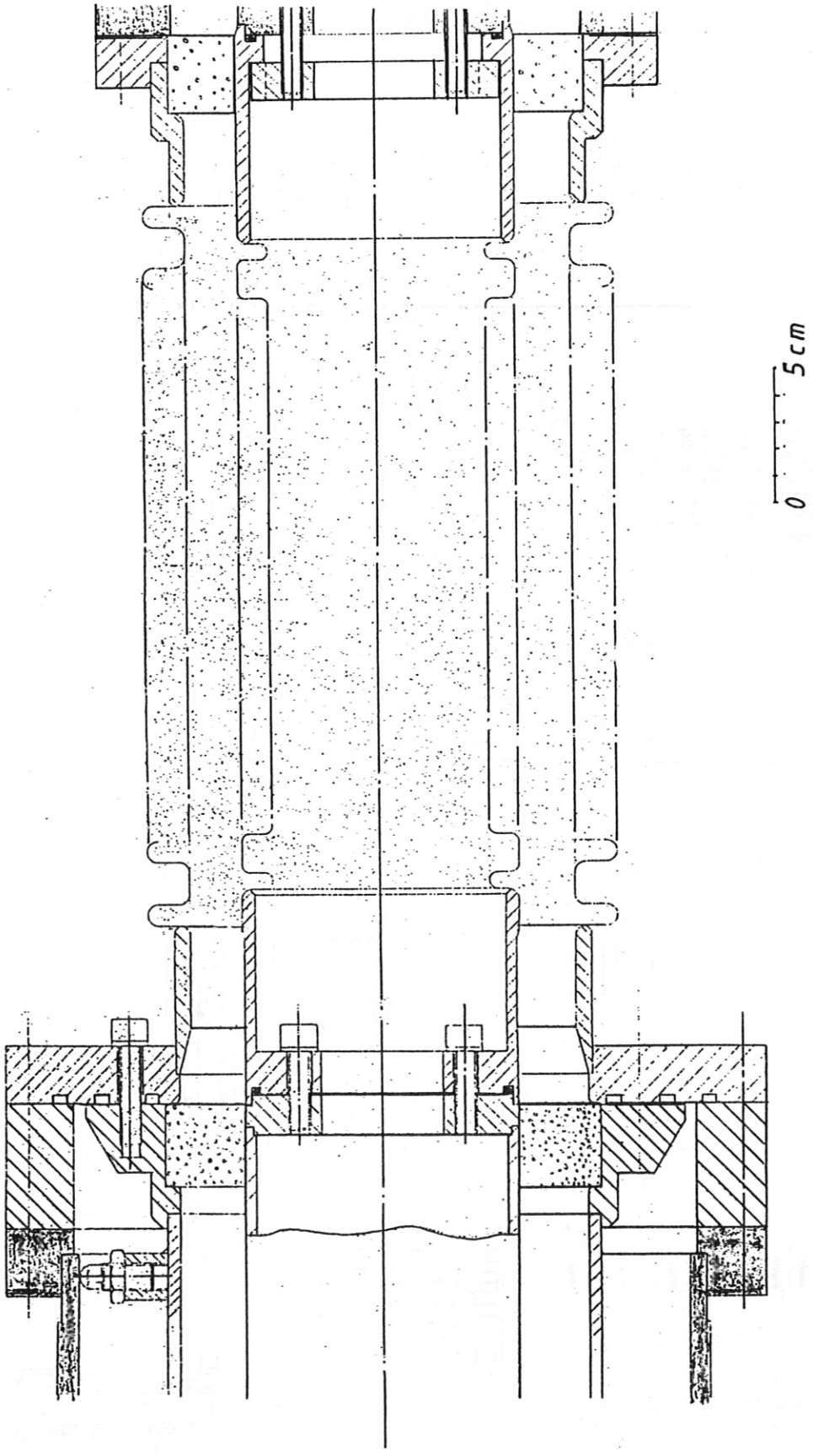

Fig. 3.34: Bellows to take up the thermal expansion. (schematic layout)

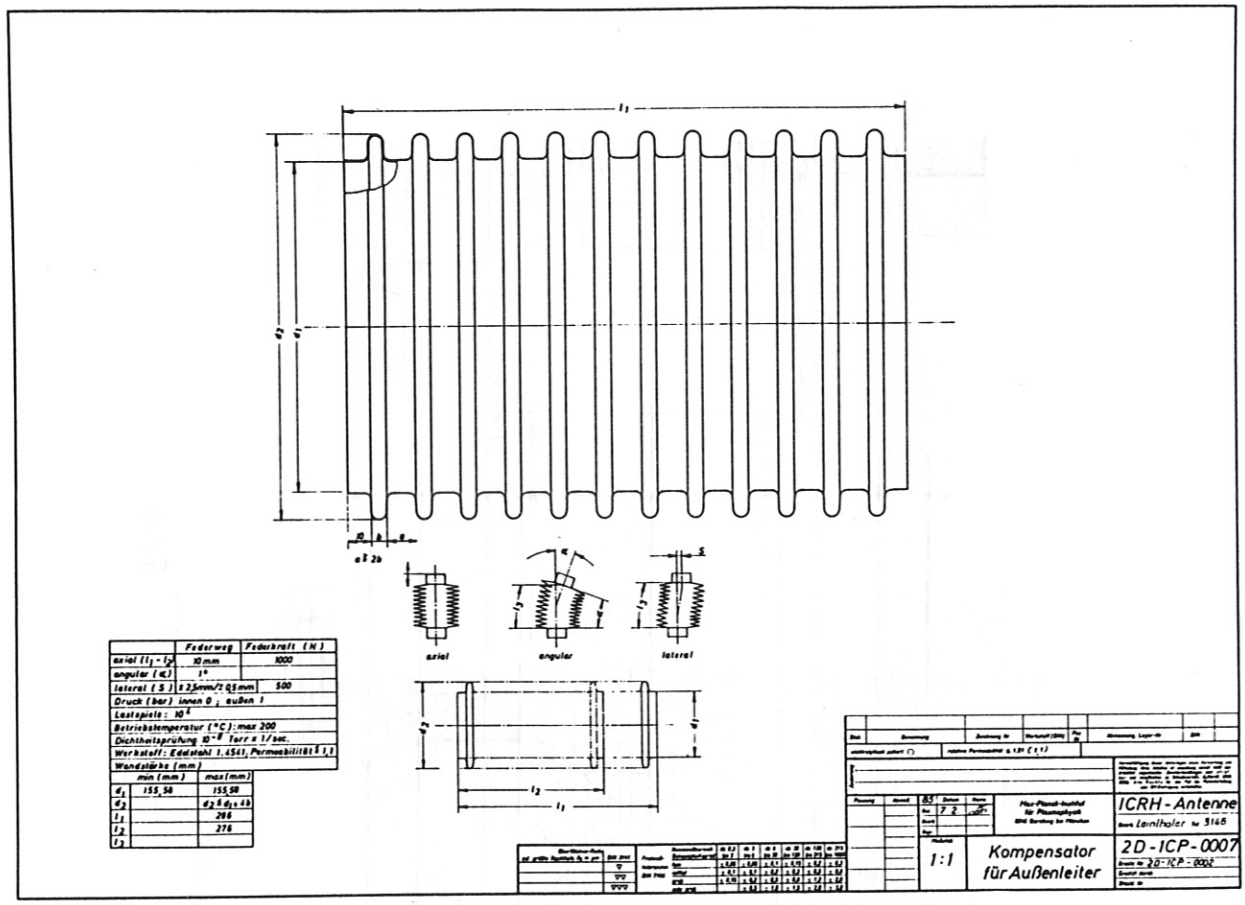

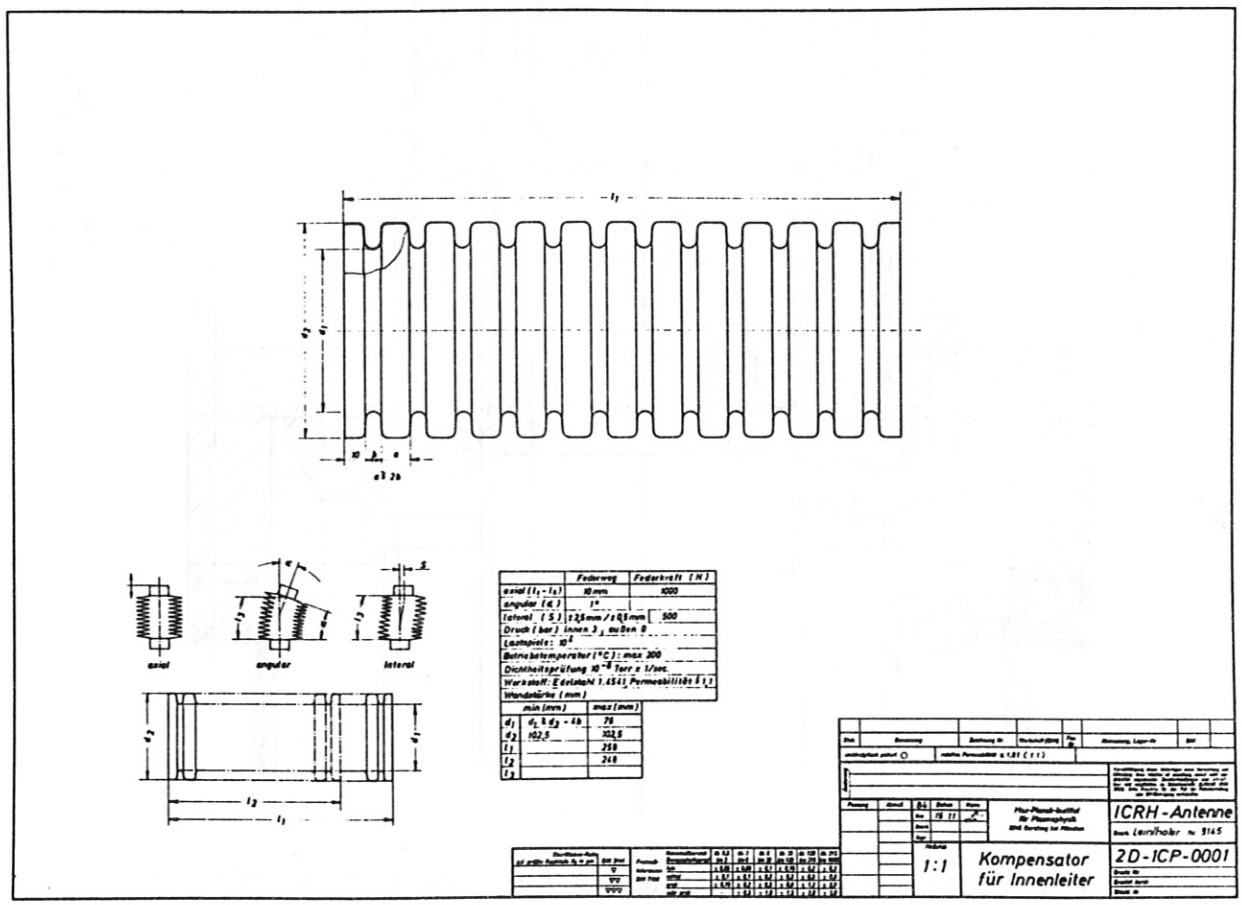

Fig. 3.35: Details of the bellows.

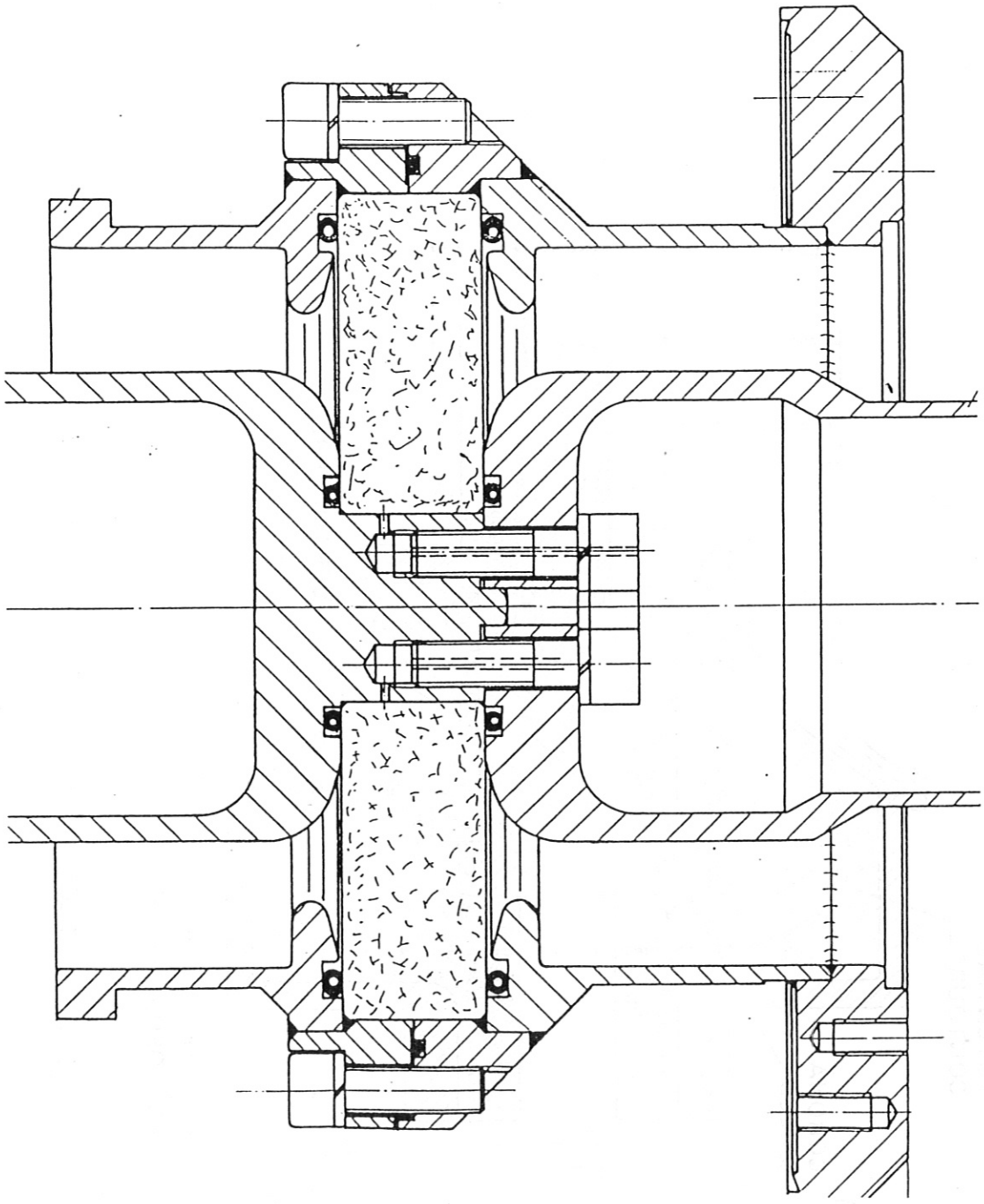

Fig. 3.36: Demountable feed-through being developed at IPP

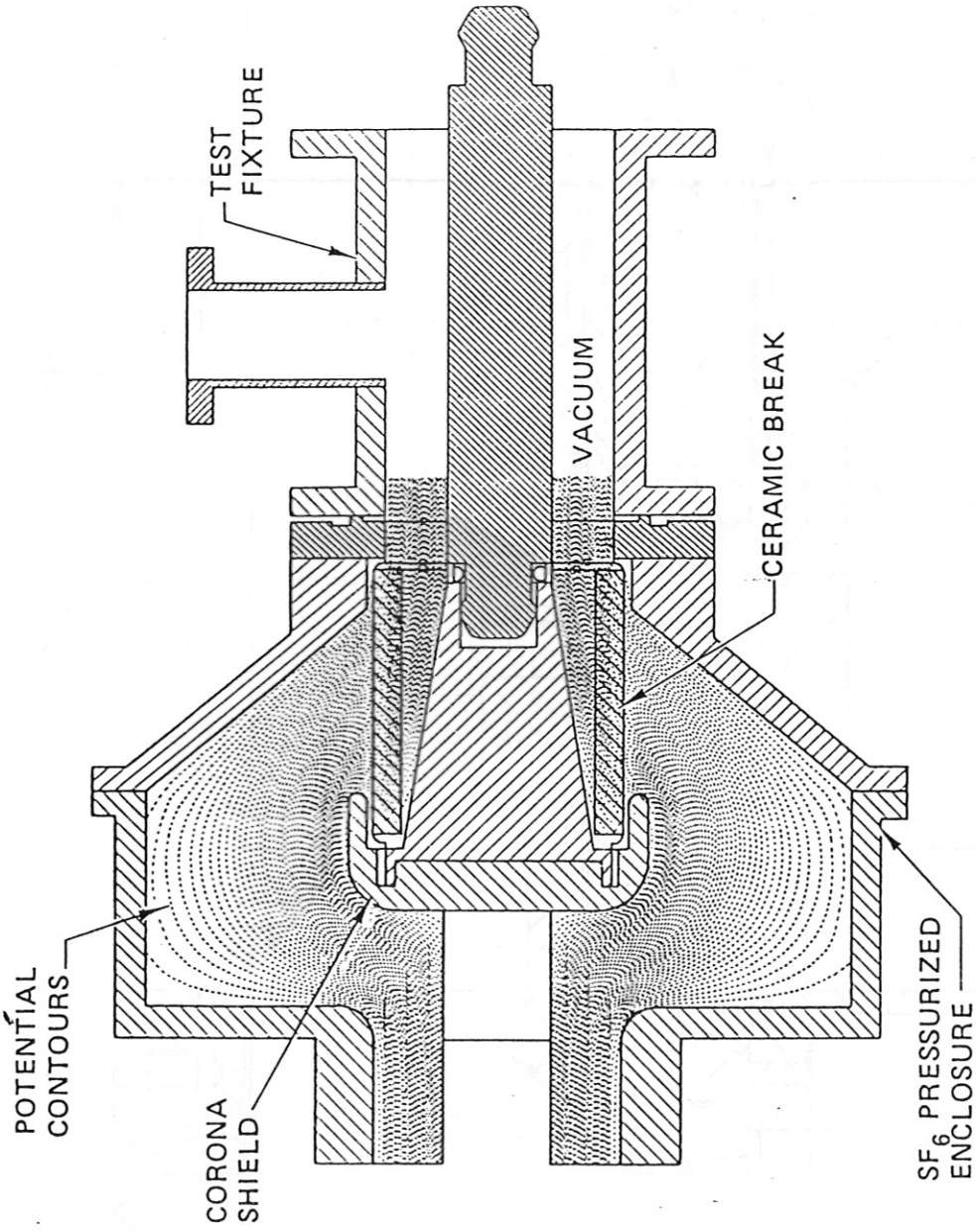

Fig. 3.37: Oak Ridge National Laboratory-type feed-through

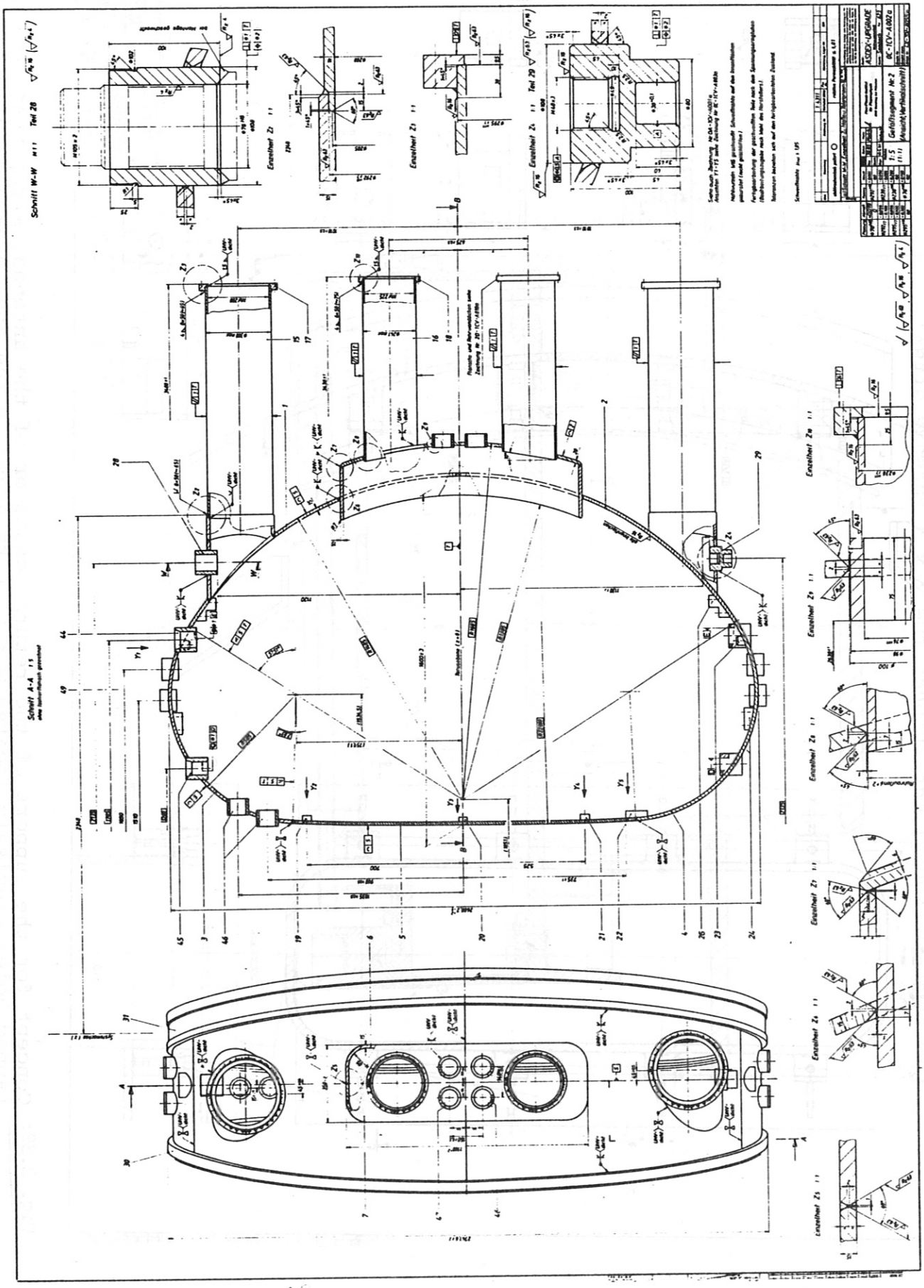

Fig. 3.38: Sector of the vacuum chamber in which the antenna is mounted.

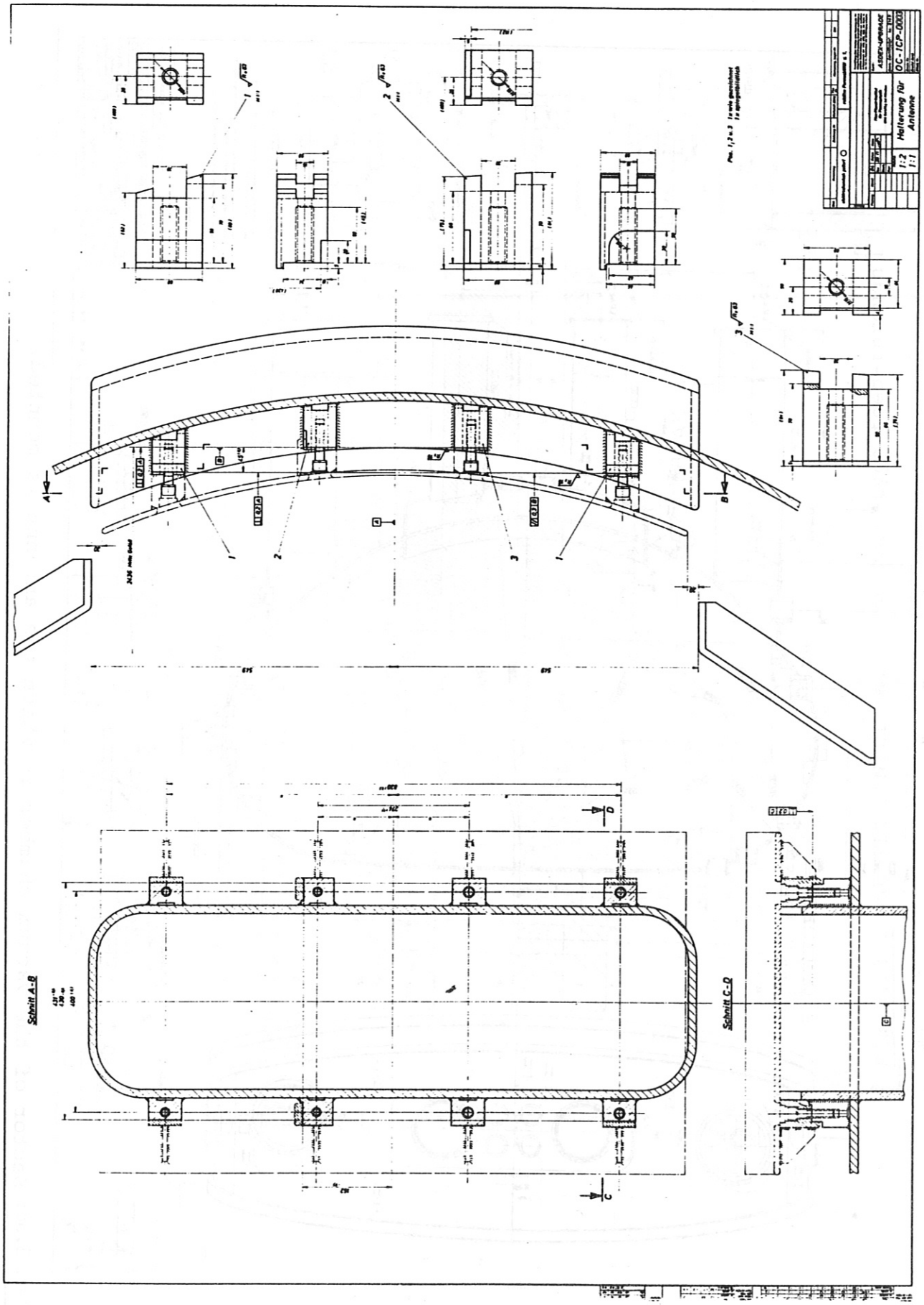

Fig. 3.39: Concept for the support of the return conductor of the antenna. Eight bushings with tapped holes precisely located w.r.t. a reference plane and to each other allow the bolting of the return conductor

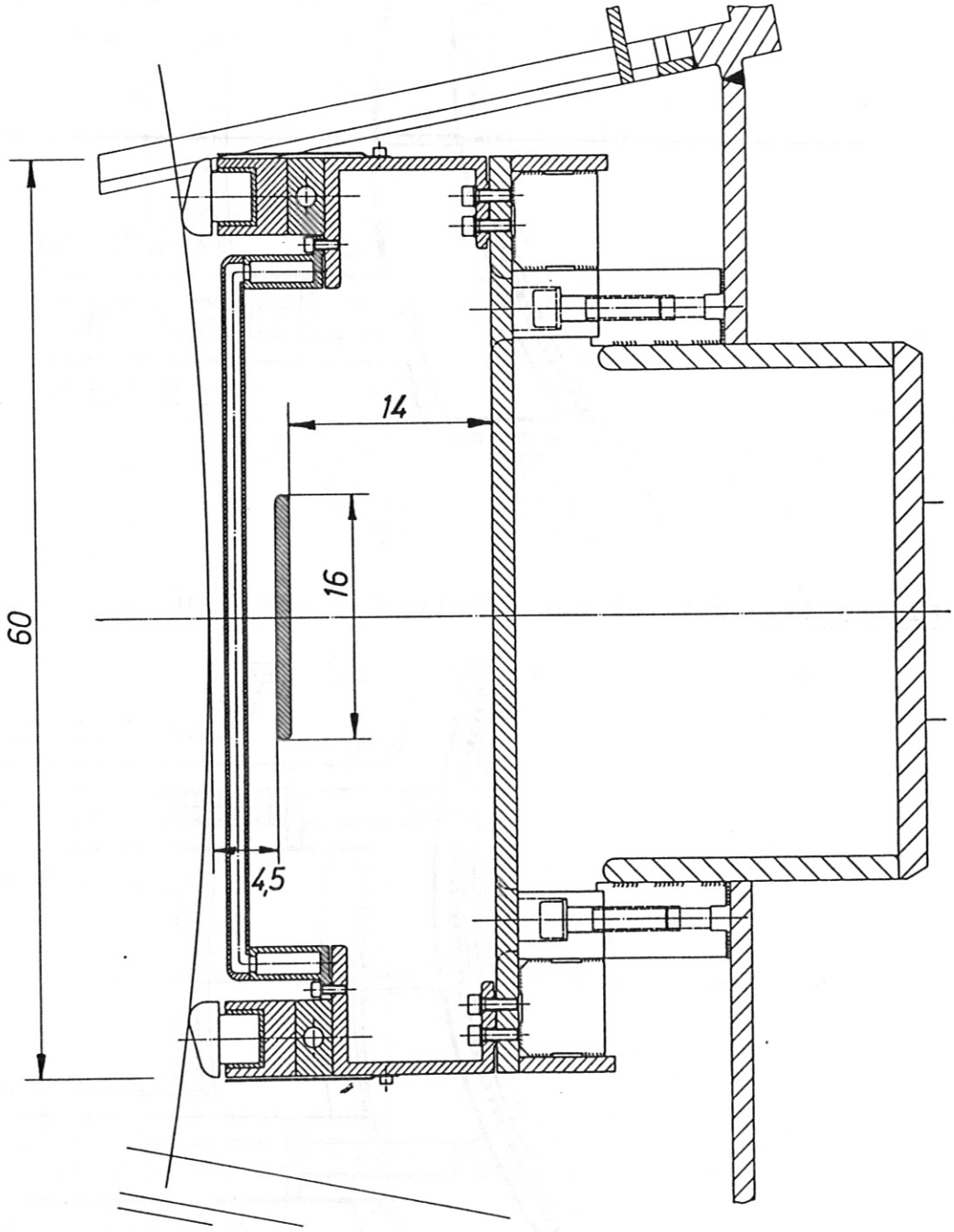

Fig. 3.40: Horizontal cut through the 1 x 2 antenna array.

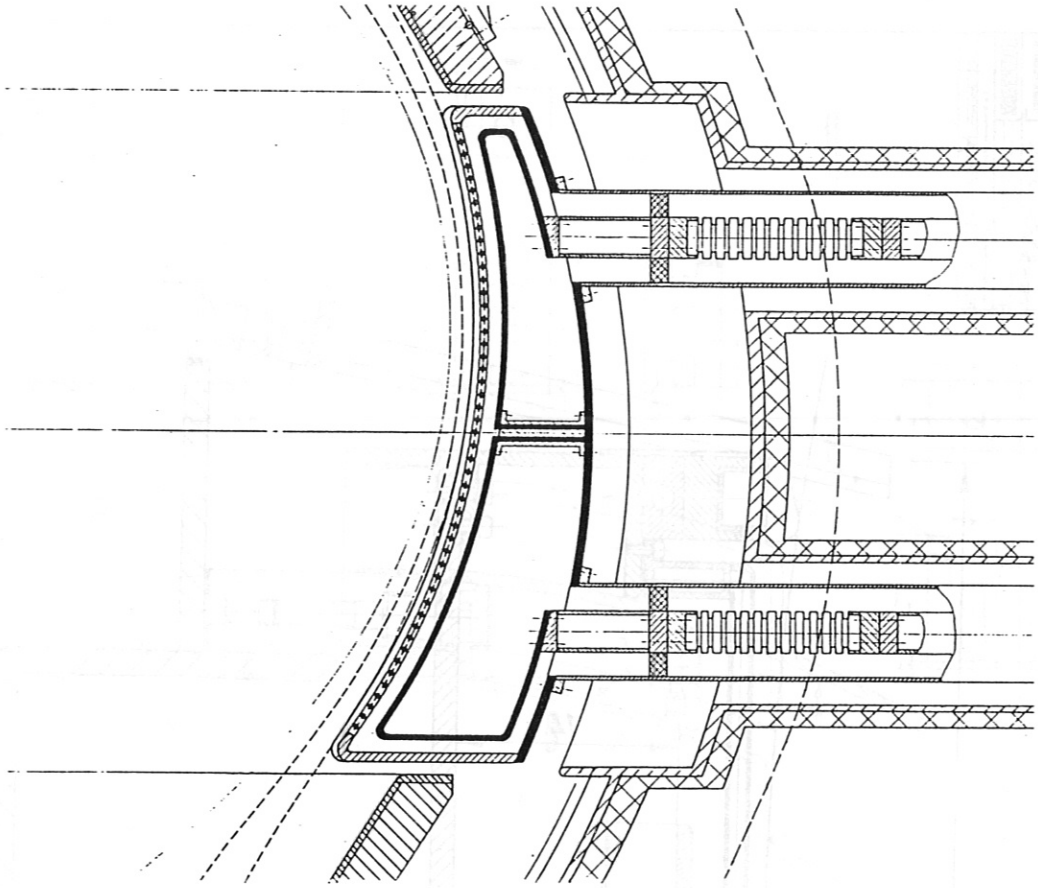

Fig. 3.41: Vertical cut JET-type trombone antenna

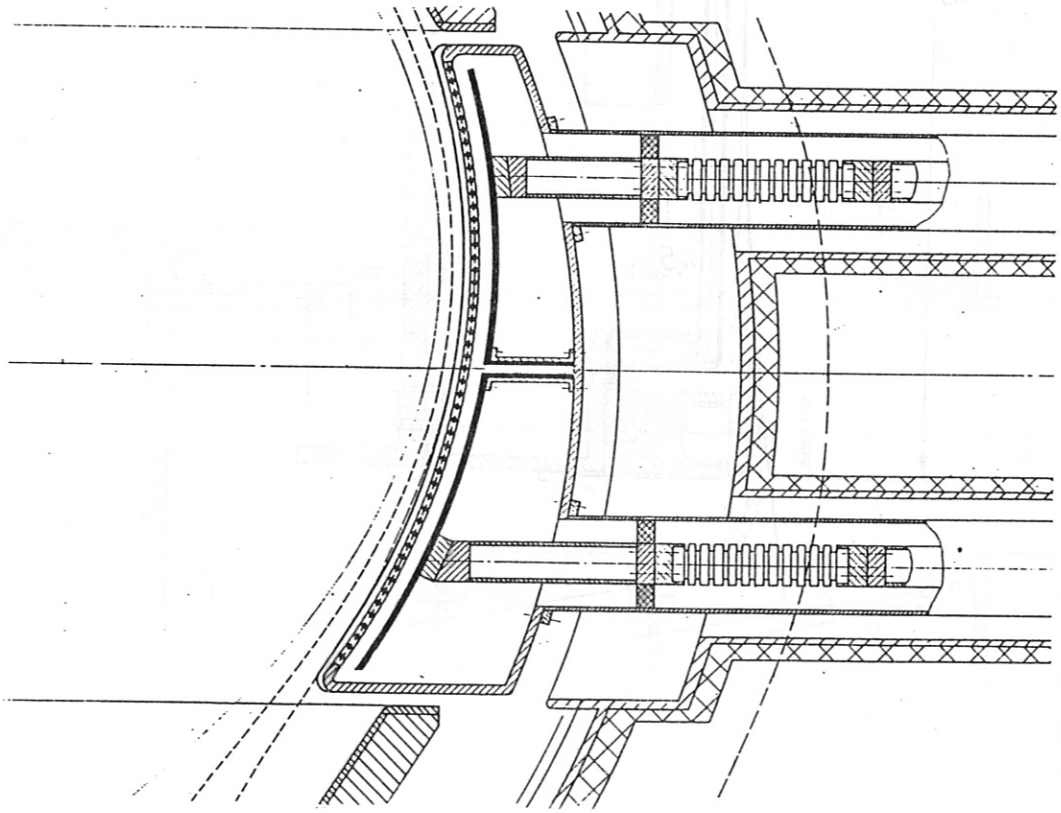

Fig. 3.42: Vertical cut straight-type antenna

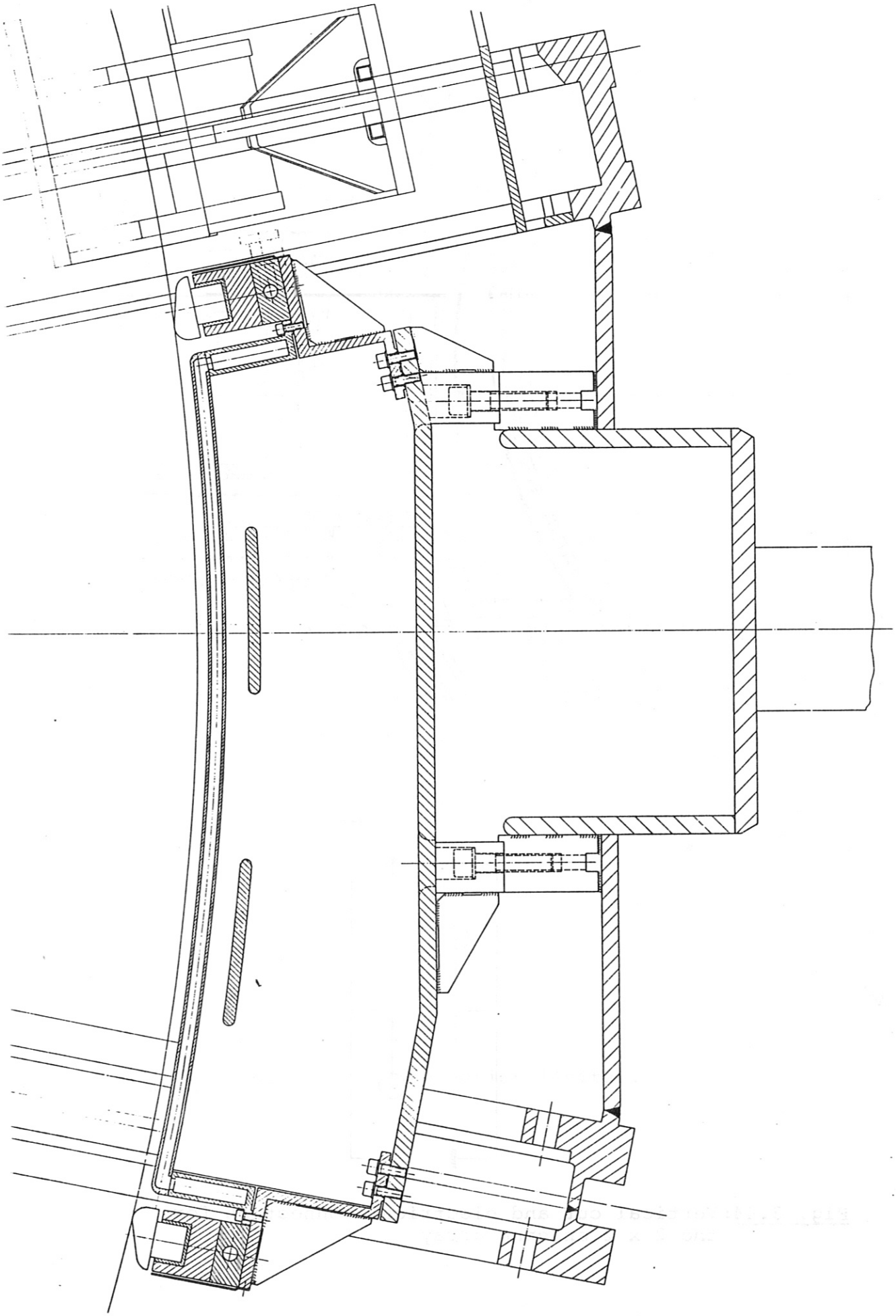

Fig. 3.43: Horizontal cut through the 2 x 2 antenna array.

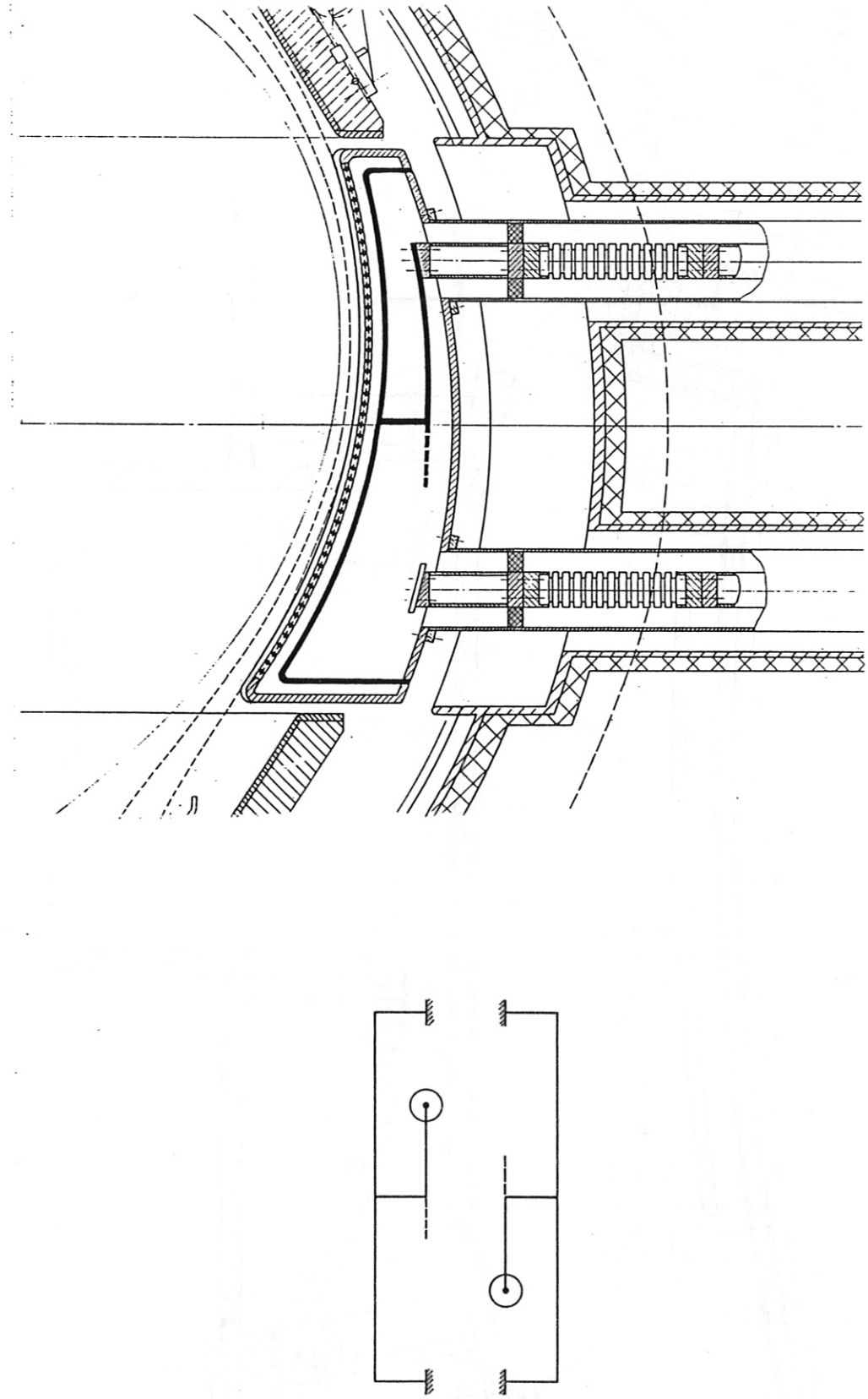

Fig. 3.44: Vertical cut and electrical connection for the 2 x 2 antenna array

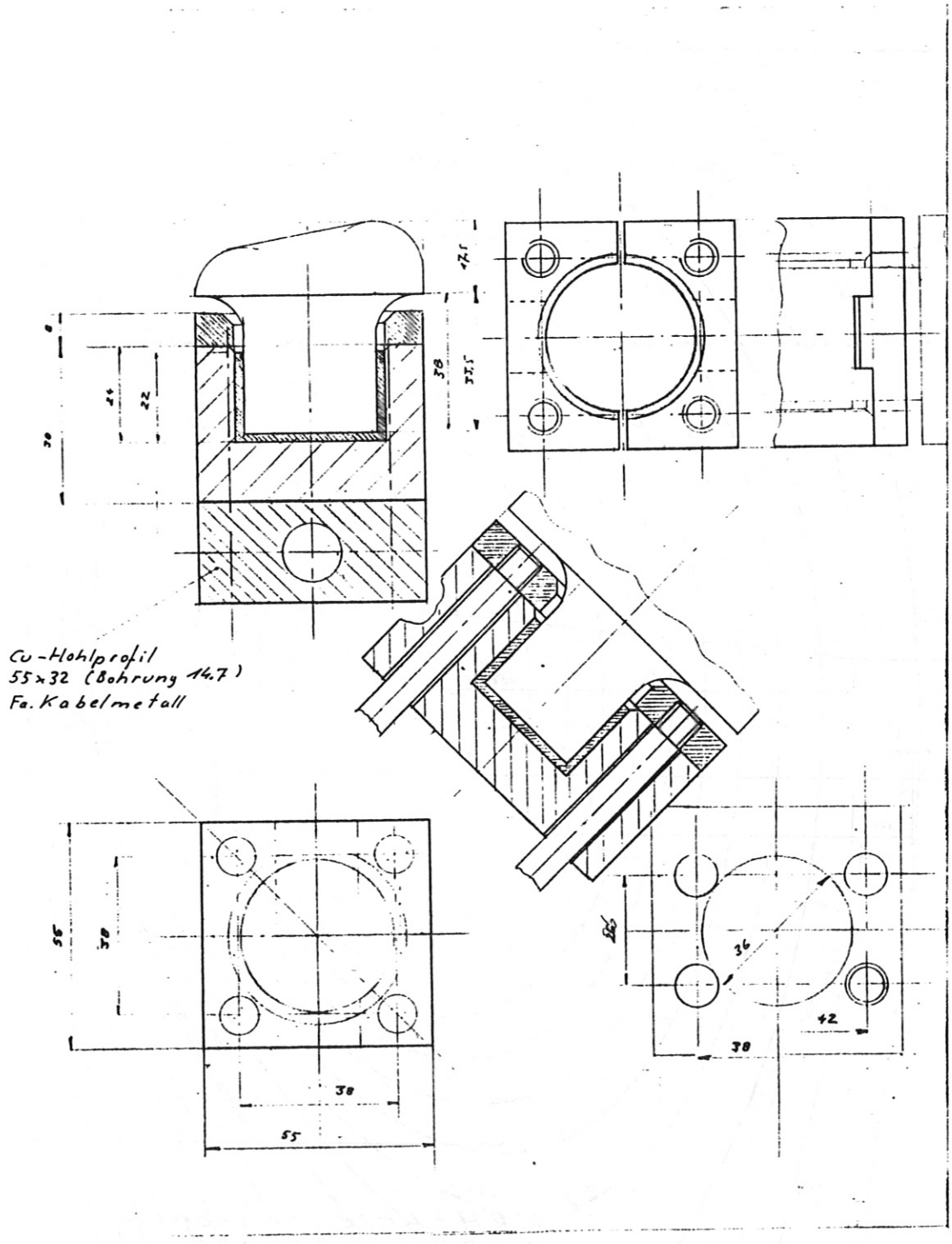

Fig. 3.45: Detail of the protection limiter.

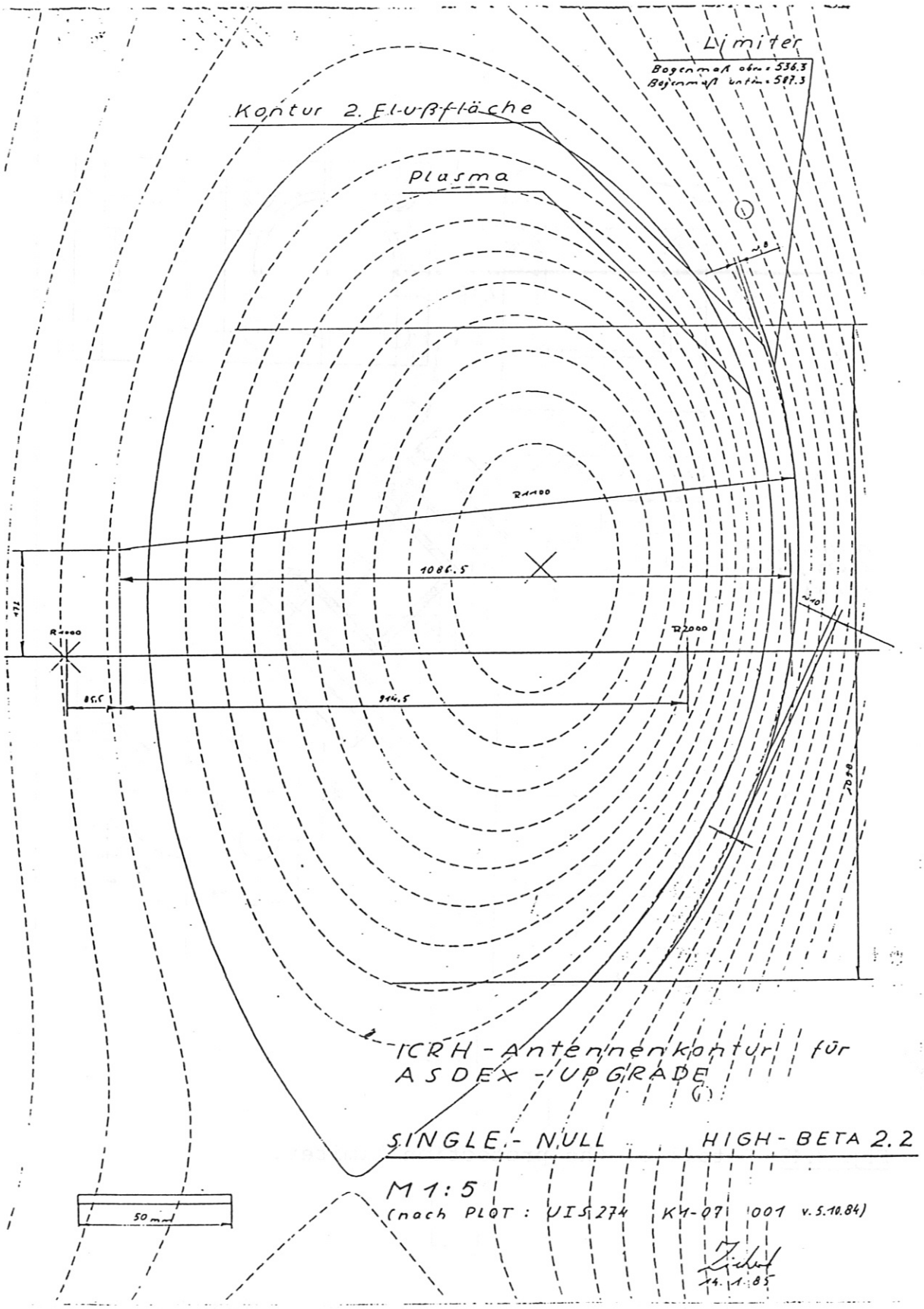

Fig. 3.46: Relation between the contour of the protection limiter and the flux surface for single null, high ß.

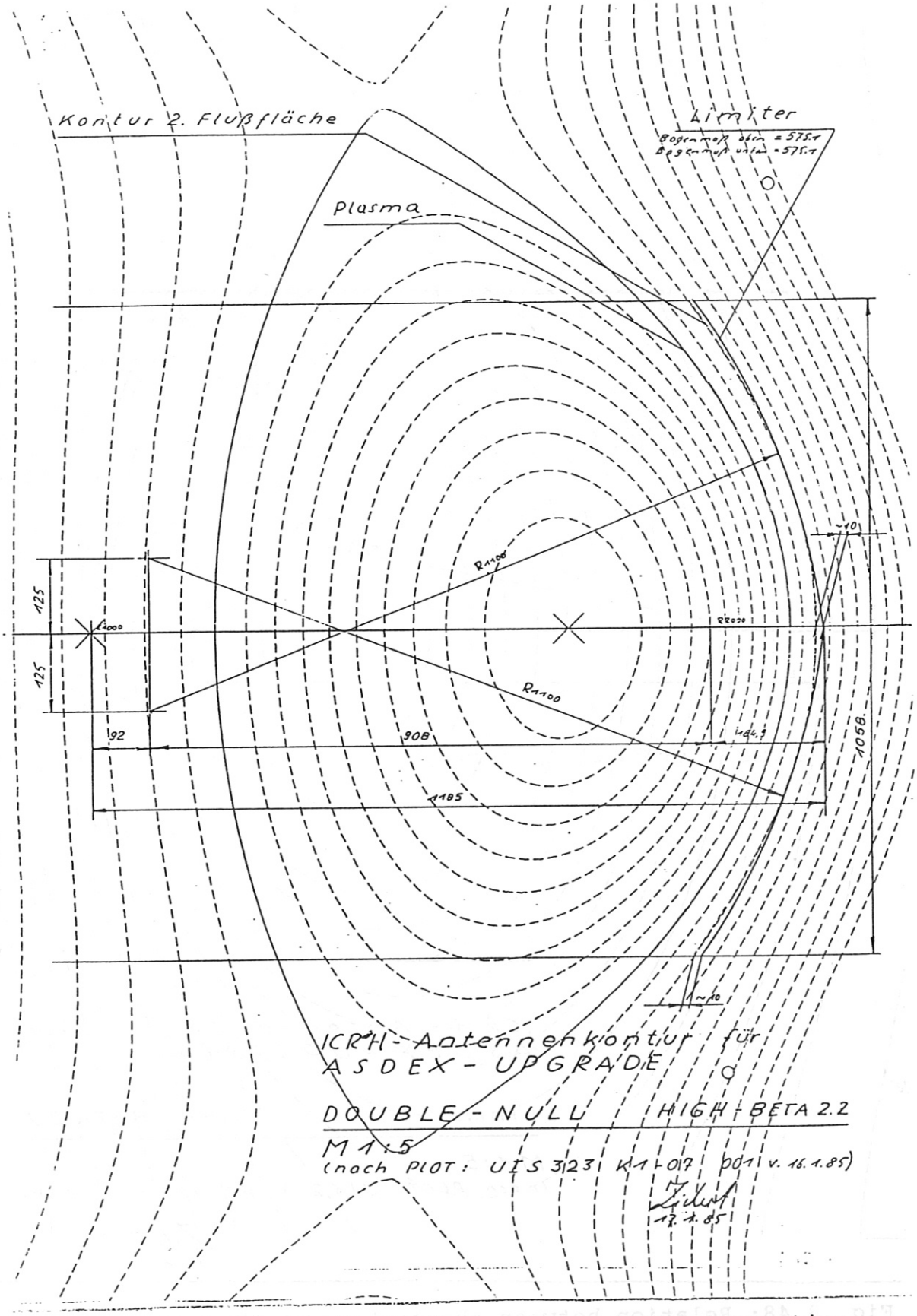

Fig. 3.47: Relation between the contour of the protection limiter and the flux surface for double null, high ß.

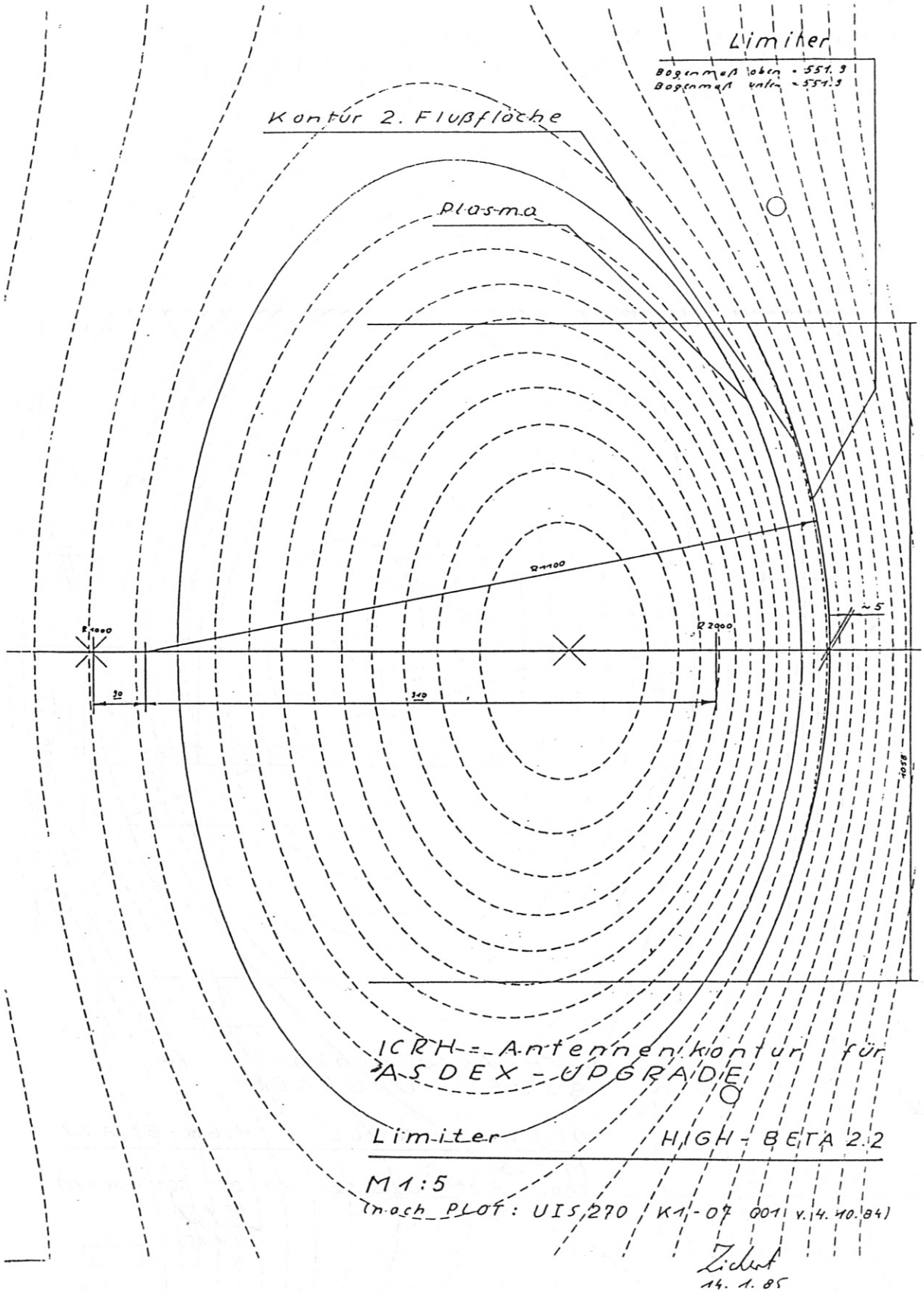

Fig. 3.48: Relation between the contour of the protection limiter and the flux surfaces for the limiter case, high ß.

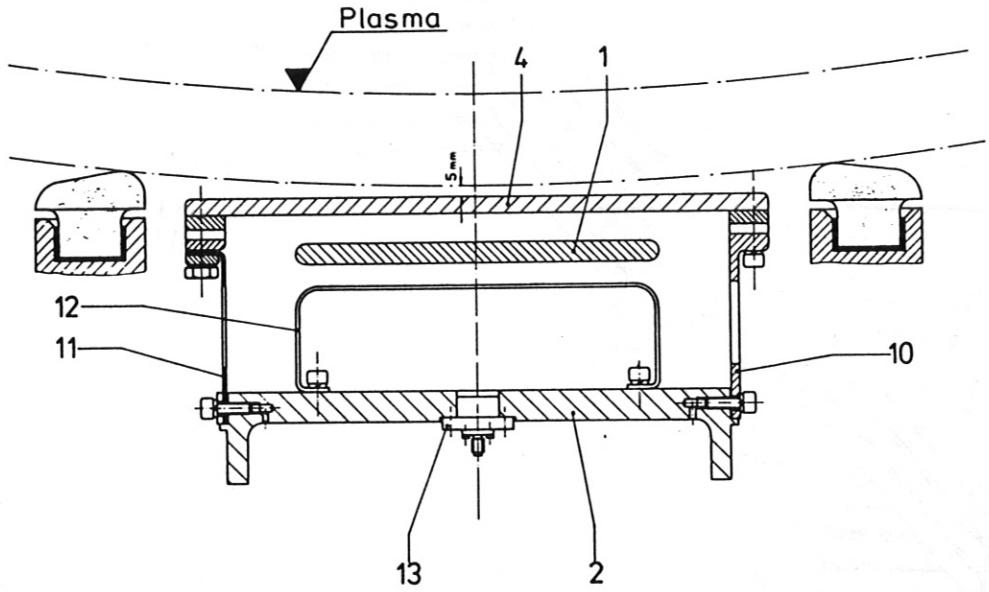

Fig. 3.49: Horizontal cut through the ASDEX antenna.

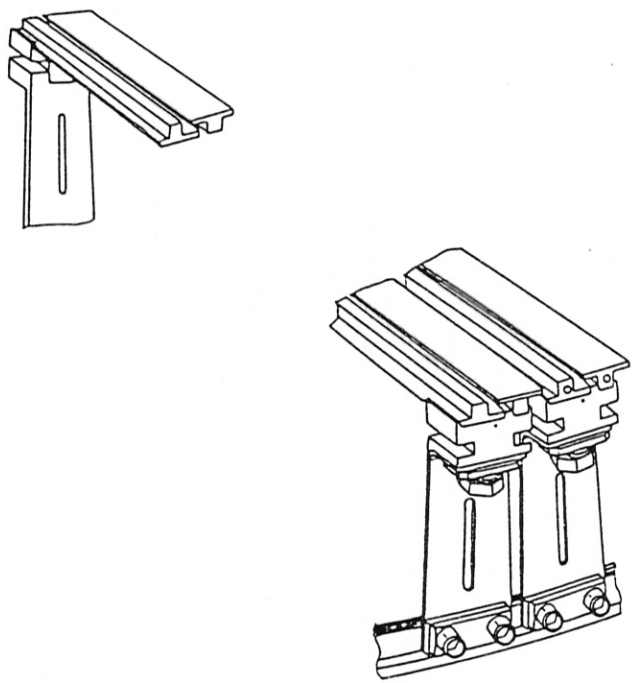

Fig. 3.50: Optically closed Faraday screen for ASDEX

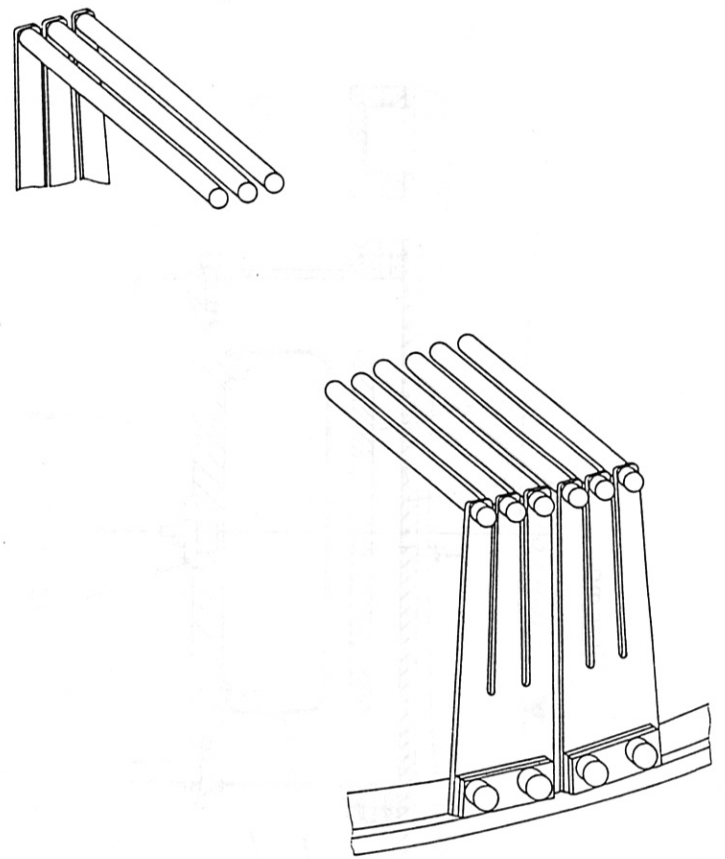

Fig. 3.51: Optically open Faraday screen for ASDEX

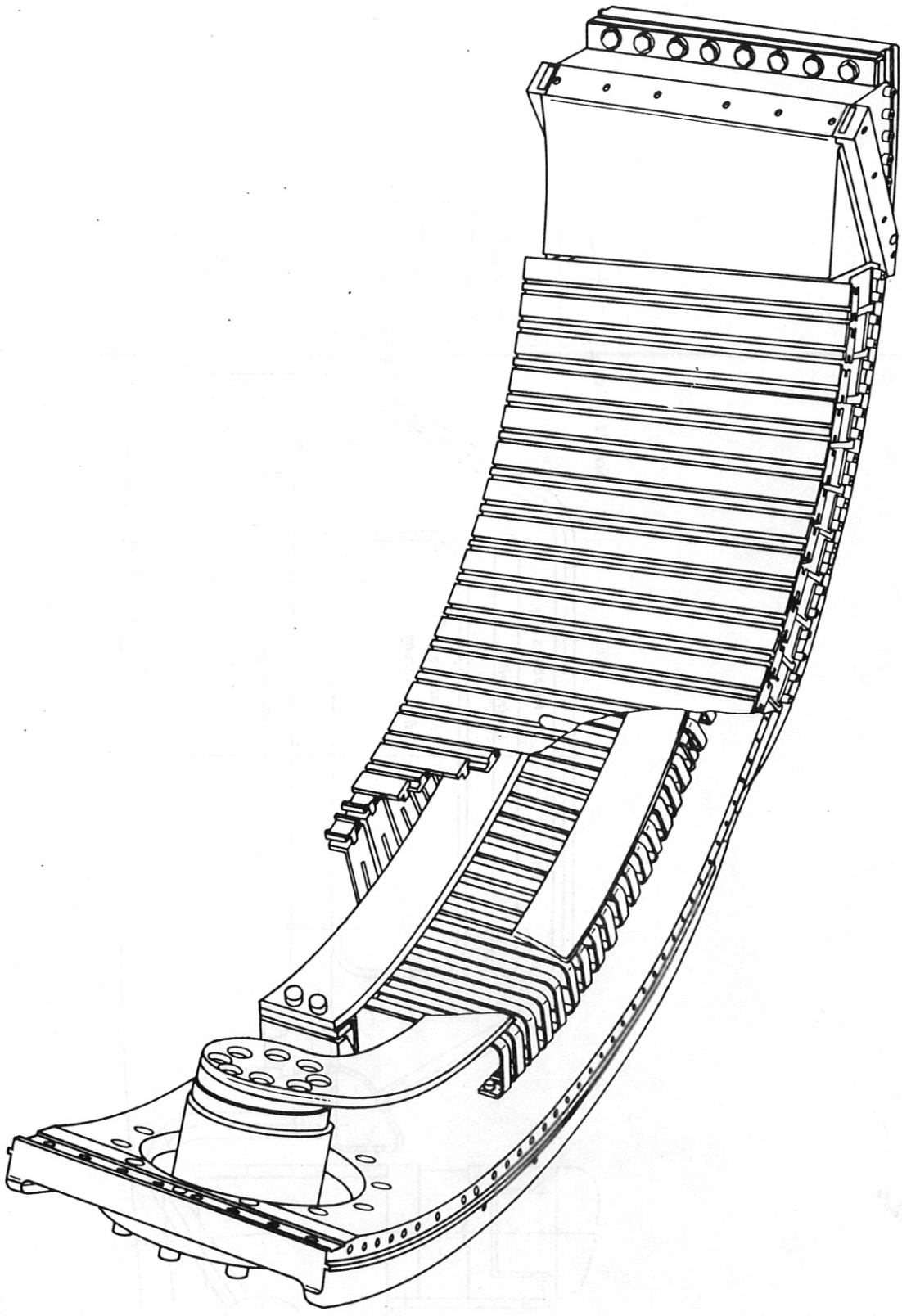

Fig. 3.52: 2 x 1 antenna array for ASDEX.

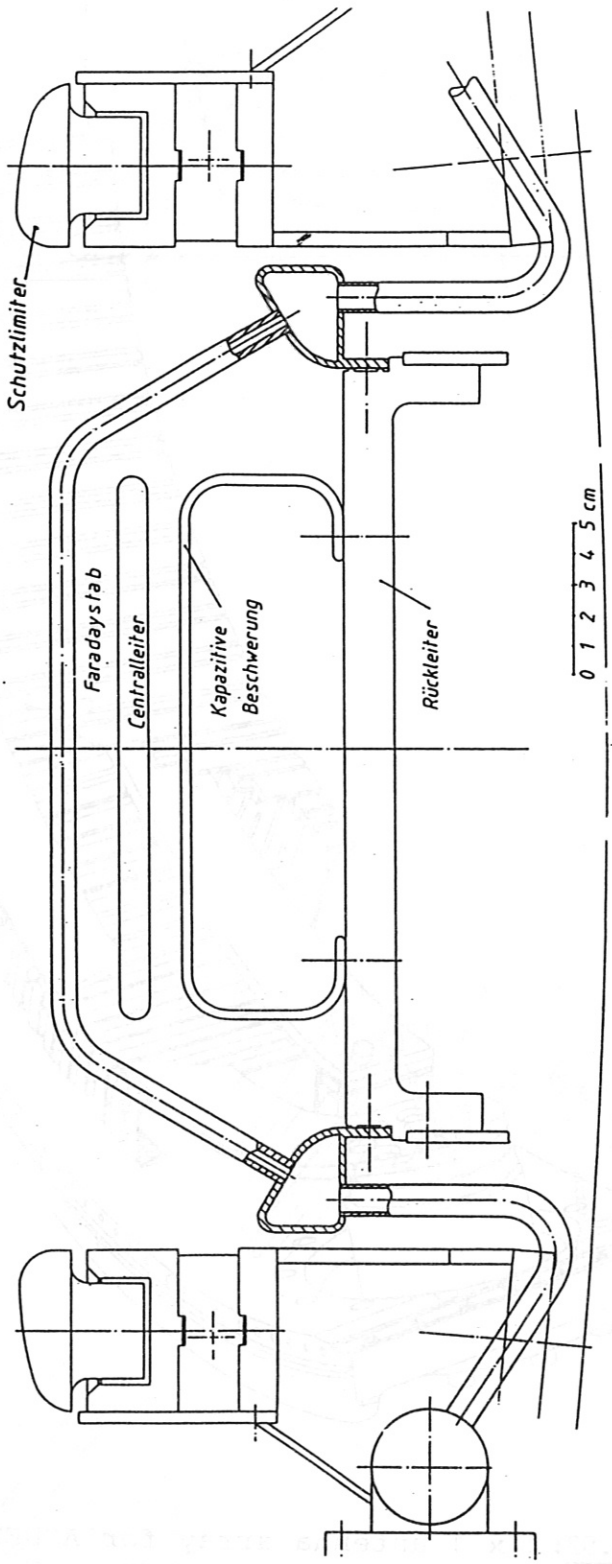

Fig. 3.53: Cooled Faraday screen for ASDEX.